2014

Development of a mechanical vapor-compression distiller incorporating concentrated solar power

Garrett Tyler Rinker

DEVELOPMENT OF A MECHANICAL VAPOR-COMPRESSION DISTILLER INCORPORATING CONCENTRATED SOLAR POWER

by

Garrett Tyler Rinker

Thesis submitted to the
Benjamin M. Statler College of Engineering and Mineral Resources
at West Virginia University
in partial fulfillment of the requirements
for the degree of

Master of Science
in
Mechanical Engineering

Hailin Li, Ph.D., Chair
Kenneth H. Means, Ph.D., PE
Lian-Shin Lin, Ph.D., PE

Department of Mechanical and Aerospace Engineering

Morgantown, West Virginia
2014

Keywords: Produced Water; Desalination; Distillation; Mechanical Vapor-Compression; Solar Energy

Abstract

DEVELOPMENT OF A MECHANICAL VAPOR-COMPRESSION DISTILLER INCORPORATING CONCENTRATED SOLAR POWER

Garrett Tyler Rinker

The demand for a reliable energy supply has promoted the development of the Marcellus Shale gas industry in the past few years. However, the produced water from hydraulic fracturing (also known as fracking) poses a hazard to human and environmental health because of its dissolved solid, hydrocarbon, and heavy metal content. This research proposes to develop a portable solar power assisted water distiller which can process produced water on-site for natural gas wells.

The distillation technology developed is a small scale mechanical vapor-compression (MVC) distillation unit. The thermal energy for the evaporation of the water is provided by the solar energy, while the recirculation pumps and compressor are driven by electrical motors. The research works completed include the in-house and on-site demonstration of the 1st generation design, and the design of the 2nd generation solar aided MVC distillation unit. The main design features of this research include an insulation system, a heat capacity analysis of heat exchangers, a compressor which requires less power input, and options for making the entire system operate on solar power alone. The potential of the insulation system in reducing the heat loss of the system and the demand for thermal energy was examined. The regeneration system developed was able to recover approximately 91% of the thermal energy released during the condensation and cooling process of the distilled water vapor, which dramatically decreased the consumption of thermal energy and the size of parabolic dish reflectors (PDRs) needed. Also, the insulation system will reduce the rate of heat loss to the ambient air by approximately 86% compared to an un-insulated system. A theoretical model was developed to examine the performance of the 2nd generation design and has been presented. The on-site demonstration of the 1st generation system confirmed that the proposed system was able to process the high-salt produced water and extract clean water with the potential to recycle the salts for commercial use. The numerical simulation results show the 2nd generation system with redesigned components and insulation was able to process produced water at a rate of 20 gallon/hour with a power consumption of approximately 4.6 kW, which includes 3.2 kW from solar energy for heating purposes and 1.4 kW from electricity to run the compressor and the recirculation pump.

Acknowledgements

I would like to thank Dr. Hailin Li for his continued support and belief in me, which has been an influential part of my academic career since the early stages of my undergraduate studies. Also, many thanks go to Dr. Kenneth Means and Dr. Lian-Shin Lin for their input toward this work.

I would like to thank my friends and family. I have greatly appreciated their unwavering support and encouragement throughout my life.

Finally, I would like to thank my colleagues at Epiphany Solar Water Systems for their funding of this project. I am very grateful to have had the opportunity to work with this group of interesting and intelligent people. None of this would be possible without them.

Table of Contents

List of Tables

List of Figures

Nomenclature

C ..... Celsius
C ..... Heat Capacity
c_p ..... Specific Heat
DEP ..... Department of Environmental Protection
EPA ..... Environmental Protection Agency
F ..... Fahrenheit
FO ..... Forward Osmosis
gal ..... Gallon
GOR ..... Gained Output Ratio
h ..... Convection Heat Transfer Coefficient
h ..... Specific Enthalpy
h ..... Head Loss
hr ..... Hour
IBC ..... Intermediate Bulk Container
k ..... Thermal Conductivity
kg ..... Kilogram
kWh ..... Kilowatt-Hour
LMTD ..... Log Mean Temperature Difference
LST ..... Local Standard Time
MED ..... Multiple Effect Distillation
min ..... Minute
MSF ..... Multistage Flash
MVC ..... Mechanical Vapor Compression
n ..... Polytropic Constant
NPSH ..... Net Positive Suction Head
NPSHA ..... Net Positive Suction Head Available
NPSHR ..... Net Postitive Suction Head Required
NREL ..... National Renewable Energy Laboratory
NTU ..... Number of Transfer Units
p ..... Pressure
P ..... Pressure
PDR ..... Parabolic Dish Reflector
PV ..... Photovoltaic
$\dot{Q}$ ..... Heat Transfer
R ..... Gas Constant
RO ..... Reverse Osmosis
s ..... Second
SG ..... Specific Gravity
T ..... Temperature
TDS ..... Total Dissolved Solids
v ..... Specific Volume
VC ..... Vapor Compression
$\dot{W}$ ..... Power
X ..... Mass Fraction

Greek Letters

α ..... Convection Heat Transfer Coefficient
ε ..... Effectiveness
ρ ..... Density
μ ..... Dynamic Viscosity
η ..... Efficiency

Subscripts

0 ..... Initial
1 ..... Inlet
2 ..... Outlet
c ..... Compressed
comp ..... Compressor
e ..... Evaporated
GS ..... Gassy Steam
major ..... Major Head Loss
min ..... Minimum
minor ..... Minor Head Loss
max ..... Maximum
sat ..... Saturated

Chapter 1: Introduction

This research seeks to produce clean water by proposing a distiller design which can be incorporated in water purification units manufactured by Epiphany Solar Water Systems. Epiphany is a company which specializes in utilizing concentrated solar energy to assist the process of water purification in a system referred to as the E3H. The basic process of the E3H is shown in Figure 1 [1]. Sunlight is concentrated at a focal point by PDRs. A heat transfer receiver is located at the focal point, and these receivers convert solar energy into thermal energy. Heat transfer fluid is pumped through these receivers, which raises the temperature of the fluid to approximately 200°C. The heat transfer fluid gathers in an insulated hot fluid storage tank. This storage tank acts as a thermal "battery" which can keep the unit operational while the sun is discontinuous and at night. The hot heat transfer fluid is sent through a distillation unit and is used to vaporize contaminated water. The vaporized water is condensed and collected in a clean water tank.

This technology has recently attracted interest from oil and gas companies as a means to treat produced water from hydraulic fracturing (also known as fracking). Hydraulic fracturing is a process in which several million gallons of fluid are injected into a horizontal well at extreme pressures in order to fracture shale and release natural gas. The injected fluid usually consists of more than 90% water, almost 9% sand, and less than 0.5% chemical additives. The chemical additives function as friction reducers, scale inhibitors, iron controls, and biocides [2]. Most wells have 10-40% of the injected fluid return to the surface when natural gas is released from the shale [2, 3, 4], but this percentage may vary greatly from well to well. The fluid which returns to the surface is referred to as produced water. Produced water poses a hazard to human

and environmental health because of its dissolved solid, hydrocarbon, heavy metal content, and high salt concentration [2]. Some toxic chemical elements found in produced water include barium, strontium, and radium. The US Environmental Protection Agency (EPA) and the Pennsylvania Department of Environmental Protection (DEP) recognize that disposal of produced water to publicly owned wastewater plants is not a sustainable water management strategy [2].

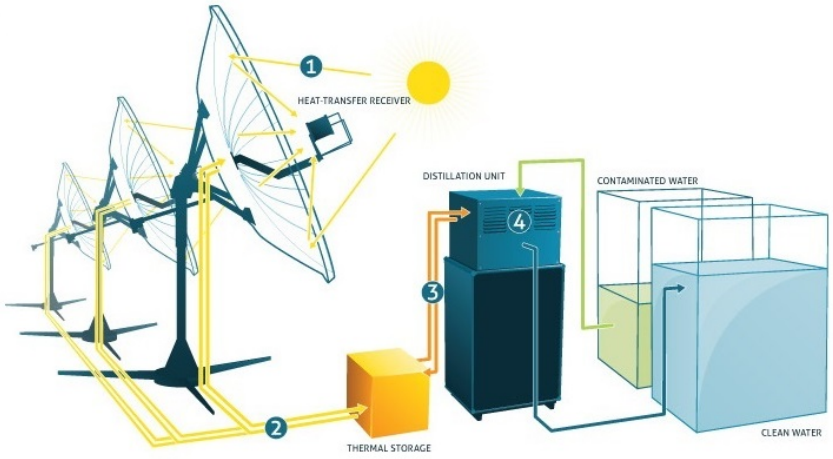

Figure 1: Epiphany's Water Purification Unit [1]

Deep-well injection is not a sustainable option either and has several negative aspects. As mentioned by Tofflemire and Brezner [5], there is always a chance that fresh water can be contaminated if these wells fail, long-term geological effects of deep-well injection are not well known, and it will be difficult to correct these negative effects if they become evident. Hauling the produced water to treatment facilities may not be the best economical option for companies, especially if these facilities are a great distance away from the natural gas well.

This research proposes to develop a solar power assisted distiller capable of processing the produced water from hydraulic fracturing. The distillation unit previously installed in the E3H was not designed to handle water containing high salt concentrations, which is in the range

of 10-15% of the mass of produced water from hydraulic fracturing. Therefore, a new distillation unit must be designed in order to provide an acceptable solution for the treatment of the produced water.

A 1st generation design was developed by Epiphany before this research was conducted. The 1st generation design had many characteristics of a typical mechanical vapor-compression (MVC) distiller, but several modifications were needed so the distiller could handle the high salt concentrations of the produced water. The goal for the 1st generation design was to produce fresh water at a rate of 20 gal/hr, and have an energy consumption of less than 0.5 kWh/gal. This energy consumption included the energy provided by concentrated solar power, and electricity consumed by the compressor and recirculation pump. The physical model of the 1st generation design was able to meet the design criteria, but it was not able to maintain that level of performance for extended periods of time. This research seeks to improve upon the 1st generation design in terms of performance, reliability, durability, and cost. A theoretical model has been presented, but a physical model will need to be constructed in order to validate it. The 2nd generation design provides system arrangements for preventing pump cavitation, describes the optimum amount of insulation to be utilized, requires less power consumption for the same flow rate of purified water as the 1st generation design, and the manufacturing cost of the entire unit will be lower.

Chapter 2: Literature Review and Technical Problems

2.1 Desalination Processes

The two main categories of desalination processes are membrane and thermal processes. A membrane process involves passing water through a barrier (a membrane) in order to remove certain substances. Thermal processes produce pure water by bringing a saltwater solution to its saturation temperature, further heated to form water vapor, which can be condensed and collected as clean, salt-free liquid water.

2.1.1 Reverse Osmosis

There are numerous membrane processes, including nanofiltration, electrodialysis, and forward osmosis (FO), and reverse osmosis (RO). Among these, RO is the popular membrane process, which accounts for 44% of worldwide purified water production [6]. The RO process is illustrated in Figure 2 [7]. A pressure is applied to the input water which is greater than its osmotic pressure, and the water is forced to flow through a semipermeable membrane. The osmotic pressure of seawater is approximately 30 bar, and a pressure of 40-70 bar is usually applied [8]. The pressure applied is related to the salt concentration of the input water. RO is effective at removing salts from solutions which have salt concentrations up to 45,000 mg/L. The recovery rate of RO is the volume of clean water obtained divided by the volume of feedwater processed. The recovery rate for RO processes ranges from 30 to 85% [6, 9].

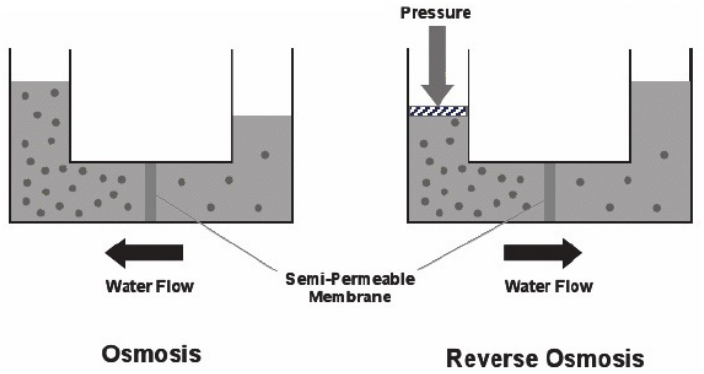

Figure 2: Concept of Reverse Osmosis [7]

2.1.2 Thermal Distillation

During thermal distillation, the input feedwater is heated to its saturation temperature and vaporized, which separates pure water from the brine. The water vapor is then condensed and collected from the system. The three most popular thermal distillation processes in terms of worldwide desalination are multistage flash (MSF), multiple effect distillation (MED), and MVC.

Single Effect Distillation

One of the simplest forms of distillation is a unit which consists of only one effect (evaporation column), as shown in Figure 3 [10]. Input feedwater is injected into the evaporator where it is heated to its saturation temperature. The heat source in Figure 3 [10] is a steam loop connected to a boiler. The water vapor generated in the evaporator is sent to a cooling tank, where a cool water loop causes the vapor to condense. The condensed water is collected in a storage tank. It is important to note that the latent heat of condensation is not recovered during this process as it is transferred to a separate cooling water loop.

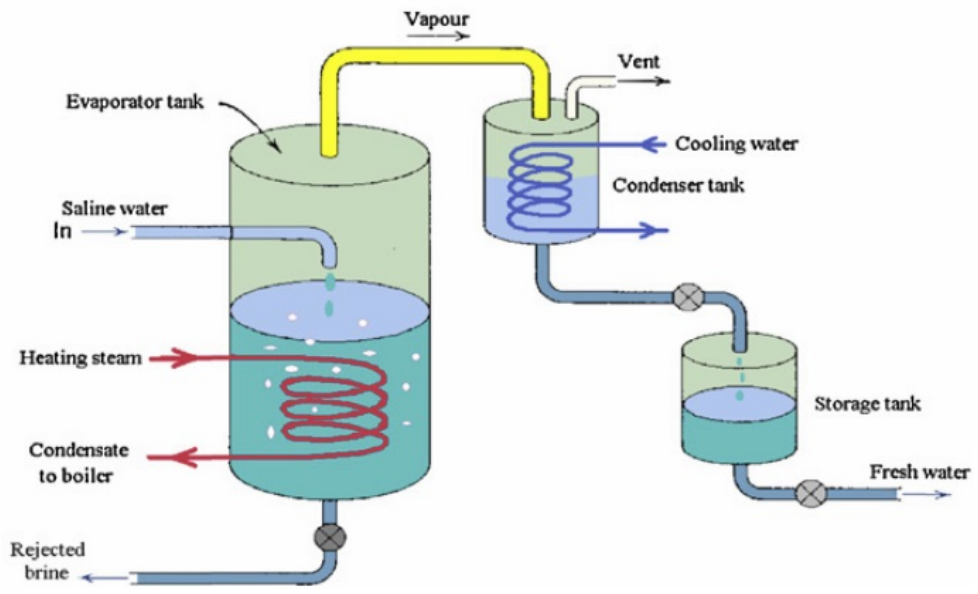

Figure 3: Schematic of a Single Effect Distiller [10]

Single effect distillation is generally utilized where compact size of a unit is required, and where heating steam is abundant and cheap [10]. However, these distillers produce less fresh water compared to MED, and a greater amount of heating steam is needed per unit volume of fresh water production compared to MED and MVC [11].

Multistage Flash Distillation

The boiling temperature of water decreases as pressure decreases. Vaporization of water due to decreased pressure is termed “flashing”. A schematic of a typical MSF distillation unit is shown in Figure 4 [12]. In MSF distillation, the pressure of the second stage is less than that of the first stage. The pressure of the third stage is lower than that of the second stage. This pattern continues until the last stage of the unit. Pipes containing input feedwater are passed through each effect to preheat the feedwater. The feedwater passes through a heat exchanger and recovers

energy from steam produced in a boiler. Vaporization occurs when the feedwater is released into the effects.

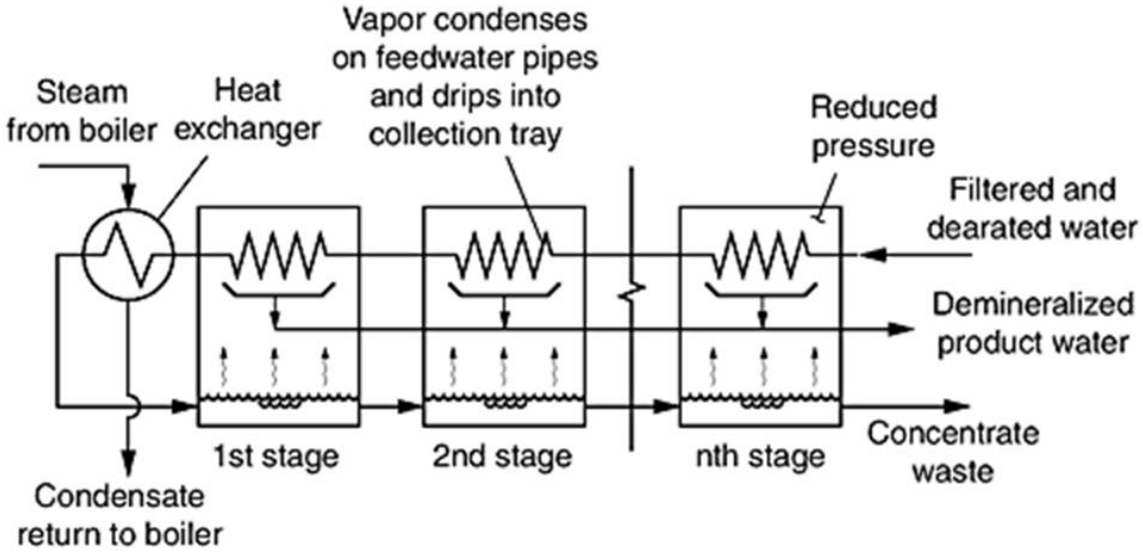

Figure 4: MSF Schematic [12]

Multiple Effect Distillation

MED is similar to MSF in that it utilizes a series of low-pressure effects. However, in MED, input water is sprayed onto pipes containing water vaporized in the effects. This helps to condense the vapor in the pipes and causes the sprayed water to vaporize [13]. Figure 5 [12] is a schematic of a typical MED unit. Steam from a boiler is used as the initial heat source to vaporize the input water. This steam is usually supplied at 790 to 1130 kPa [11]. After the first effect, vapor produced in the previous effect is used to heat and vaporize input water in the next effect. Water which does not vaporize (and contains salts) in each effect in sent to a concentrate waste location. The concentrate waste can be recirculated back through the distiller in order to create more product water.

The efficiency of MED is increased when more effects are added to the system. This reduces the amount of input steam required. MED units typically contain anywhere from three to sixteen effects [7, 11]. However, as the number of effects increases, the initial cost of the system increases. MED has a range of recovery of about 20 to 35% when seawater is used as the input water. The operating cost of a MED unit is usually less than that of a MSF unit because of reduced energy consumption due to vapor from previous effects heating input water in later effects [7]. This concept is similar to regeneration in steam engines for power plants.

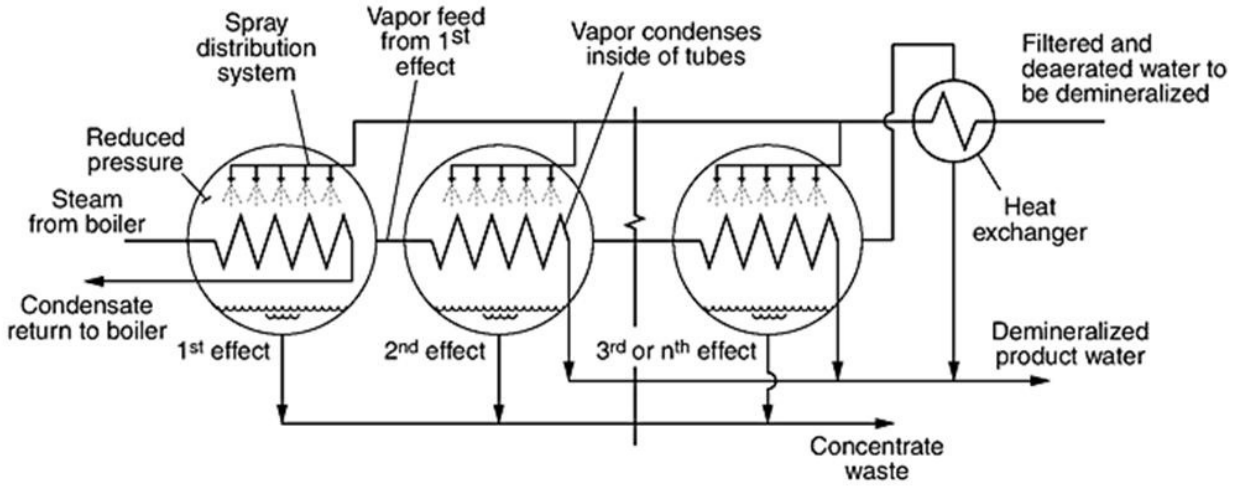

Figure 5: MED Schematic [12]

Mechanical Vapor Compression

MVC is a process in which steam generated in the evaporator is compressed to raise its temperature. Figure 6 [12] shows a schematic diagram of a basic MVC distiller. Initial heating from another source is needed to start the evaporation process. Input feedwater passes through a series of heat exchangers before reaching an evaporator. The input water then comes into contact with pipes containing pressurized, superheated steam and vaporizes. Water which does not

vaporize can be recirculated through the system or sent to a concentrate waste collection container. The compressed vapor condenses as it gives energy to the input feedwater in a heat exchanger. MVC distillers usually have a range of recovery between 40 to 50% for seawater desalination [7]. As reported by Ettouney et al. [14], the MVC process is considered to be the most attractive single-stage distillation method as it is compact, suitable for remote and low population areas, and recovers a significant amount of energy through the condensation of fresh water vapor within the system . MVC distillers with one effect are as beneficial as a MED unit with 15-20 effects [10].

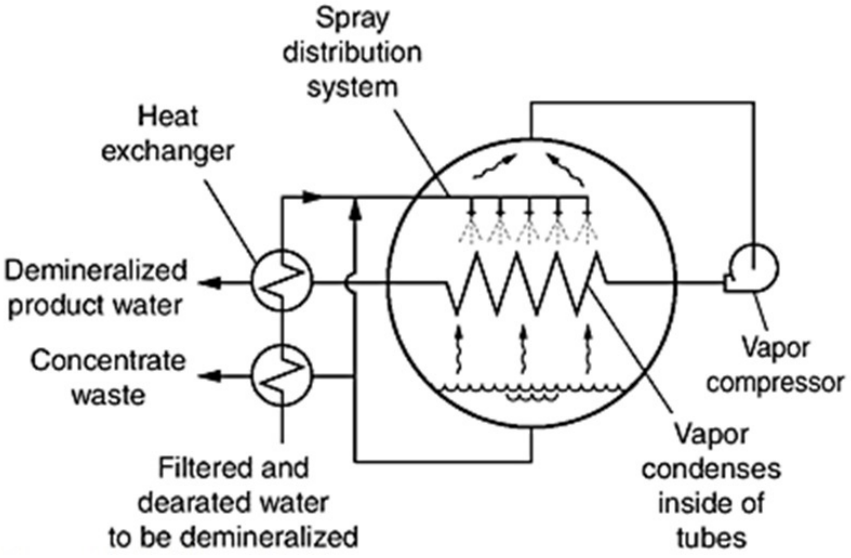

Figure 6: MVC Schematic [12]

Solar Distillation

Solar distillation is a process in which solar energy is collected and utilized to produce purified water from a reservoir of saline water. Figure 7 [15] shows a schematic of a typical solar still. The basin liner is usually painted black in order to absorb as much solar radiation as possible. When the water from the reservoir evaporates, it will gather on the sloped glass cover.

The evaporated water will condense on the glass and trickle down into a trough, where it is collected as distillate. This technique has several advantages over other distillation methods, such as the still is easy to construct, it has no moving parts, and only renewable forms of energy are required for its operation. However, with a distillate production rate of approximately 0.88 kg m^{-2} day^{-1}, this technique will not produce enough water to meet the design goal of this document. Active solar stills add components to passive solar stills (Figure 7 [15] is an example of a passive solar still) which serve to increase the distillate production rate. Some examples of these components are parabolic concentrators, heat pipes, and heat exchangers. Even with these modifications, active solar stills will only produce about 3 to 4.5 kg m^{-2} day^{-1} [15].

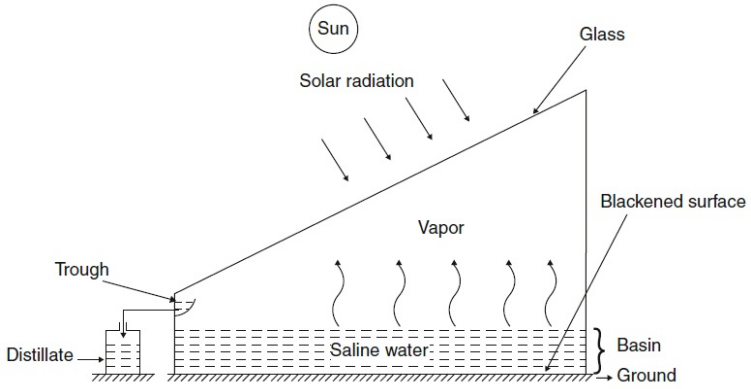

Figure 7: Solar Still System Schematic Diagram [15]

2.2 Additional Distiller Components

A variety of components have been developed to improve upon the performance of desalination units. One of these components is demisters, devices which remove entrained water droplets from vapor. Demisting pads are knitted meshes which can remove droplets as small as 1μm from vapor. These pads are available in a wide range of materials, thicknesses, and densities [16]. Another approach which can be utilized to remove water from vapor is placing a

baffle in the flow. A baffle forces the vapor to rapidly change directions, and water droplets are thrown against a solid wall by centrifugal force. The droplets then run into a lower liquid section of the vessel [17].

The majority of process steam is superheated. Superheated vapor is not as efficient at transferring heat as saturated vapor. The most common method for desuperheating steam is to introduce finely atomized cooling water into the flow, which brings the temperature of the steam closer to that of the saturation temperature. This process is shown in Figure 8 [18]. Another approach is to use a venturi desuperheater, but these units tend to be more expensive and produce greater pressure drops than mechanical atomizing units [19].

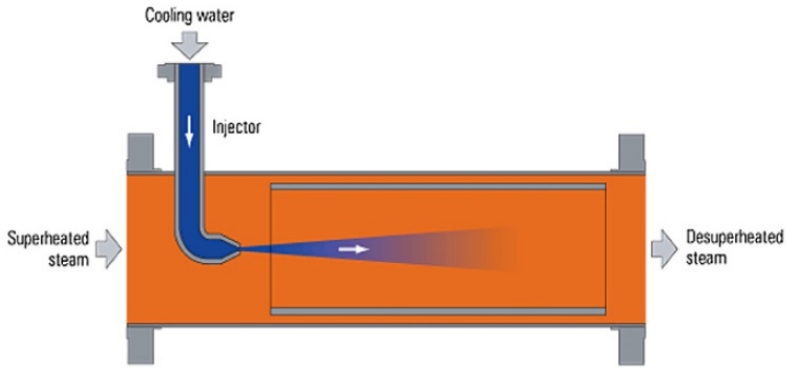

Figure 8: Typical Desuperheater [18]

Other components include trays, nozzles, and vacuum pumps. Trays may be placed inside the evaporator to add more surface area for evaporation. Nozzles may increase the rate of evaporation by finely atomizing water droplets. Vacuum pumps may be installed on the evaporator to remove non-condensable gases from the generated steam. These pumps also create a vacuum within the evaporator, which lowers the saturation temperature of water, and increases the rate of evaporation.

2.3 Measurement of Desalination Energy Consumption

Certain relationships have been established in order to compare desalination technologies to each other. Semiat [20] described several of these relationships, including energy consumption per amount of water produced, "gained output ratio" (GOR), and the Carnot efficiency. Energy consumption per amount of water produced usually has units of kWh/m^3. GOR is described as being "number of times the heat of evaporation is reused" and is defined as the ratio of the mass of water produced to the mass of steam utilized in the process [20]. The Carnot efficiency, as with all other engineering systems, is the ratio of the minimum theoretical work required to the actual work invested. A more detailed explanation of the Carnot efficiency applied to desalination systems is presented in a later section in this document. Values for energy consumption vary greatly depending on the technology utilized. MSF plants typically produce clean water at an energy consumption of 55-80 kWh/m^3 or a GOR of 8-12, whereas MED plants have a typical energy consumption of 40-60 kWh/m^3 or a GOR of 10-16 [20].

2.4 Selection of Distillation Method

The design of the distiller for this research will incorporate many MVC technology and process aspects. It has been recognized as an excellent solution for small-scale applications, and is considered to be the most efficient thermal distillation process. Some design modifications to the typical MVC schematic will be needed in order to handle the relatively high salt concentrations of produced water from hydraulic fracturing. Membrane processes were not considered because the high salt concentration will diminish the performance of the membranes.

2.5 MVC Case Studies

Veza [21] presented an investigation of the Las Palmas Port Authority Desalination Plant in the Canary Islands (an autonomous community of Spain off the coast of northwest Africa) which had two VC units. Each unit was able to produce purified water at a rate of 500m^3/day. A schematic diagram of these VC units is shown in Figure 9 [21].

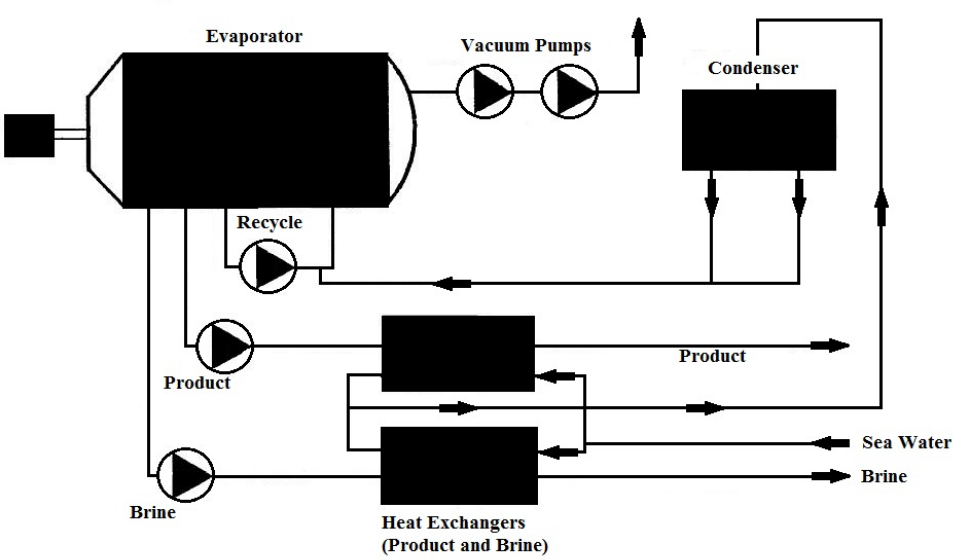

Figure 9: Schematic of the MVC Units Analyzed by Veza [21]

The compressors had an efficiency of approximately 58.9%, and the plant had an energy consumption of 10.4-11.2 kWh/m^3. The product water had a conductivity which was consistently below 20 µS/cm. The tubes of the evaporator-condenser units were 5.13 m long with a total surface area of 2598 m^2, and the vessels were 4 m in diameter. The operating temperature of the evaporator-condenser units was 59°C. This low temperature was utilized to reduce scaling in the components and heat loss from the system to the ambient air. The compressors produced a vacuum in the evaporator, and the vapor passed through a demister mesh before reaching the

compressor. The compressors were radial centrifuge types with aluminum rotors and titanium blades. Vacuum pumps removed non-condensable gases from the systems.

Aly and El-Fiqi [22] presented an investigation of a small-scale VC unit in the heat transfer laboratory of the Atomic Energy Authority of Egypt. The unit had a capacity of 5 m^3/day, and the evaporator was designed to operate at 70°C. The condenser containing the produced steam was located within the evaporator, and the inside of the evaporator was a horizontal spray film design. The experimental and theoretical results showed the production rate increased with an increase in the operating temperature from 70°C to 98°C. The authors claimed that VC distillation was generally used for small to medium-scale purposes. The operating temperature was chosen in order to minimize both scale and the requirement for thermal isolation. Feed water was preheated in two plate-type heat exchangers. Electrical immersion heaters were utilized to generate the initial and make-up steam. The usage of the heaters depended on the temperature of the feed water and the compressor load. A centrifugal-type compressor was turned on after a sufficient amount of steam has been generated. The compressor created a vacuum within the evaporator as it drew vapor through mesh separators. The conductivity of the product water was usually below 15 μs/cm. A vacuum pump was utilized to create a vacuum in the evaporator before the compressor was turned on and it removed non-condensable gases. The evaporator had a glass observation window for viewing the interior of the evaporator shell, as well as liquid level glasses, drains, a vent, and safety valves.

Bahar et al. [23] presented an analysis of a VC distiller which had a rated capacity of 1 m^3/day. The distiller had two stages, i.e. two vertical evaporator-condenser units. VC systems with multiple effects have been shown to increase the performance ratio (the authors define this as the mass of distillate produce in kilograms divided by 2326 kJ of heat input), decrease the

power consumption, and better utilize heating sources. An experiment was conducted to observe the effects of increasing the brine recirculation rate and the compressor speed. The salt concentration of the brine had different values ranging from 20,000 ppm to 33,000 ppm. The temperature of the brine in the first and second effect was 103°C and 101°C, respectively. The temperature of the heating steam for the first and second effect ranged from 103°C-110°C and 101°C-102°C, respectively. The compressor was a rotary-lobe type, had a capacity of 42 m^3/hr, and a maximum compression ratio of 2.2. The power input for the compressor ranged from 0.59 kW to 1.75 kW. It was found that increasing the concentration of the input water had a negative effect on the production rate at each recirculation rate tested. However, increasing the recirculation rate increased the production rate since more latent heat was absorbed. The flow rate of product water increased linearly with increasing compressor speed. Figure 10 [23] shows of schematic of this distiller.

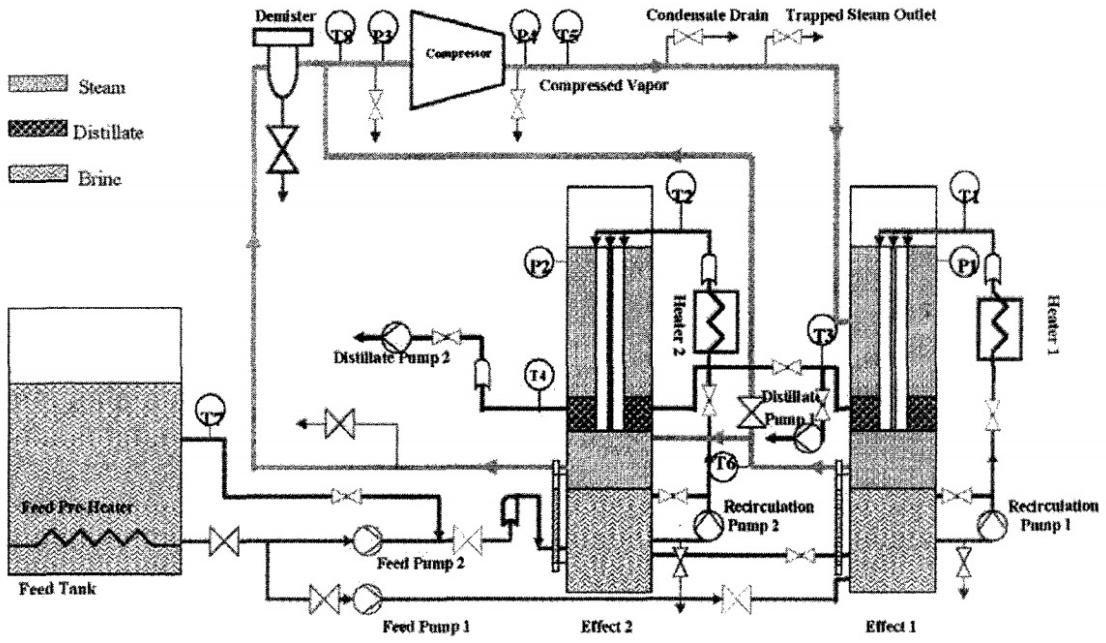

Figure 10: Schematic of the MVC Unit Analyzed by Bahar et al. [23]

2.6 Temperature-Entropy Diagram

Figure 11 [24] is a T-S diagram of a typical VC process. The feed water enters the system at point A. It is then heated to its boiling point B at pressure P_1, usually in a heat exchanger with the condensate as the hot fluid. The feed water is then vaporized by a constant temperature and pressure process within the evaporator to point C. A compressor then compresses the vapor to a greater pressure P_2 at point D, so the water is now a superheated vapor. The compressed vapor is condensed along the line D-E-F, and it transfers its latent heat of vaporization to the cross-hatched area. The thermodynamic advantage of the VC process is the ratio of the area bounded by BCDEF (the compressor work region) to the cross-hatched area. The condensate is subcooled in another heat exchanger with the feed water acting as the coolant. From this diagram, one can find that the lower the value of ΔT, the higher the thermodynamic advantage will be due to lower energy consumption from the compressor. However, the required surface area within the evaporator to carry out the process is increased, raising the capital cost [24].

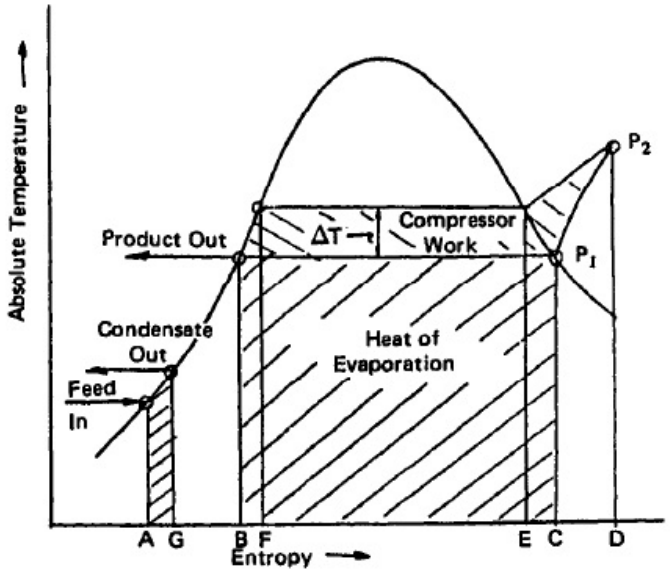

Figure 11: Temperature-Entropy Diagram of a General VC Process [24]

2.7 Scaling

The deposition of solids from water to pipes is referred to as scaling. Water containing relatively high total dissolved solids (TDS) levels usually has more severe and varied scale problems compared to fresh water [25]. Due to the scope of this research, scaling must be taken into serious consideration. As described by Cowan and Weintritt [25], scaling leads to many problems, such as reduced area for flow through a pipe, reduction of heat transfer through the wall of the pipe, and corrosion attacks. Scaling can lead to greater costs due to inefficiencies, downtime and maintenance, and increased safety hazards.

Three factors must be present at the same time in order for scale deposition to occur: supersaturation, nucleation, and an adequate amount of contact time [25, 26]. Figure 12 [25] shows a flowchart of the scale deposition process. It shows some of the important controlling parameters for each stage of scale deposition. Supersaturation occurs when a solution contains more solvent than the equilibrium concentration. Cowan and Weintritt [25] describe supersaturation as being the primary cause of scaling, and list the following ways to supersaturate a solution: temperature fluctuation, pH alteration, addition of solid seeding material, commingling of two incompatible waters and pressure reduction (common in gas/oil production), agitation, evaporation or concentration, etc. Gooch [27] defines nucleation as “the formation of short range ordered polymer aggregates in a melt or solution, which acts as growth centers for crystallization.” Nucleation occurs faster at higher levels of supersaturation.

Prevention of scaling requires at least one of these three factors to be removed. Since contact time is not a factor which can be changed in this project, either supersaturation or nucleation must be considered [26]. Since evaporation is recognized as one of the causes of supersaturation, the water through the recirculation loop should be kept as a condensed liquid

until it reaches the evaporator. Though there are a variety of other factors affecting supersaturation as previously described, having a set location where the water will evaporate is one method for reducing the degree of supersaturation throughout the system. The highest amount of scaling will most likely be located in the evaporator. Cleaning the evaporator of scale will be less difficult than removing scale from the pipes and heat exchangers comprising the recirculation loop.

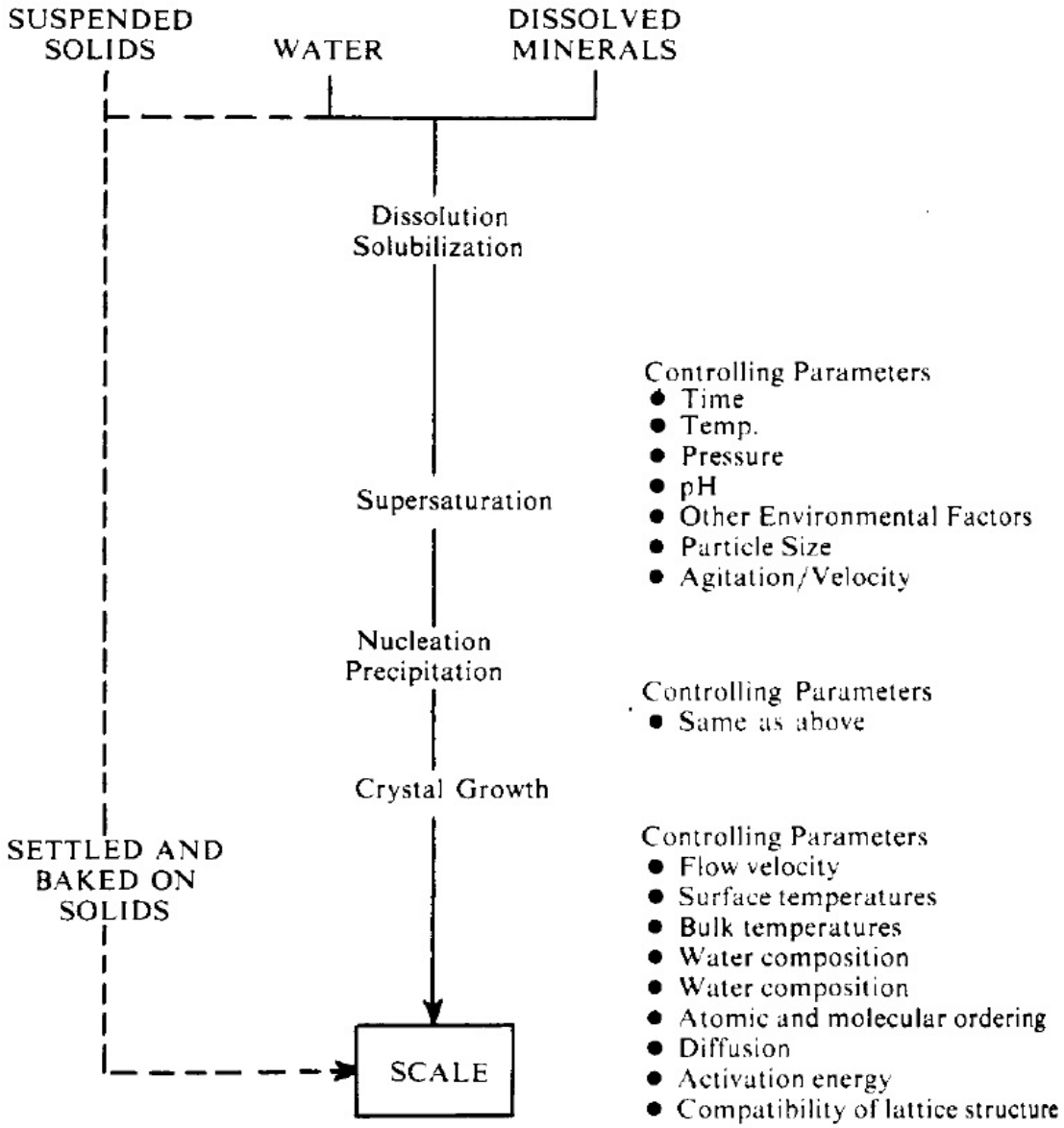

Figure 12: Scale Deposition Flow Chart [25]

2.8 Solubility

Solubility is defined as the maximum amount of solute which can be dissolved in a solvent. Table 1 [28] shows the solubility of salt (NaCl) in water as a function of temperature [28]. The table shows the solubility increases with temperature, which means this is an endothermic process.

Table 1: Mass of Salt in a Saturated Solution with 100 grams of Water [28]

Temperature (°C)	0	10	20	30	40	60	80	90	100
Mass of Salt (grams)	35.7	35.8	35.9	36.1	36.4	37.1	38	38.5	39.2

2.9 Total Dissolved Solids and Salinity

Total dissolved solids (TDS) is the concentration of salts in water measured in part per million (ppm). Another popular value describing salt concentrations is salinity, which is usually given as grams of salt per kilogram of seawater. Seawater has a salinity of approximately 35 g/kg (or TDS = 35,000 ppm) [29].

During operation, the salt concentration within the recirculation loop will continually increase, or scale will form in the evaporator. This is due to the fact that salt will not leave the system until it is removed during downtime.

2.10 Pump Cavitation

Cavitation is a phenomenon caused by the formation of vapor bubbles in localized low pressure regions below the saturation pressure of the fluid at a given temperature. When these vapor bubbles are later exposed to a pressure increase, they collapse and cause negative effects

on pump performance [30]. An important parameter in preventing cavitation is known as the net positive suction head (NPSH). NPSH is the total energy (from pressure and velocity) above the vapor pressure of the liquid at the pump inlet [30]. The net positive suction head available (NPSHA) and the net positive suction head required (NPSHR) are variables utilized by pump manufacturers to designate how a pump should be placed and/or operated in order to prevent cavitation. Measures should be taken to ensure that the NPSHA is always greater than or equal to the NPSHR. The NPSHR can be reduced by making a variety of design modifications. For example, pump manufactures may offer devices known as inducers and other impellers for certain pumps, both of which are intended to lower the NPSHR. Larger pumps operated at lower speeds can lower the NPSHR [31].

The NPSHA can be calculated by using the equation shown below [31]. It is important to note that each term must be expressed in feet of head. Each variable in the equation is described in Table 2. A visual aid depicting how these variables affect cavitation is shown in Figure 13 [31].

For the design of the distiller, increasing the vertical distance between the liquid level and the pump may be the simplest solution for preventing cavitation. The pump was already placed below the liquid level in the 1st generation design, but this distance may not have been adequate as far as the NPSHA value is concerned. Also, it may be necessary to install a vacuum breaker on the evaporator to ensure that there is never a negative gauge pressure within the evaporator if cavitation continues to be a problem.

$$\mathrm{NPSHA} = h_{atm} + h_p + h_{el} - h_f - h_{vp} \qquad \textbf{Equation 1}$$

Table 2: NPSHA Energy Terms

Variable	Pressure	Description
h_{atm}	Atmospheric pressure	This value is always positive
h_p	Gauge pressure	The value is negative for a vacuum, zero for an open tank, and positive for a positive pressure
h_{el}	Static liquid level height	The value is negative if the pump is above the liquid level, and positive it is below the liquid level
h_f	Friction losses	This value is always negative
h_{vp}	Vapor pressure of the pumped fluid	This value is always negative

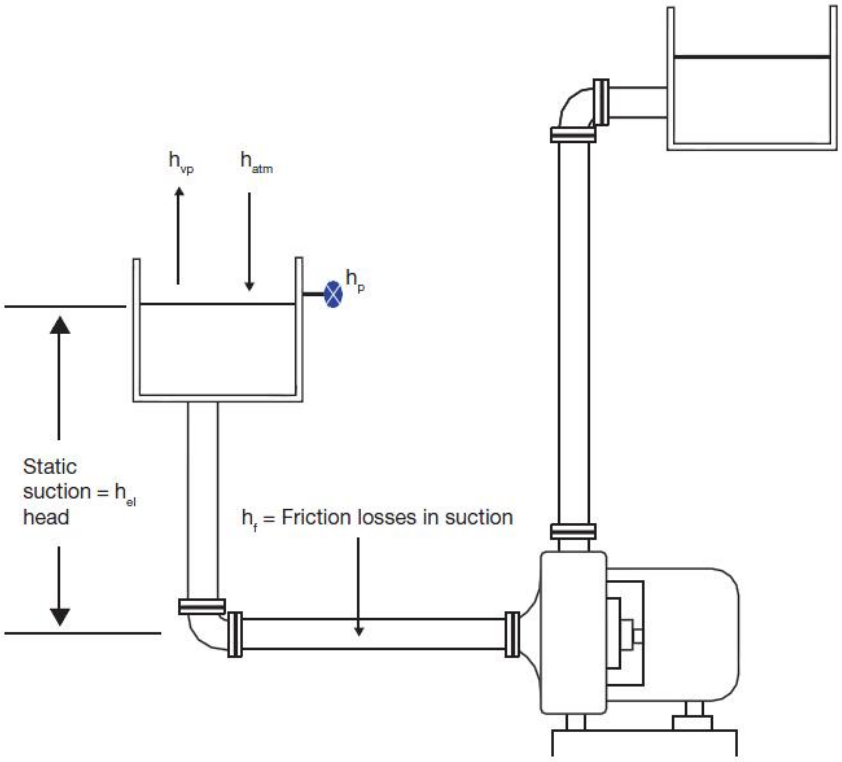

Figure 13: Energy in a Pumping System [31]

2.11 Non-Condensable Gases in the Product Steam

The condensation heat transfer coefficient is significantly reduced if non-condensable gases such as air are present along with steam [32]. This will increase the surface area needed in the condenser. An estimate of the percent reduction of the heat transfer coefficient is shown in Figure 14 [33]. The variable α_0 is the heat transfer coefficient of pure steam, and α_{GS} is the heat transfer coefficient of gassy steam. As shown in Figure 14 [33], an air weight percentage of only 1% in the steam-air mixture can reduce the heat transfer coefficient by more than half the value of pure steam. It is therefore critical that the evaporator be completely sealed in order to prevent air from being drawn in by the compressor.

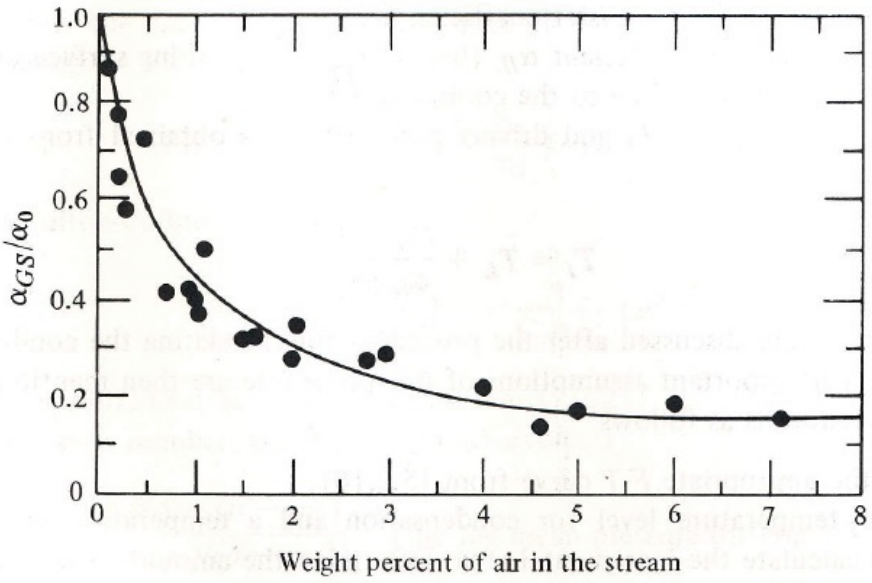

Figure 14: Effect of Air on Condensation Heat Transfer [33]

Chapter 3: In-House Testing and Field Results of the 1st Generation Design

This chapter introduces the 1st generation design of a MVC distillation unit which can separate pure water from the chemicals found in produced water from hydraulic fracturing. This concept has validated as both in-house and field testing yielded positive results. However, this design will need to be improved in certain areas in order to provide satisfactory results continuously.

3.1 In-House Testing

A schematic of Epiphany's 1st generation MVC distiller is shown in Figure 15. The solar collectors were only present in field tests, and were simulated by electric heaters during in-house testing. In-house testing was conducted at the Epiphany headquarters in Lawrenceville, Pennsylvania. Figure 16 is a picture of the testing arrangements, including instrumentation monitored by LabVIEW™. Two tests were performed, both utilizing different types of water as the input fluid. The first test involved river water, and the second test involved brine with a salt concentration of 100,000 ppm. The water for the second test was prepared by dissolving rock salt into fresh water.

The heat input from the solar panels was simulated by modifying an air tank to act as a Therminol®66 reservoir. Electrical immersion heaters were used to provide heat, and the Therminol®66 was pumped from the tank to the distiller in a continuous loop by a small gear pump.

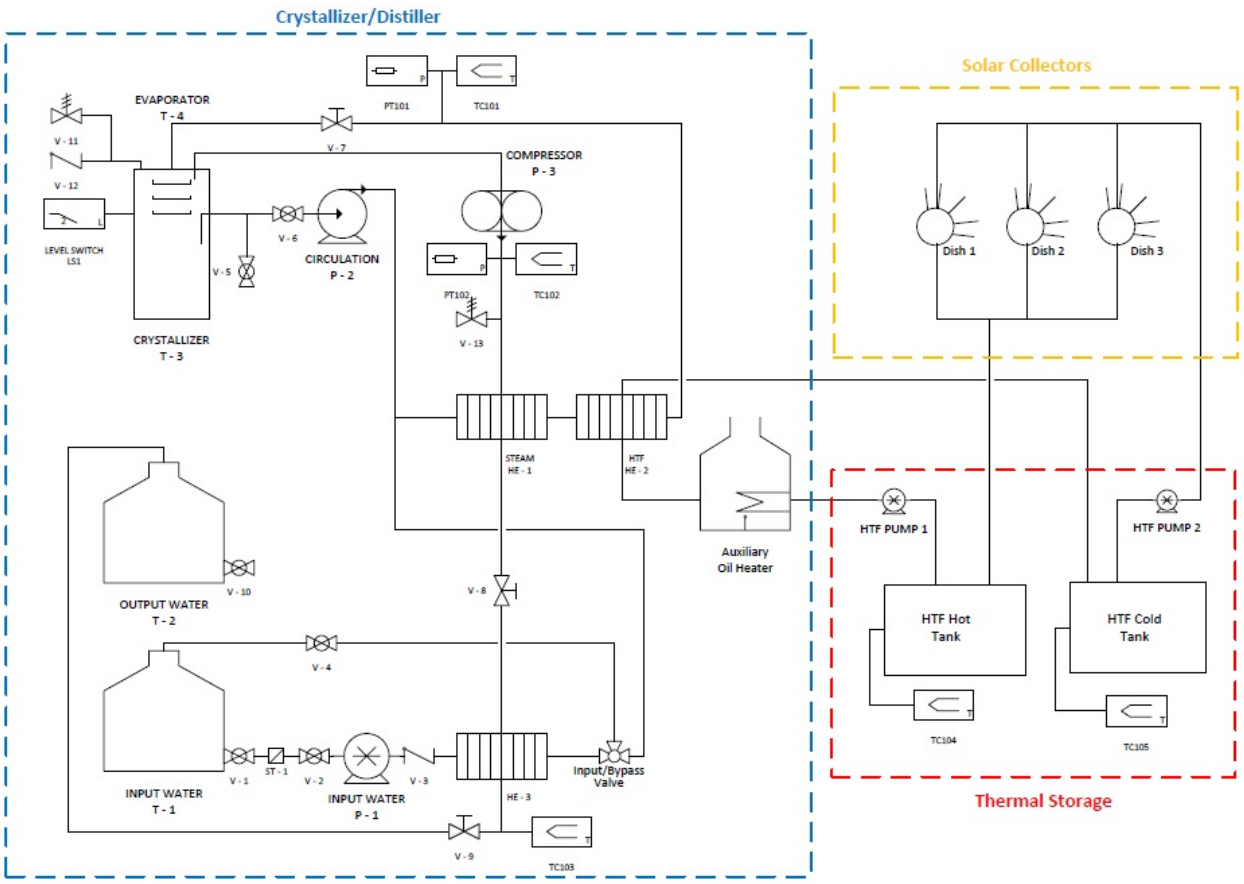

Figure 15: Schematic of Epiphany's 1st Generation MVC Distiller

Figure 16: In-House Testing Arrangements

Table 3 shows the results of the in-house testing. The brine test was split into two different tests due to maintenance. The distillate flow rate ranged from 20-40 gal/hr, and the water purity was always less than 225 ppm TDS.

Figure 17 through Figure 25 are selected graphs of many of the important aspects of the distiller performance during the test involving river water. All graphs involving temperatures and pressures were directly measured by thermocouples and pressure transducers, respectively. Graphs involving flow rates and heat transfer were calculated based on the measured temperature differences across heat exchangers.

Table 3: In-House Testing Results

	River Water Test	Brine Test 1	Brine Test 2
Date	6-Aug	8-Jun	21-Jun
Operating Hours	10:00	3:45	12:00
Volume of Water Fed (gal)	275	175	310
Volume of Distillate Produced (gal)	200	100	300
TDS of Distillate (mg/L)	20	225	200
Mass of Crystallizer Byproduct Disposed (lb)	-	50	300
Electrical Energy Input Compressor (kWh)	62.00	26.00	74.00
Electrical Energy Input Heaters (kWh)	70.00	30.00	80.00
Electrical Energy Controls (kWh)	7.50	3.00	9.00
Total Energy Input (kWh)	139.50	59.00	163.00
Efficiency (kWh/gal)	0.51	0.34	0.53
Generator % of total	44%	44%	45%

Figure 17 shows the volumetric flow rate of the recirculation loop, which, according to Figure 15, starts in the crystallizer, goes through Heat Exchangers 1 and 2, and ends back in the crystallizer again. The curve of the graph is erratic, which cannot occur in future modifications of the system if predictable results are desired.

Figure 18 shows the temperature at three different locations along the recirculation loop. The graph shows that the majority of the heat transfer to the recirculation loop occurs within Heat Exchanger 1, which explains the large temperature difference between “Recirc Post Pump” and “Recirc Pre-Auxiliary Heat.” The recirculation loop then receives more heat from the Therminol®66 loop within Heat Exchanger 2, and enters the evaporator at a temperature shown

by “Recirc to Crystallizer.” The recirculation loop receives more heat from Heat Exchanger 1 than Heat Exchanger 2 because it absorbs the latent heat of condensation from the output water path at this point.

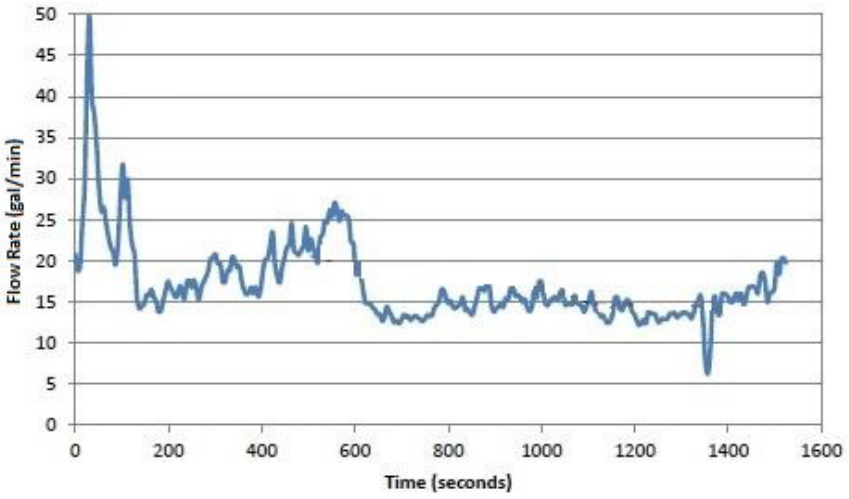

Figure 17: Recirculation Loop Volumetric Flow Rate

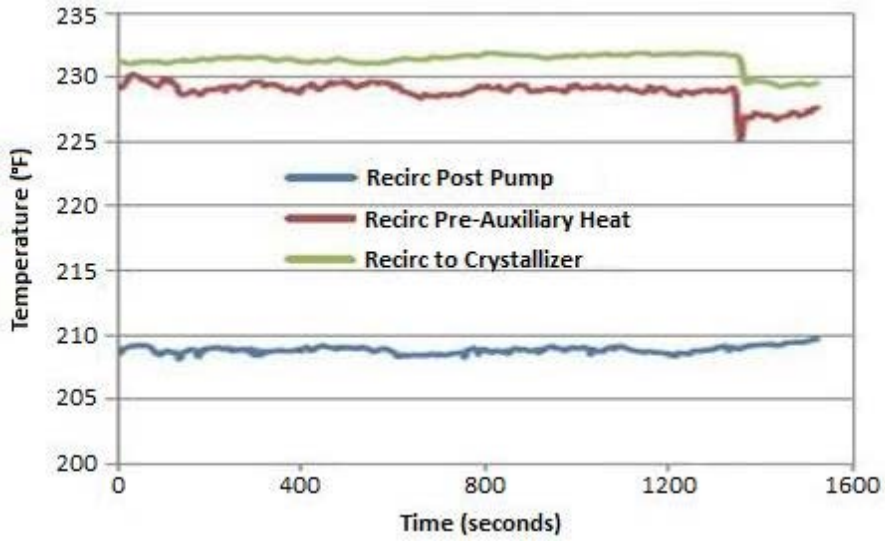

Figure 18: Recirculation Loop Temperatures

Figure 19 shows the pressure at the outlet of the steam compressor. The pressure is fairly consistent in the graph, but it was known that air was present in the flow, which has been shown

to significantly reduce the convection coefficient of steam. Future modifications to the distiller must therefore be made to ensure that no air can enter the distiller.

Figure 20 shows the rate of heat transfer calculated by utilizing the known temperatures of the recirculation loop and its calculated volumetric flow. The curve of Figure 20 varies in the same manner as Figure 17 for this reason.

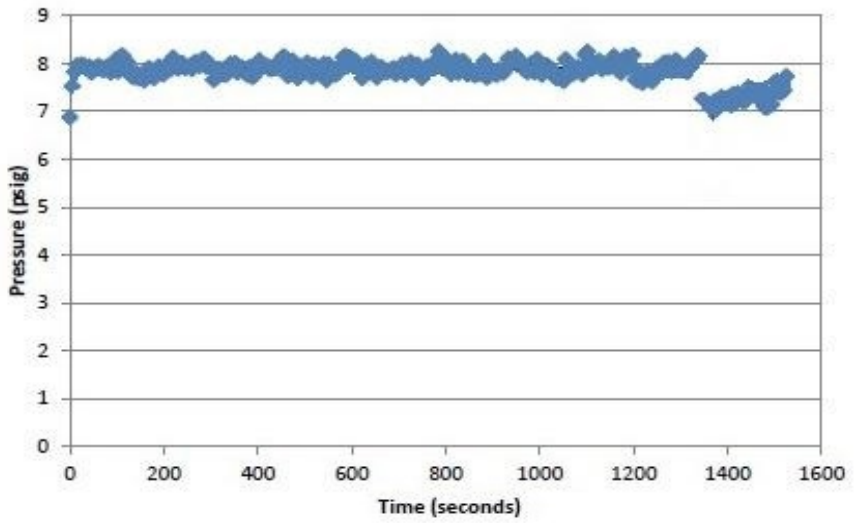

Figure 19: Compressed Steam Pressure

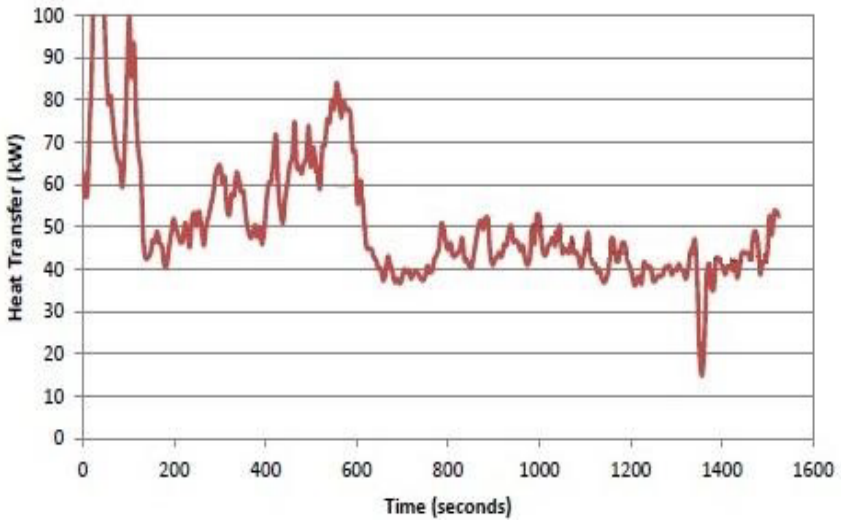

Figure 20: Heat Transfer from the Steam Path to the Recirculation Loop

Figure 21 shows the inlet and outlet temperatures of the input water. Figure 22 was constructed by using this temperature data along with a known mass flow rate and specific heat of the input water to calculate the rate of heat transferred to the path in Heat Exchanger C.

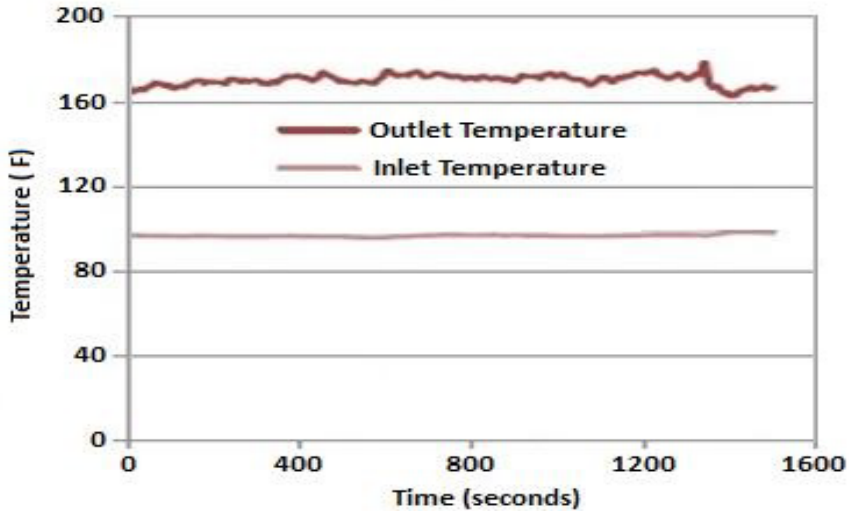

Figure 21: Input Water Temperatures at the Inlet and Outlet of Heat Exchanger 3

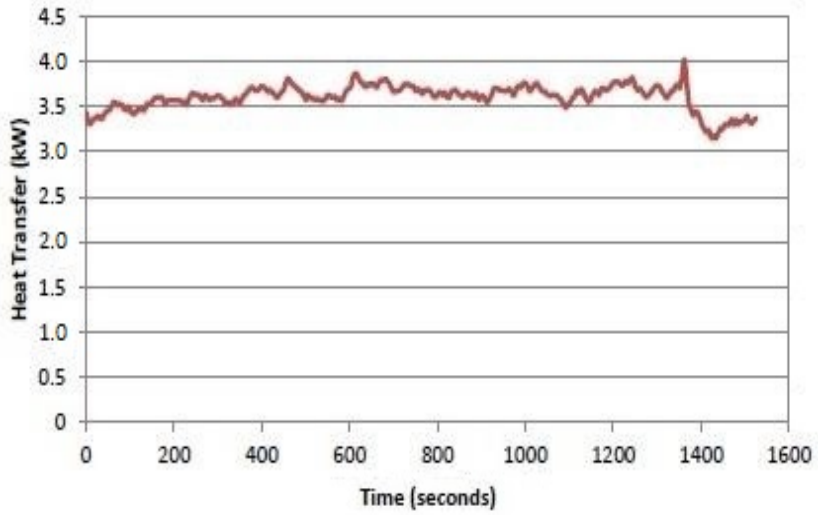

Figure 22: Heat Transfer from the Output Water Path to the Input Water Path

Figure 23 shows the temperature of the Therminol®66 at the inlet and outlet of Heat Exchanger 2. Figure 24 was constructed by using this temperature data, the value of a measured

mass flow rate of the fluid, and known specific heat based on temperature to calculate the rate of heat transfer. A 5.5 kW electric heater was utilized to provide heat to the Therminol®66 reservoir, so the calculated rate of heat transfer to the recirculation loop is in close agreement with the expected rate under the assumption that there is negligible heat loss to the environment.

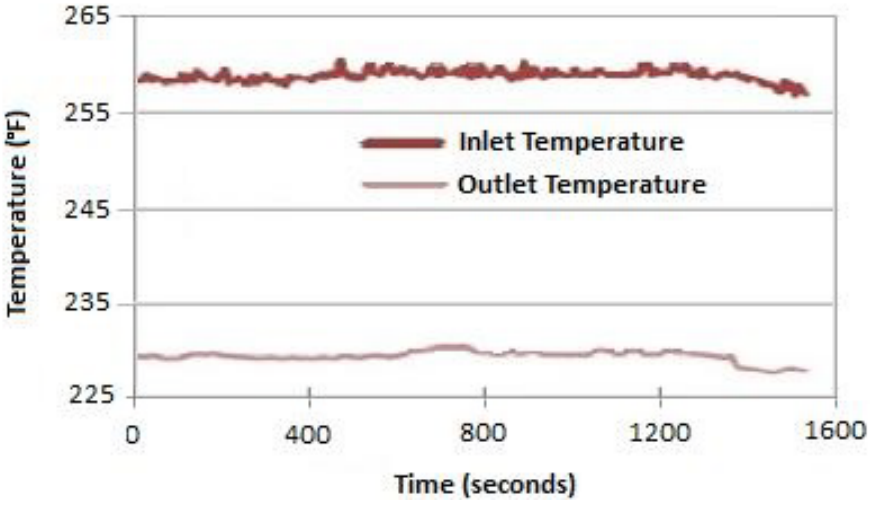

Figure 23: Therminol®66 Temperatures at the Inlet and Outlet of Heat Exchanger 2

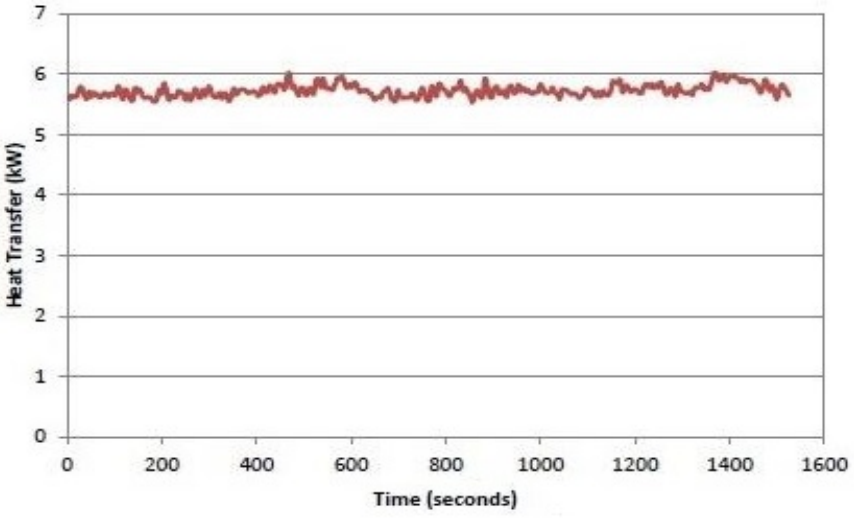

Figure 24: Heat Transfer from the Therminol®66 to the Recirculation Loop

Figure 25 shows the temperatures of the output water at the inlet and outlet of Heat Exchanger 1. The inlet temperature of Heat Exchanger 1 is the temperature of the steam at the outlet of the compressor. However, it should be noted that this fluid is not entirely steam, as some air was entrained in the flow as well due to leaks in the evaporator. The large temperature drop shows that Heat Exchanger 1 brings the water from the superheated steam phase to a saturated vapor. It was known that Heat Exchanger 1 was not always able to completely condense the steam, so other alternatives will need to be taken into consideration. These alternatives may be a de-superheater or a heat exchanger with more surface area.

The in-house testing confirmed that the 1st generation distiller can be steadily operated to separate fresh water from an aqueous NaCl solution and meet the design requirements.

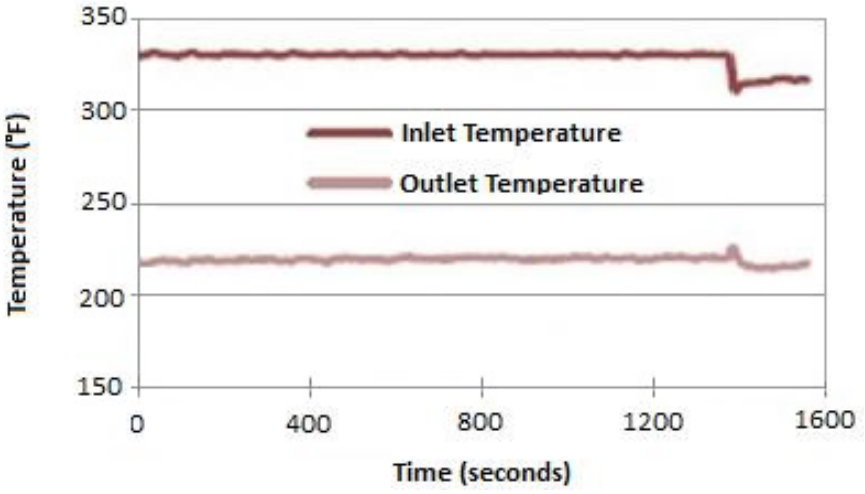

Figure 25: Output Water Temperatures at the Inlet and Outlet of Heat Exchanger 1

3.2 Field Demonstration

After the in-house testing was completed, field testing of the distillation unit was conducted at Consol's GH-10 well pad, located in Greene County, Pennsylvania. The left side of

Figure 26 shows the E3H unit at the GH-10, and the right side shows the inside of the container, which houses the distiller. An auxiliary propane heater was added to the distiller to simulate sunlight on cloudy days.

Samples of produced and distillate water, as well as precipitated salt during crystallizer cleanouts, were sampled on regular intervals. These samples were submitted to Consol's R&D laboratory for analysis. Figure 27 is a picture of some samples gathered from the GH-10 well pad distillation unit. The produced water contained about 180,000 ppm TDS of impurities, whereas the distillate had a purity of about 50 ppm TDS. The precipitated solids had a salt concentration of about 93%. Table 4 is an analysis of the water samples gathered from the GH-10 well pad. All parameters and substances tested for were found to be within an acceptable range.

Figure 26: Epiphany's E3H Unit and MKII Distiller at the GH-10 Well Pad

From the in-house and field testing results, it can be concluded that the 1st generation can distill produced water for the production of fresh water. It can also be a potential solution to the environmental concerns raised by produced water from hydraulic fracturing. The distiller was able to produce clean water at a performance level of less than 0.5 kWh/gal, so it met the design

goal. However, further modifications must be made in order to ensure that the distiller can reliably perform at this level consistently, or if a better performance level is desired.

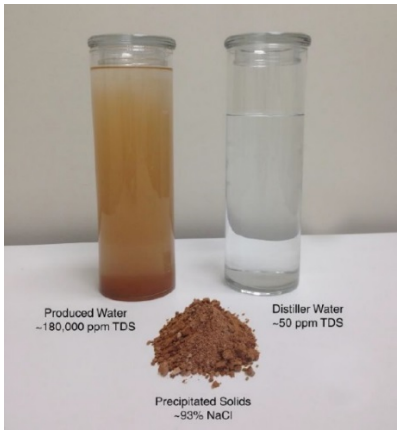

Figure 27: Water and Salt Samples from the GH-10 Well Pad

Table 4: GH-10 Water Sample Analysis

10/3/2013	Description	Pre Treatment	Post Treatment	Percent Reduction
s.u	pH	4.02	8.57	N/A
mg $CaCO_3$/L	Alkalinity, Total	0	42	N/A
mg/L	TSS	740	<6	99.19
	TDS	147100	78	99.95
Concentration (mg/L)	Al	2.33	0.22	90.56
	Ca	15330	1.43	99.99
	Fe	74.2	0.1	99.87
	Mg	1548	0.13	99.99
	Mn	13.4	0.1	99.25
	K	299	0.1	99.97
	Na	38370	2.83	99.99
	pH	2.03	0.2	90.15
	Si	3.08	0.65	78.90
	Total Sulfur as SO_4	<25	1.3	94.80
	Cl	91000	9	99.99
µg/L	Ba	1750	0.11	99.99
	Sr	2386	0.17	99.99

Chapter 4: 2nd Generation Design

The 2nd generation design improves upon several aspects of the 1st generation design. For example, cavitation was often observed after the water in the evaporator/crystallizer had reached its saturation temperature. Calculations have been performed to recognize the NPSHA and NPSHR for the 2nd generation distiller setup, which will help prevent cavitation. The 2nd generation design will also require less power input and components than the 1st generation design, which also lowers the cost.

4.1 Design Criteria of the Distiller

The performance of the distiller was evaluated by finding the energy consumed per volume of fresh water produced (kWh/gal). The significant contributions to the total energy input are the recirculation pump, the compressor, and the solar panels. The goal of this research is to design a distiller which can produce clean water at a rate of 20 gal/hr and have a performance of less than 0.5 kWh/gal. The total energy input must be limited to 10 kW in order to meet these goals. Table 5 gives the design parameters for the 2nd generation MVC design.

Table 5: 2nd Generation Design Criteria

Distilled Water Flow Rate (gal/hr)	20
Total Heat and Work Input (kW)	≤10
Performance (kWh/gal)	≤0.5

4.2 Removal of Salt from the System

Crystallization is the process of removing solid solutes (in the form of crystals) from a solution. If the salt is allowed to gather in the crystallizer, the salt particles may bind together, which is referred to as caking. Salt which has caked will not flow freely, and will require an external force to break the block of salt into a more manageable form [34].

Several approaches could be taken in order to remove the salt from the system, including pumping the saturated saltwater solution to a solar pond, manually removing the salt after an appreciable quantity of salt has gathered in the crystallizer, or installing an auger in the evaporator/crystallizer. During the in-house and field testing, the salt was manually removed from the evaporator/crystallizer once the system was stopped. This research recommends an auger system, which might be a better solution for the 2nd generation design, especially since it is desired that the system be completely automated. The auger can be placed at the bottom of the evaporator/crystallizer. Once the distillation unit has stopped running, a valve at the bottom of the evaporator/crystallizer will be opened, and the auger will force the majority of the salt out of the system.

4.3 Minimum Work Input to Obtain Fresh Water

Equation 2 through Equation 5 are from Çengel and Boles [35]. For Equation 2, the mass fraction of salt (mf_s) is determined simply by dividing the TDS value (in ppm) of the solution by one million. The mass fraction of water (mf_w) is determined by subtracting the mass fraction of salt from 1. Once these mass fraction values are obtained, the molar mass of the solution (M_m) can be calculated. For these calculations the value of M_s will be that of NaCl, which is 58.44 kg/kmol. The molar mass of water (M_w) is approximately 18 kg/kmol.

$$M_m = \frac{1}{\sum \frac{mf_i}{M_i}} = \frac{1}{\frac{mf_s}{M_s} + \frac{mf_w}{M_w}}$$ **Equation 2**

The molar fraction of water and salt can be found by using Equation 3 and Equation 4, respectively.

$$y_w = mf_w M_m / M_w$$ **Equation 3**

$$y_s = 1 - y_w$$ **Equation 4**

The following relationship for calculating the minimum work input required to separate 1 kg of fresh water from brackish water, which has been provided by Çengel and Boles [35]:

$$w_{min,in} = R_w T_0 \ln(1/y_w)$$ **Equation 5**

R_w is 0.4615 kJ/(kg K), T_0 is the temperature of the reservoir of brackish water in Kelvin, and $w_{min,in}$ has units of kJ/kg fresh water. This equation shows that as the TDS value increases, the minimum input required to separate 1 kg of fresh water from brackish water increases.

Table 6 shows sample calculations utilizing Equation 2 through Equation 5. When calculating the minimum work input, a T_0 value of 300 K was assumed. The maximum TDS value given in Table 6 is 70,000 ppm, which is twice the concentration expected in the input feed water. The table shows that the minimum work requirement increases as TDS levels increase.

Table 6: Composition and Minimum Work Requirements Based on TDS Values

TDS (ppm)	mf_s	mf_w	M_m (kg/kmol)	y_s	y_w	$w_{min, in}$ (kJ/kg fresh water)
0	0	1	18	0	1	0
25000	0.025	0.975	18.3	0.008	0.992	1.09
50000	0.05	0.95	18.6	0.016	0.984	2.23
75000	0.075	0.925	19.0	0.024	0.976	3.42
100000	0.1	0.9	19.3	0.033	0.967	4.66
125000	0.125	0.875	19.7	0.042	0.958	5.96
150000	0.15	0.85	20.1	0.052	0.948	7.33

4.4 Thermodynamic Properties of the Fluids Involved in this Research

Pure Water

Pure water will be present in the compressed steam path, and it will be condensed from a gas to a liquid. The properties of pure water as a saturated vapor and superheated steam must be considered. The properties of pure water have been well documented in the literature. The tabulated data presented by Çengel and Boles [35] will be utilized to approximate the thermodynamic property values at various temperatures and pressures.

Therminol®66

Therminol®66 will be utilized as the heat transfer fluid which is pumped through the PDRs and distillation unit. Equations for this fluid's thermodynamic properties as functions of temperature are given in Table 7 [36].

Table 7: Therminol®66 Thermodynamic Property Equations [36]

Property	Units	Equation
Density	kg/m^3	$-0.614254 * T(°C) - 0.000321 * T^2(°C) + 1020.62$
Heat Capacity	$\frac{kJ}{kg * K}$	$0.003313 * T(°C) + 0.0000008970785 * T^2(°C) + 1.496005$
Thermal Conductivity	$\frac{W}{m * K}$	$-0.00003 * T(°C) - 0.00000015 * T^2(°C) + 0.118294$
Kinematic Viscosity	mm^2/s	$e^{\left(\frac{586.375}{T(°C)+62.5} - 2.2809\right)}$
Vapor Pressure	kPa	$e^{\left(\frac{-9094.51}{T(°C)+340} + 17.6371\right)}$

Aqueous NaCl Solutions

Equations and tables for the thermodynamic properties of aqueous NaCl solutions are given in Appendix A of this document. This information, found in the literature, was derived primarily by empirical methods.

4.5 Steam Compressor

A compressor is necessary for the operation of a VC distiller, and minimizing its power consumption greatly impacts the performance of the distiller. The simple block diagram shown in Figure 28 will be utilized to derive an equation for the required power input of the compressor. In Figure 28, the inlet and outlet of the compressor is designated by 1 and 2, respectively.

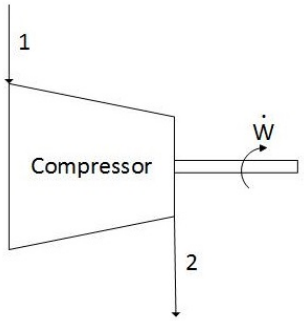

Figure 28: Block Diagram of a Compressor

The equation for calculating the power consumption of a steadily operating compressor with one inlet and one outlet can be derived from the 1st Law of Thermodynamics:

$$\dot{Q}_{in} + \dot{W}_{in} + \dot{m}(h + ke + pe)_1 = \dot{Q}_{out} + \dot{W}_{out} + \dot{m}(h + ke + pe)_2 \qquad \textbf{Equation 6}$$

Power is not produced by the system, so $\dot{W}_{out}$ is eliminated. The mass flow rate at the inlet equals that of the outlet due to conservation of mass. Neglecting heat transfer, kinetic energy, and potential energy, the above equation can be reduced to:

$$\dot{W}_{in,rev} = \dot{m}(h_2 - h_1) \qquad \textbf{Equation 7}$$

If the efficiency of the compressor is to be included, then the equation becomes:

$$\dot{W}_{in,actual} = [\dot{m}(h_2 - h_1)]/\eta_{rev} \qquad \textbf{Equation 8}$$

Table 8 shows other equations which have been utilized by authors analyzing VC distillers. These equations will not be utilized in the design of this distiller because they consider water vapor to be an ideal gas, which is only a valid assumption for certain conditions [35].

Table 8: Compressor Work Equations from VC Case Studies

Work Equation	Reference
$W = \frac{n}{n-1} p_1 v_1 \left\{ \left(\frac{p_2}{p_1} \right)^{\frac{n}{n-1}} - 1 \right\}$	[21]
$w_{comp} = \frac{nRT_e}{\eta_{comp}(n-1)} \left[\left(\frac{P_c}{P_e} \right)^{(n-1)/n} - 1 \right]$	[37]

The actual phase of water at the exit is usually superheated. This raises the power input compared to the theoretical situation where the fluid is a saturated vapor at the outlet. For example, Table 9 shows two processes where saturated vapor at 100°C with a mass flow rate of 0.0211 kg/s (a volumetric flow rate of 20 gal/hr) at the inlet is compressed to a pressure of 150 kPa by a compressor which has a compressor efficiency of 80%. For the specific scenarios given, the power consumption is approximately 5.59 times greater for producing a superheated vapor at the outlet compared to a saturated vapor. In order to transfer all of the latent heat of evaporation to the recirculation loop, the steam must have a saturation temperature greater than the elevated boiling temperature of the saltwater.

Table 9: The Effect of Compressor Outlet Conditions on Power Consumption

Outlet Conditions [35]	Power Calculation
Saturated Vapor P = 150 kPa T_{sat} = 111.35°C h = 2693.1 kJ/kg	$\dot{W} = \frac{\dot{m}(h_2 - h_1)}{\eta_{comp}} = \frac{0.0211 \frac{kg}{s} \left(2693.1 \frac{kJ}{kg} - 2675.6 \frac{kJ}{kg} \right)}{0.8} = 0.46\ kW$
Superheated Vapor P = 150 kPa T = 150°C h = 2772.9 kJ/kg	$\dot{W} = \frac{\dot{m}(h_2 - h_1)}{\eta_{comp}} = \frac{0.0211 \frac{kg}{s} \left(2772.9 \frac{kJ}{kg} - 2675.6 \frac{kJ}{kg} \right)}{0.8} = 2.57\ kW$

4.6 2nd Generation MVC Distiller Design

Figure 29 is the schematic of the 2nd generation MVC distiller proposed in this research. The distiller in many ways functions as a typical MVC distiller, but several important modifications to the conventional design have been made. Salt will be expected to precipitate out of the saltwater solution in the evaporator/crystallizer as time progresses during operation. The water in the evaporator/crystallizer and recirculation loop will eventually become saturated with salt. Due to scaling concerns, all heat exchangers are located outside the evaporator/crystallizer. The higher pressure of the recirculation loop will prevent the liquid from evaporating until it reaches the evaporator/crystallizer, which will be maintained at about atmospheric pressure.

The compressor will be turned on once the liquid in the evaporator/crystallizer reaches the designed boiling temperature. It will be assumed that the water at the inlet of the compressor is a saturated vapor, and the water at the outlet is superheated. The superheated steam will be cooled by injecting low-temperature purified water into the flow so it becomes a saturated vapor at the inlet of Heat Exchanger B. The compressor serves to raise the pressure, and therefore the saturation temperature, of the vapor in this path so heat transfer is possible between the vapor and the saltwater solution of the recirculation loop. The temperature of the recirculation loop will be less than that of the output water path, so the saturated vapor will transfer its latent heat of condensation to the recirculation loop, and leave Heat Exchanger B as a saturated liquid. This saturated liquid will be cooled in Heat Exchanger A when it transfers heat to the flow of input water.

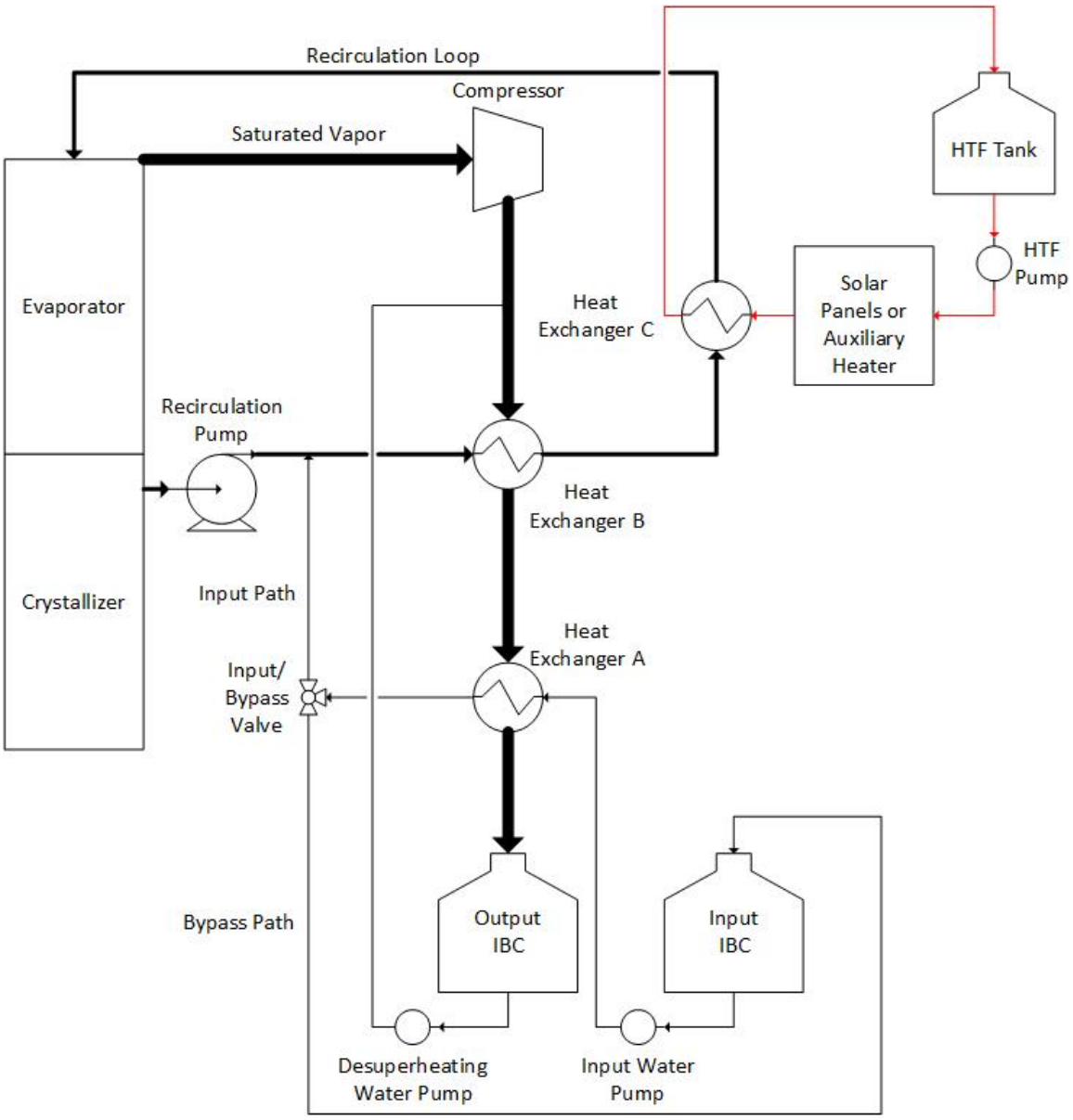

Figure 29: Schematic Diagram of the Proposed VC Distiller

The input water pump must always be on as long as the compressor is drawing water vapor out of the evaporator/crystallizer. If the water level in the evaporator/crystallizer is above a certain point, it will be sent back to the Input Water Intermediate Bulk Container (IBC). If the water level is lower than this point, the input water will be injected into the recirculation loop before Heat Exchanger B.

4.7 Design Calculations

Boiling Point Elevation

Using Equation A2, the mass fraction of salt at the saturation limit (X_{SAT}) value for a solution at 100°C is 0.280. Using Equation A1, a mass fraction of 0.280 equals a molality of 6.65 mol salt/kg water. Using Equation A9, the boiling temperature of this solution is 106.9°C. Therefore, the compressor must generate enough pressure at its outlet to ensure the saturation temperature of the steam is greater than 106.9°C.

Heat Transfer in Heat Exchanger B

The specific enthalpy of saturated water vapor at 106.9°C is 2686.3 kJ/kg by using linear interpolation of the tabulated data from Çengel and Boles [35]. Using Equation A5, the specific enthalpy of an aqueous NaCl solution at this temperature and a mass fraction of 0.280 is 328.72 kJ/kg. Using Equation A6, the latent heat of vaporization of this solution is 2357.6 kJ/kg. Using Equation A7, the recirculation loop must receive 49.5 kW of heat in order to have an output water vapor mass flow rate of 0.021 kg/s.

The saturation pressure of water at 110°C is 143.38 kPa [35]. The specific enthalpy of a saturated vapor and saturated liquid at 110°C is 2691.1 kJ/kg and 461.42 kJ/kg, respectively. The latent heat of vaporization of water at 110°C is 2229.7 kJ/kg. The heat transfer out of the output water through Heat Exchanger B is 46.8 kW. The temperature of the recirculation loop cannot be greater than that of the output water at any point in Heat Exchanger B. Assuming the temperature of the recirculation loop is 109°C at the outlet of Heat Exchanger B, the mass flow rate of the recirculation loop must be 6.97 kg/s.

Heat Transfer in Heat Exchanger C

The required heat input from the Therminol®66 in Heat Exchanger C is 2.7 kW. The temperature of the recirculation loop at the inlet of Heat Exchanger C is 109°C, and it will be assumed that the specific heat of an aqueous NaCl solution at this temperature is approximately the same as that at 106.9°C since there is only a difference of 2.1°C between these two temperatures. The temperature of the recirculation loop at the outlet of Heat Exchanger C will be 109.12°C. A gear pump may be the best option for the pump of the Therminol®66 loop because of their ability to handle high temperatures. Gear pumps usually have relatively low flow rates, and the design volumetric flow rate for the Therminol®66 loop will be 3 gal/min (1.89×10^{-4} m^3/s). It will be assumed that the maximum temperature of this loop is 190°C. In actuality, the maximum temperature of the loop will vary with solar radiation throughout the day. The temperature variation throughout the day will be discussed in more detail later in this chapter. It will also be assumed that the average temperature of the loop through the heat exchanger is 186°C. Using the equations found in Table 7, the density and specific heat of Therminol®66 at 186°C is 895.3 $kg/m^3$and 2.143 kJ/(kg K), respectively. Solving for the temperature of the loop at the outlet of Heat Exchanger C:

$$\dot{Q}_{out} = \dot{m}c_p(T_{in} - T_{out})$$

$$T_{out} = T_{in} - \frac{\dot{Q}_{out}}{\dot{m}c_p} = T_{in} - \frac{\dot{Q}_{out}}{\rho\dot{V}c_p}$$

$$T_{out} = 190°C - \frac{2.7\ kW}{895.3\frac{kg}{m^3} \times 1.89 \times 10^{-4}\frac{m^3}{s} \times 2.143\ \frac{kJ}{kg\ K}} = 182.6°C$$

The above result shows 186°C is a reasonable assumption for the average temperature of the loop through the heat exchanger. The mass flow rate of the Therminol®66 is 0.17 kg/s based on

the above calculations. The mass flow rate will actually need to vary with the maximum temperature in the loop. However, the calculated temperatures and mass flow rate above were utilized to simplify the heat exchanger design calculations.

Heat Transfer in Heat Exchanger A

It was assumed that the output water enters Heat Exchanger A as a saturated liquid at 110°C and leaves as a subcooled liquid at 60°C. The specific enthalpy of pure liquid water at 110°C and 60°C is 461.42 kJ/kg and 251.18 kJ/kg, respectively [35]. Calculating the heat transfer out of the output water path through Heat Exchanger A:

$$\dot{Q}_{out} = \dot{m}(h_{in} - h_{out}) = 0.021\frac{kg}{s}\left(461.42\frac{kJ}{kg} - 251.18\frac{kJ}{kg}\right) = 4.42\ kW$$

It was assumed that the input water has a NaCl concentration of 0.1 kg salt/kg water (a mass fraction equal to 0.091) and it has a temperature of 35°C at the inlet of Heat Exchanger A. It was assumed that the flow rate of the input water path is 2 gal/min (1.26×10^{-4} m^3/s) and the average temperature of the path through Heat Exchanger A is 40°C. Using Equation A4, the density of the input water at this average temperature is 1056.2 kg/m^3. Using Equation A5 and Equation A8, the specific heat of the input water is 3.77 kJ/(kg K). Solving for the temperature of the input water at the outlet of Heat Exchanger A:

$$\dot{Q}_{in} = \dot{m}c_p(T_{out} - T_{in})$$

$$T_{out} = T_{in} + \frac{\dot{Q}_{in}}{\dot{m}c_p} = T_{in} + \frac{\dot{Q}_{in}}{\rho\dot{V}c_p}$$

$$T_{out} = 35°C + \frac{4.42\ kW}{1056.2\frac{kg}{m^3} \times 1.26 \times 10^{-4}\frac{m^3}{s} \times 3.77\frac{kJ}{kg\ K}} = 43.8°C$$

The above result shows 40°C is a reasonable assumption for the average temperature of the path through the heat exchanger.

Summary of Temperatures and Mass Flow Rates

Figure 30 shows the schematic of the 2nd generation distiller with numbered locations. These locations are listed in Table 10 along with each of their temperatures and mass flow rates.

Table 10: Conditions of Each Location of the Distiller

Location	Temperature (°C)	Pressure (kPa)	Phase	Mass Flow Rate (kg/s)
Input Water Path				
1	35	239	Compressed Liquid	0.133
2	43.8	239	Compressed Liquid	0.133
Recirculation Loop				
3	106.9	207	Compressed Liquid	6.97
4	109	207	Compressed Liquid	6.97
5	109.1	207	Compressed Liquid	6.97
Output Water Path				
6	106.9	101.3	Saturated Vapor	0.021
7	120	143.4	Superheated Vapor	0.021
8	110	143.4	Saturated Vapor	0.021
9	110	143.4	Saturated Liquid	0.021
10	60	143.4	Compressed Liquid	0.021
Desuperheating Water Path				
11	60	377	Compressed Liquid	3.03×10^{-4}
Therminol®66 Loop				
12	190	207	Compressed Liquid	0.17
13	182.6	207	Compressed Liquid	0.17

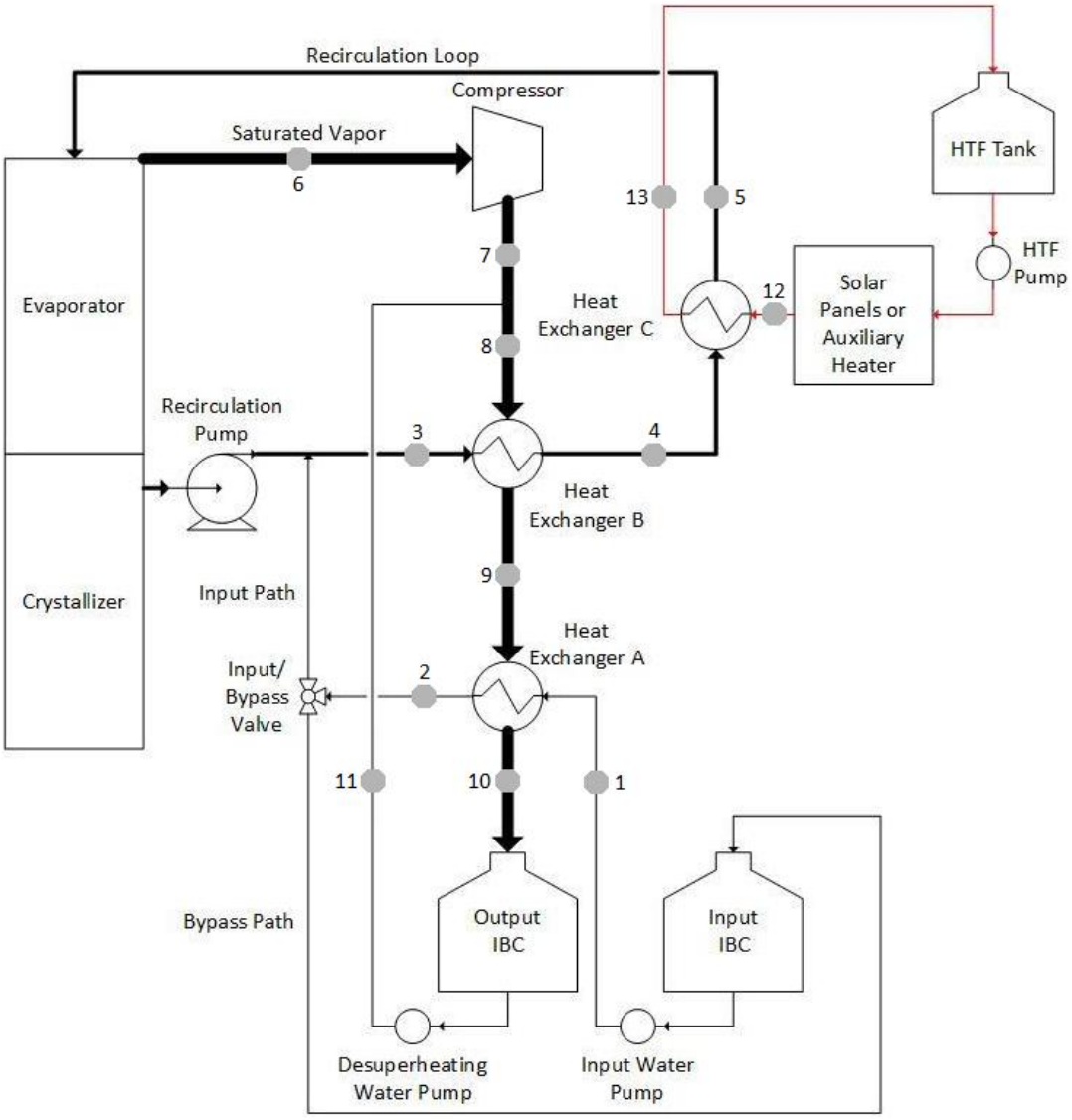

Figure 30: 2nd Generation Schematic with Location Markers

4.8 Heat Exchanger Design

The inlet and outlet temperatures, the overall heat transfer coefficient, and the total surface area of the heat exchanger are important parameters in the design of heat exchangers [38]. For this design, the unknown parameter to be calculated is the total surface area. Due to space limitations in the shipping container which houses the distiller, each heat exchanger must be kept at a reasonable size. The log mean temperature difference (LMTD) method will be

implemented in the design of the Heat Exchanger A and Heat Exchanger C. Due to the complexity of designing a heat exchanger involving a phase change, an appropriately sized heat exchanger will be selected from McMaster-Carr®.

Concentric, Counterflow Tube Heat Exchangers

One of the simplest types of heat exchangers is one involving two concentric tubes. The two arrangements of this type of heat exchanger are parallel-flow and counterflow. A counterflow heat exchanger requires less surface area compared to a parallel-flow arrangement for a prescribed set of inlet and outlet temperatures [38]. Therefore, only the counterflow arrangement will be considered for this research.

Figure 31 is a schematic of a typical concentric tube heat exchanger. These heat exchangers consist of two tubes, with one tube passing through the center of the larger tube. One fluid flows through the central tube, and the other fluid passes between the space between the outer wall of the central tube and the inner wall of the larger tube. This space is called the annulus. It will be assumed that the outer wall of the larger tube is well insulated, so heat can only pass through the wall of the central tube. It will also be assumed that the thickness of the wall of the central tube provides negligible resistance to the heat transfer between the fluids. The tube diameters will be selected based on commercially available pipe sizes. The inner diameters of 1” and 1.5” Schedule 40 pipes are approximately 0.027 m and 0.04 m, respectively. For both Heat Exchanger A and Heat Exchanger C, the values of D_i and D_o will be set as 0.027 m and 0.04 m, respectively.

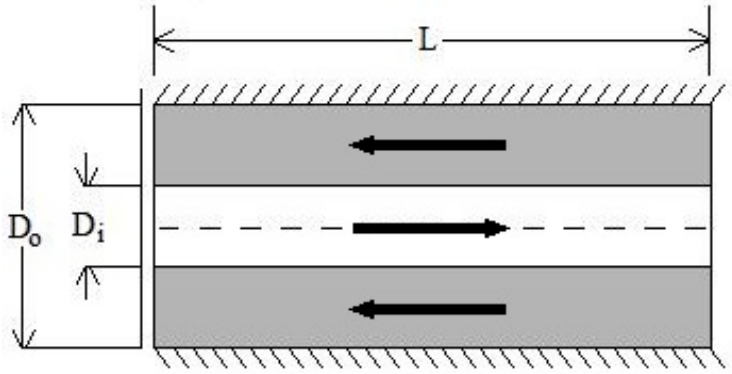

Figure 31: Schematic of a Concentric, Counterflow Heat Exchanger

LMTD Method

Bergman et al. [38] provide Equation 9 through Equation 20 for the analysis of a concentric, counterflow tube heat exchanger. Equation 9 is the general equation for relating the LMTD to heat exchanger size.

$$\dot{Q} = U\Delta T_{lm}A \qquad \textbf{Equation 9}$$

In the above equation, $\dot{Q}$ is the rate of heat transfer, U is the overall heat transfer coefficient, A is the surface area, and ΔT_{lm} is the mean temperature difference. The mean temperature difference is defined in Equation 10.

$$\Delta T_{lm} = (\Delta T_1 - \Delta T_2)/\ln(\Delta T_1/\Delta T_2) \qquad \textbf{Equation 10}$$

For a counterflow heat exchanger, ΔT_1 and ΔT_2 are calculated by utilizing Equation 11 and Equation 12, respectively. In these equations, the subscripts h, c, i, and o are hot, cool, inlet, and outlet, respectively.

$$\Delta T_1 = T_{h,i} - T_{c,o} \qquad \textbf{Equation 11}$$

$$\Delta T_2 = T_{h,o} - T_{c,i}$$ **Equation 12**

The overall heat transfer coefficient from Equation 9 can be found by utilizing Equation 13. For this equation, it is assumed that the resistances due to fouling and wall thickness are negligible.

$$U = 1/[(1/h_i) + (1/h_o)]$$ **Equation 13**

The convection coefficient for flow through the inner channel (h_i) and the annulus (h_o) can be found by utilizing Equation 14. The diameter (D) in Equation 14 is D_i for the inner channel. However, the hydraulic diameter must be utilized for the annulus, which can be found by utilizing Equation 15.

$$h = k \cdot Nu/D$$ **Equation 14**

$$D_h = D_o - D_i$$ **Equation 15**

Equation 16 can be utilized to find the Nusselt number for a flow which is fully turbulent passing through a circular tube and is receiving heat through a constant temperature wall. According to Young et al. [39], laminar flow occurs in a round pipe if the Reynolds number is less than approximately 2,100, and turbulent flow occurs when the Reynolds number is greater than approximately 4,000. However, this equation cannot be used for flow in a circular annulus. Table 11 provides values for the Nusselt number for fully developed laminar flow in a circular annulus based on the ratio of tube diameters. Linear interpolation will be used to find the values for Nusselt number for a certain ratio of diameters which is between those listed in the table.

$$Nu_D = 0.023 Re_D^{0.8} Pr^{0.4}$$ **Equation 16**

Table 11: Nusselt Number for Fully Developed Laminar Flow in a Circular Tube Annulus [38]

D_i/D_o	Nu
0	N/A
0.05	17.46
0.1	11.56
0.25	7.37
0.5	5.74
≈1.00	4.86

The Prandtl number of a fluid is defined by Equation 17. The Prandtl number does not depend on heat exchanger arrangement, and is an intensive property of the fluid.

$$Pr = c_p \mu / k \qquad \textbf{Equation 17}$$

The Reynolds number of the flow through the central channel and the annulus are calculated by utilizing Equation 18 and Equation 19, respectively. Once all other parameters have been solved for, the required length of the counterflow, concentric tube heat exchanger can be calculated by utilizing Equation 20.

$$Re_D = 4\dot{m}/(\pi D_i \mu) \qquad \textbf{Equation 18}$$

$$Re_D = 4\dot{m}/[\pi(D_o - D_i)\mu] \qquad \textbf{Equation 19}$$

$$L = \dot{Q}/(U\pi D_i \Delta T_{lm}) \qquad \textbf{Equation 20}$$

Heat Exchanger A

This heat exchanger is located between the input feed water path and the output distilled water path. The output water entering this heat exchanger is a saturated liquid, and it is desired that the temperature of this water be as low as possible at the outlet to supply more heat to the

input water path. The output water will flow through the annulus of the heat exchanger, and the input water will flow through the central tube.

Table 12 shows all the design parameters for Heat Exchanger A. Equation 9 through Equation 20 as well as Table 11 were utilized to calculate all the values in Table 12 based on inlet and outlet temperatures, flow rates, and fluid properties. The Reynolds number of the output water through the heat exchanger is 1,203, so the flow is laminar and the values in Table 11 are valid. The Reynolds number of the input water through the central tube is 7,711, so the flow is turbulent and Equation 16 is valid. The required length of the heat exchanger is 5.34 m for this arrangement.

Table 12: Heat Exchanger A Design Parameters

Parameter	Value	Parameter	Value
$T_{h,i}$ (°C)	110	Re_h	1203
$T_{h,o}$ (°C)	60	Re_c	7711
$T_{c,i}$ (°C)	35	k_h (W/m*K)	0.673
$T_{c,o}$ (°C)	43.8	k_c (W/m*K)	0.617
ΔT_1 (°C)	66.2	$c_{p,h}$ (J/kg*K)	4202
ΔT_2 (°C)	25	$c_{p,c}$ (J/kg*K)	3813
ΔT_{lm} (°C)	42.3	Pr_h	2.07
$\dot{Q}$ (W)	4420	Pr_c	5.03
$\dot{m}_h$ (kg/s)	0.021	d_i/d_o	0.675
$\dot{m}_c$ (kg/s)	0.133	Nu_h	5.43
d_o (m)	0.04	Nu_c	56.5
d_i (m)	0.027	h_h (W/(m^2*K))	281
μ_h (N*s/m^2)	0.0003316	h_c (W/(m^2*K))	1291
μ_c (N*s/m^2)	0.0008134	U (W/(m^2*K))	231
ρ_h (kg/m^3)	969	L (m)	5.34
ρ_c (kg/m^3)	1056.2		

Heat Exchanger B

This heat exchanger is located between the recirculation loop and the output water path. The purpose of this heat exchanger is to completely condense the output water, which is a saturated vapor at the inlet of the heat exchanger. Table 13 shows the mass flow rates of both fluids through the heat exchanger, all inlet and outlet temperatures, and the rate of heat transfer between the fluids. Table 14 shows the specifications of a heat exchanger selected from McMaster-Carr® which will be utilized as Heat Exchanger B. This heat exchanger is referred to as a "space-saving heat exchanger" or a "brazed-plate exchanger", and it consists of stacked, corrugated plates. This heat exchanger has a maximum pressure and temperature of 435 psi and 450°F, respectively. The rated heat transfer capacity and flow rate for the heat exchanger are more than what it will experience for this application.

Table 13: Heat Exchanger B Design Parameters

Parameter	Recirculation Loop	Output Water Path
Mass Flow Rate (kg/s)	6.97	0.021
Inlet Temperature (°C)	106.9	110
Outlet Temperature (°C)	109	110
Heat Transfer (kW)	46.8	-46.8

Table 14: Specifications of the Heat Exchanger from McMaster-Carr®

Heat Transfer Capacity (Btu/hr)	Surface Area (ft^2)	Flow Cap. (gpm)	Pipe Size (NPT)	Height (in.)	Width (in.)	Depth (in.)	Item Number	Cost ($)
380,000	82.8	126	2	24 5/16"	7 ½	11 ½	8546T17	1,837.45

Heat Exchanger C

This heat exchanger is located between the recirculation loop and the Therminol®66 loop. The purpose of this heat exchanger is to transfer additional heat to the recirculation loop

needed to generate the appropriate amount of steam in the evaporator. The temperature of both fluids at their outlets depends upon the desired heat transfer rate to the recirculation loop. Table 15 shows all the design parameters for Heat Exchanger C. Equation 9 through Equation 20 as well as Table 11 were applied to calculate all the values in Table 15 based on inlet and outlet temperatures, flow rates, and fluid properties. The Reynolds number of the Therminol®66 through the heat exchanger is 3,311, so the flow is in the transitional stage. The values in Table 11 will still be utilized even though the table is for laminar flow. This will cause some error in the calculation of the Nusselt number, and the calculated value for the required length of the heat exchanger will be greater than what is actually needed. The Reynolds number of the input water through the central tube is 604,200, so the flow is turbulent and Equation 16 is valid. The required length of the heat exchanger is 9.27 m for this arrangement.

4.9 Heat Loss through the Walls of the Heat Exchangers

For the preliminary design of the 2nd generation system, it was assumed that all the components were adiabatic. Accordingly, there is a need to estimate the heat loss from the system to ambient air. A method presented by Bergman et al. [38] will be utilized to get a more accurate estimate of the heat loss to the environment. This method involves modeling the system in question as a thermal circuit. Figure 32 is a schematic showing how the concentric-tube heat exchangers will be analyzed by this method. It will be assumed that the temperature of the outer wall of the heat exchanger (T_i) in Figure 32 is the average temperature of the fluid flowing through the annulus. The thermal resistance of the outer wall of the heat exchanger will be neglected. The heat loss will be calculated as a function of the thickness of insulation utilized. The thickness of the insulation is the difference between the outer radius of the insulation (r) and

the outer radius of the heat exchanger (r_i). The temperature of the ambient air (T_∞) will be set to 28°C. Bergman, et al., [38] suggested a value of 10 W/m^2·K for a typical value of free convection in air (h_∞).

Table 15: Heat Exchanger C Design Parameters

Parameter	Value	Parameter	Value
$T_{h,i}$ (Celsius)	190	Re_h	3311
$T_{h,o}$ (Celsius)	182.2	Re_c	604200
$T_{c,i}$ (Celsius)	109	k_h (W/m*K)	0.107
$T_{c,o}$ (Celsius)	109.1	k_c (W/m*K)	0.654
ΔT_1 (Celsius)	80.9	$c_{p,h}$ (J/kg*K)	2143
ΔT_2 (Celsius)	73.2	$c_{p,c}$ (J/kg*K)	3195
ΔT_{lm} (Celsius)	77.0	Pr_h	19.4
$\dot{Q}$ (W)	2700	Pr_c	2.66
$\dot{m}_h$ (kg/s)	0.169	d_i/d_o	0.675
$\dot{m}_c$ (kg/s)	6.97	Nu_h	5.43
d_o (m)	0.04	Nu_c	1434
d_i (m)	0.027	h_h (W/(m^2*K))	44.7
μ_h (N*s/m^2)	0.000970	h_c (W/(m^2*K))	34719
μ_c (N*s/m^2)	0.000544	U (W/(m^2*K))	44.6
ρ_h (kg/m^3)	895	L (m)	9.27
ρ_c (kg/m^3)	1161		

The two sources of thermal resistance considered in Figure 32 are conduction through the insulation and convection of the ambient air. The thermal resistance of conduction and convection for the radial system depicted in Figure 32 can be calculated by Equation 21 and Equation 22, respectively. The variable L is the total length of the heat exchanger. The total resistance of the thermal circuit is the sum of the individual resistances, as shown in Equation 23.

Once the total thermal resistance is known, Equation 24 will be used to calculate the rate of heat transfer to the environment.

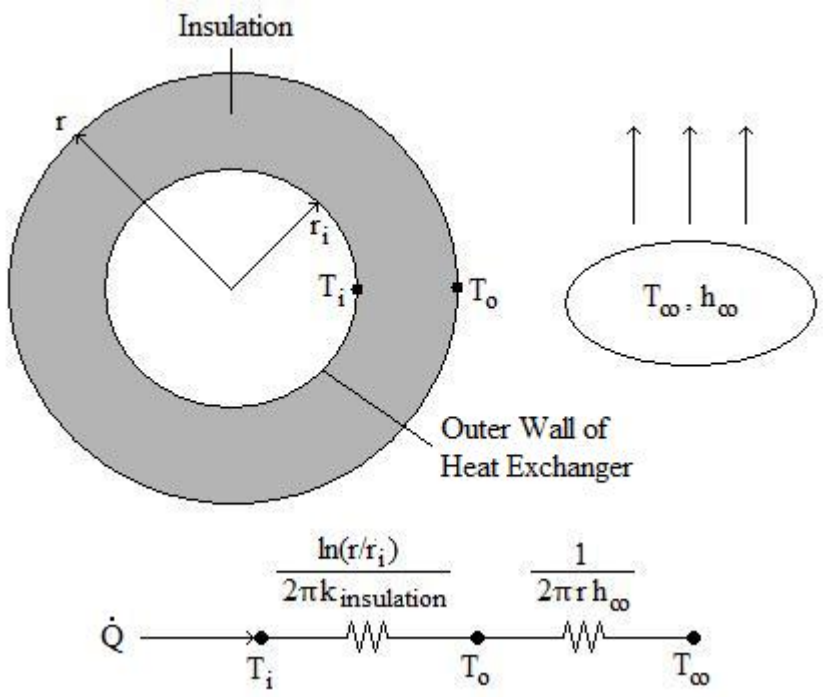

Figure 32: Thermal Circuit for the Concentric-Tube Heat Exchangers (Heat Exchangers A and C)

$$R_{t,cond} = \ln(r/r_i)/(2L\pi k_{insulation}) \quad \textbf{Equation 21}$$

$$R_{t,conv} = 1/(2\pi r L h_\infty) \quad \textbf{Equation 22}$$

$$R_{tot} = R_{t,cond} + R_{t,conv} \quad \textbf{Equation 23}$$

$$\dot{Q} = (T_i - T_\infty)/R_{tot} \quad \textbf{Equation 24}$$

Figure 33 is a graph of the rate of heat loss to the ambient air versus the thickness of insulation applied to Heat Exchanger A. Bergman et al. [38] provide tabulated data for the insulation materials selected, which includes the thermal conductivity at various temperatures.

The values for the thermal conductivity for all materials shown in the graph were selected for 365 K. The rate of heat transfer within Heat Exchanger A is 4.42 kW.

Figure 34 is a graph of the rate of heat loss to the ambient air versus the thickness of insulation applied to Heat Exchanger C. The same materials for insulation are considered as in Figure 33. The rate of heat transfer within Heat Exchanger C is 2.7 kW.

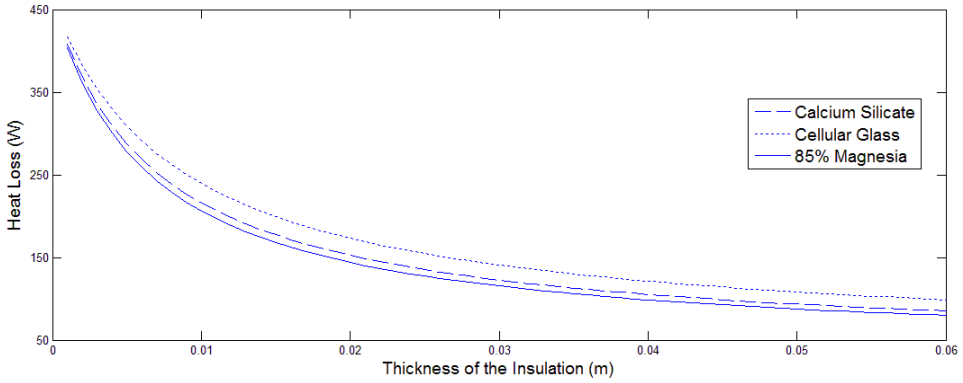

Figure 33: Heat Loss vs Thickness of the Insulation for Heat Exchanger A

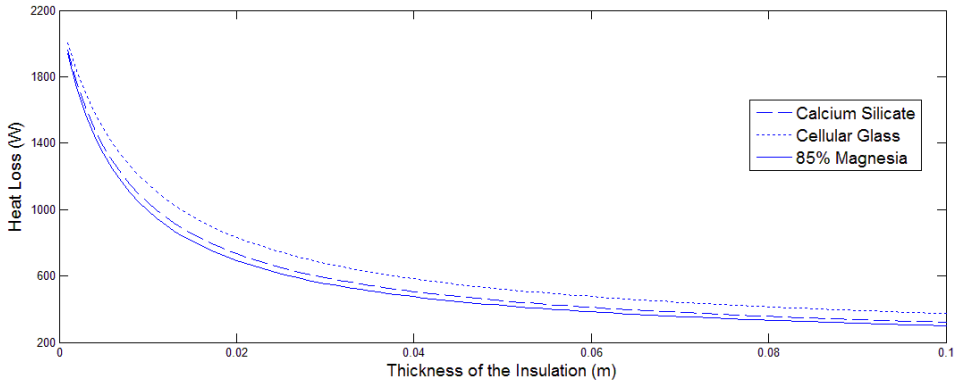

Figure 34: Heat Loss vs Thickness of the Insulation for Heat Exchanger C

Bergman et al. [38] also present how to analyze heat loss through a plane wall via the thermal circuit method. Figure 35 is a schematic showing how the space-saving heat exchanger utilized for Heat Exchanger B can be analyzed by this method. It will be assumed that the

temperature of the outer wall of the heat exchanger (T_i) is the same temperature of the condensing water vapor (110°C). This assumption will result in the maximum possible heat loss from the heat exchanger since this is the greatest temperature of either fluid. As with the heat loss calculations for Heat Exchangers A and C, the thermal resistance of the wall of the heat exchanger will be neglected, and the heat loss will be calculated as a function of the thickness of the insulation.

The thermal resistance of conduction and convection for the plane wall system depicted in Figure 35 can be calculated by Equation 25 and Equation 26, respectively. Equation 23 and Equation 24 apply to the plane wall system as well as a radial system.

$$R_{t,cond} = x/(k_{insulation}A) \qquad \textbf{Equation 25}$$

$$R_{t,conv} = 1/(h_{\infty}A) \qquad \textbf{Equation 26}$$

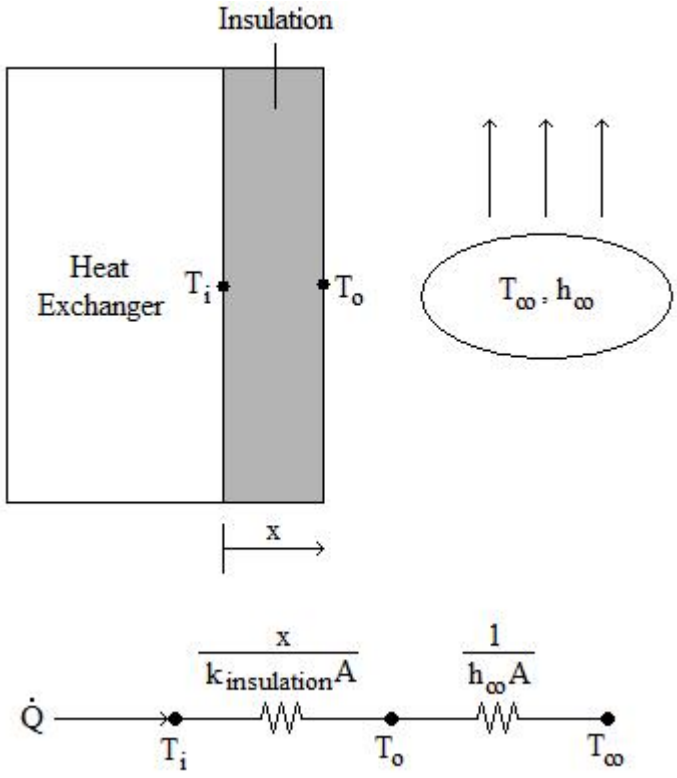

Figure 35: Thermal Circuit for the Space-Saving Heat Exchangers

Figure 36 is a graph of the rate of heat loss to the ambient air versus the thickness of insulation applied to Heat Exchanger B. The rate of heat transfer within Heat Exchanger B is 46.8 kW.

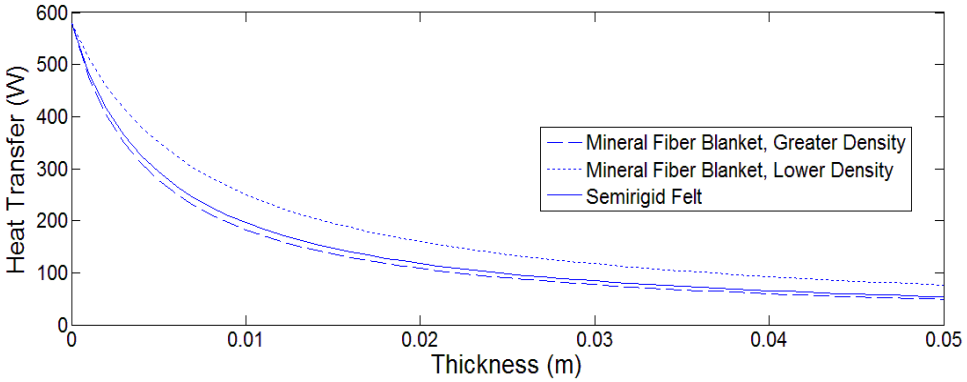

Figure 36: Heat Loss vs Thickness of Insulation for Heat Exchanger B

A space-saving heat exchanger was utilized as Heat Exchanger A in the 1st generation design. The specifications of this heat exchanger are listed in Table 16. If it is desired that this heat exchanger be utilized in the 2nd generation design, then the heat loss to the environment must be considered. Figure 37 is a graph of the rate of heat loss to the ambient air versus the thickness of insulation applied to Heat Exchanger A if the space-saving heat exchanger is utilized instead of the designed concentric-tube heat exchanger. It was assumed that the outer surface of the heat exchanger was 110°C, which is the greatest temperature in the system. By comparing Figure 33 and Figure 37, for the same thickness of insulation, the space-saving heat exchanger has less heat loss to the environment than the concentric-tube heat exchanger.

Table 16: Specifications of the Heat Exchanger from McMaster-Carr® Utilized as Heat Exchanger A in the 1st Generation Design

Heat Transfer Capacity (Btu/hr)	Surface Area (ft^2)	Flow Cap. (gpm)	Pipe Size (NPT)	Height (in.)	Width (in.)	Depth (in.)	Item Number	Cost ($)
50,000	15.6	18	1	20 11/16”	4 3/8”	4 ¼”	8546T14	566.50

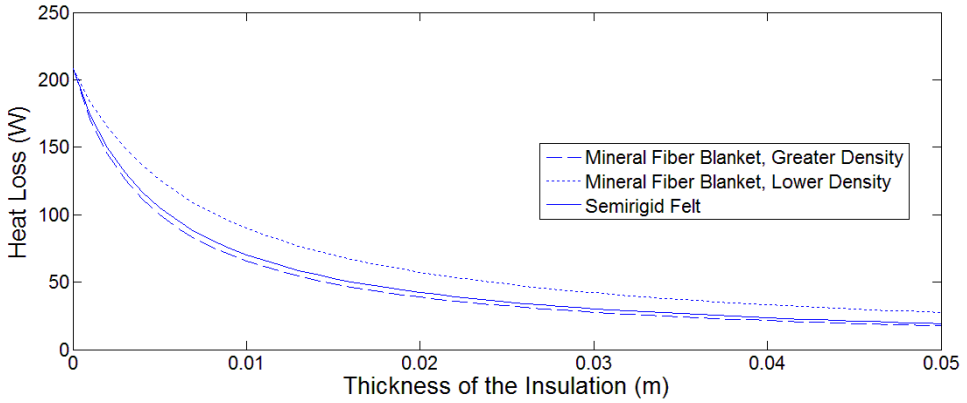

Figure 37: Heat Loss vs Thickness of the Insulation for Heat Exchanger A if a Space-Saving Heat Exchanger is utilized

The heat exchanger described by Table 14 was utilized as Heat Exchanger C in the 1st generation design. Figure 38 is a graph of the heat loss from Heat Exchanger C if this heat exchanger is used in the 2nd generation design. It was assumed that the outer wall of the heat exchanger was at 190°C, which is the greatest temperature of either fluid in the system. By comparing Figure 34 and Figure 38, it can be observed that the heat loss is much less by utilizing the space-saving heat exchanger instead of the concentric tube heat exchanger.

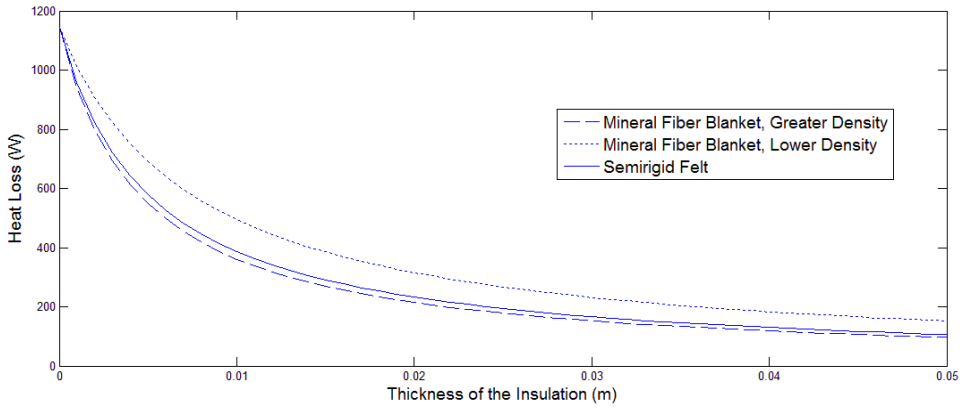

Figure 38: Heat Loss vs Thickness of the Insulation for Heat Exchanger C if a Space-Saving Heat Exchanger is utilized

4.10 Heat Loss through the Walls of the Evaporator/Crystallizer

The evaporator/crystallizer is a potential location for a significant amount of heat loss to the ambient air due to its high temperature and large surface area. The heat loss from the evaporator/crystallizer and a recommended amount of insulation will be calculated the same way as was done for the concentric-tube heat exchangers. It will be assumed that the outer surface of the evaporator/crystallizer has a temperature of 106.9°C, which is the boiling point of water saturated with salt. The 55 gallon stainless steel drums to be utilized in the construction of the evaporator/crystallizer each have a height and outer diameter of approximately 88.9 cm and 59.4 cm, respectively. Two drums will be modified in order to make one cylindrical container with a height of 177.8 cm, and the outer diameter will remain as 59.4 cm.

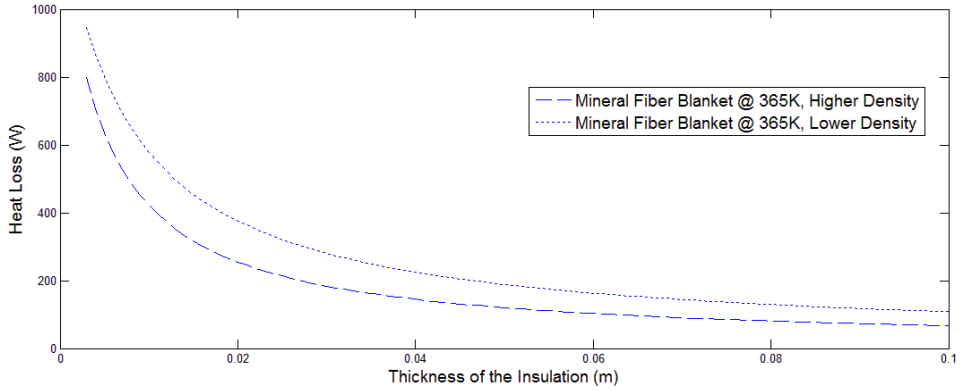

Figure 39: Heat Loss vs Thickness of the Insulation for the Curved Wall of the Evaporator/Crystallizer

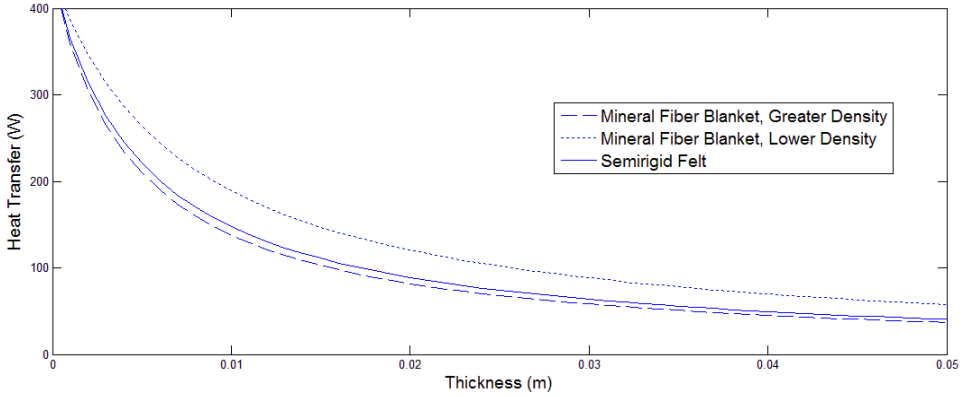

Figure 40: Heat Loss vs Thickness of the Insulation for the Flat Sides of the Evaporator/Crystallizer

4.11 Insulation Selection

It will be assumed that mineral fiber blankets (density of 96-192 kg/m^3, and a thermal conductivity of 0.038 W/m K at room temperature) will be utilized to insulate all the heat exchangers and the evaporator. Table 17 shows how the heat loss from all of these components varies with insulation thickness. Epiphany has conducted experiments with a brand of PDRs, and each PDR has been measured to provide 40.7 kWh of heat over 14 hours of daylight, which is an average heat supply of 2.91 kW. The design calculations showed that the PDRs must provide 2.7

kW of heat to the Therminol®66 loop in order to maintain the distiller's performance, which allows a single PDR to provide all the necessary heat plus an extra 210 W for inevitable heat loss.

Figure 41 is a graph of the total heat loss through the components considered in the heat loss analysis, which include the evaporator and the three heat exchangers. Table 17 shows the exact value of heat loss to the ambient air for certain insulation thicknesses. Based on the information given in Table 17 , an insulation thickness of 8 cm will ensure proper operation of the distiller with only one PDR by keeping the heat loss to the appropriate amount. However, there are more locations where heat loss will occur than what was considered during this analysis, and an insulation thickness of 8 cm is impractical. The best option may be to apply 3 cm of insulation (a reasonable thickness of one layer of insulation) and have a small immersion heater in the Therminol®66 reservoir to make up for the heat loss to the ambient air. Another possibility is to utilize a larger PDR which would be able to collect more solar energy.

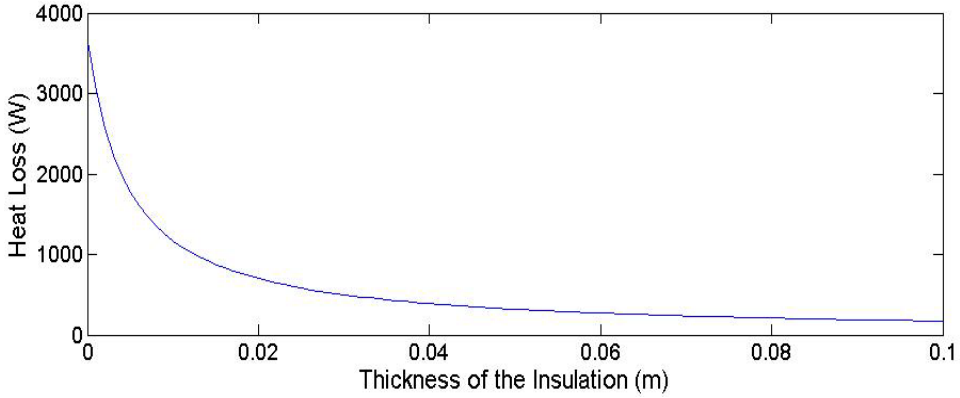

Figure 41: Total Heat Loss through the Heat Exchangers and Evaporator

Table 17: Mineral Fiber Blanket Insulation Thickness Effect on Total Heat Loss

Insulation Thickness (cm)	Heat Loss from Heat Exchanger A (W)	Heat Loss from Heat Exchanger B (W)	Heat Loss from Heat Exchanger C (W)	Heat Loss from the Evaporator (W)	Total Heat Loss (W)
0	208	580	1145	1746	3679
1	66	183	361	559	1169
2	39	108	214	336	697
3	28	77	152	242	499
4	21	60	118	190	389
5	18	49	97	157	321
6	15	41	82	134	272
7	13	36	71	117	237
8	11	32	62	105	210
9	10	28	56	94	188
10	9	25	50	86	170

Figure 42 is a graph of the ratio of heat loss with insulation to heat loss without insulation. From the figure, one can observe that the heat loss due to insulation thickness starts to level off with thickness, as the ratio for 4 cm, 6 cm, and 8 cm is approximately 11%, 7%, and 6%, respectively.

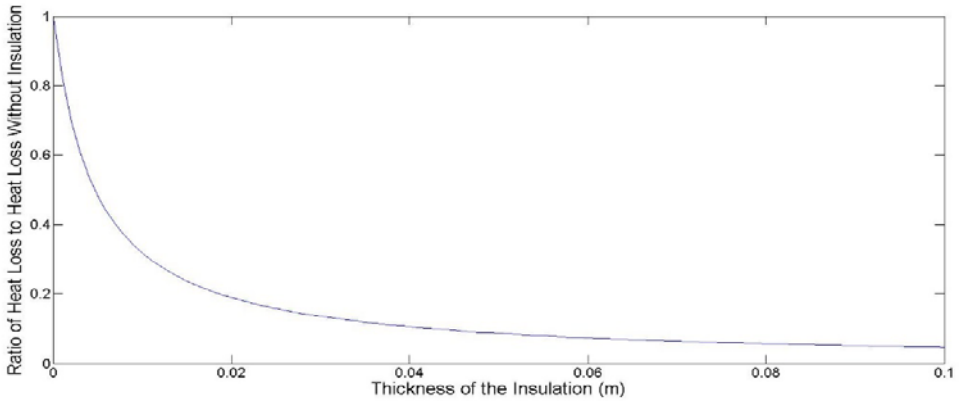

Figure 42: Ratio of Heat Loss vs Thickness of Insulation

The rate of change of heat loss with insulation thickness can be calculated by finding the derivative of Equation 24. Equation 27 and Equation 28 are the results of taking the derivative of Equation 24 with respect to thickness for a plane wall and a radial system, respectively. Figure 43 is the total change in heat loss for all the heat exchangers and the evaporator. It can be seen from the figure that adding more insulation after a thickness of 4 cm has been applied does not reduce the heat loss substantially.

Plane Wall

$$\frac{d\dot{Q}}{dt} = \frac{T_\infty - T_i}{kA[x/(kA) + 1/(hA)]^2} \qquad \textbf{Equation 27}$$

Radial System

$$\frac{d\dot{Q}}{dt} = \frac{L(T_\infty - T_i)\left[1/\left(2\pi k(x + r_i)\right) - 1/(2\pi h(x + r_i)^2)\right]}{\left[\ln(x/r_i + 1)/(2\pi k) + 1/\left(2\pi h(x + r_i)\right)\right]^2} \qquad \textbf{Equation 28}$$

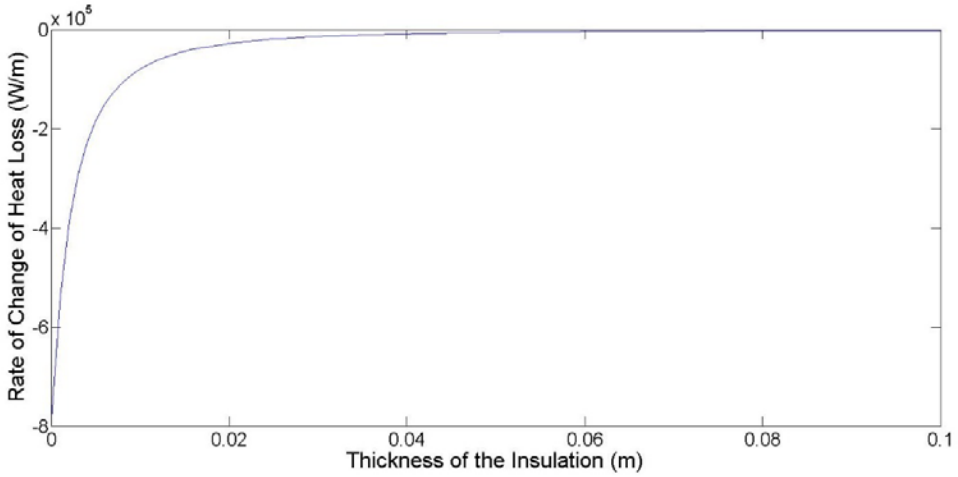

Figure 43: Rate of Change of Heat Loss vs. Thickness of Insulation

Table 18: Rate of Change of Heat Loss for Certain Insulation Thicknesses

Insulation Thickness (cm)	$d\dot{Q}/dx$ (W/m)
0	-795501
1	-79274
2	-27947
3	-14134
4	-8510
5	-5680
6	-4059
7	-3045
8	-2369
9	-1895
10	-1551

4.12 NPSHA Calculations

Approximate values of the NPSHA values for the recirculation pump and the Therminol®66 pump will be calculated in this section. Reliable operation of the 2nd generation distiller will require these pumps to never experience cavitation. Though cavitation was experienced more frequently in the recirculation pump of the 1st generation design, the relatively high temperature of the Therminol®66 loop may cause pumps for this loop in the 2nd generation design to cavitate, so this pump arrangement should be looked into.

All the energy terms described in Equation 1 must be calculated individually and in terms of feet of head. Equation 29 [31] can be utilized to convert pressure (in psi) to feet of head. In Equation 29, SG is the specific gravity of the fluid being pumped, which is obtained by dividing the density of the fluid by 1000 kg/m^3, the density of water at 4°C [39]. The pressure terms in Equation 1 include h_{atm}, h_p, and h_{vp}. The atmospheric pressure is assumed to be 14.7 psi for all

calculations, and the value of h_{atm} depends upon which fluid is being pumped. For the recirculation pump, it is has been assumed that the evaporator is maintained at 0 psig, so the h_p term is canceled out for its NPSHA calculation. However, the gauge pressure for the heat transfer fluid holding tank has been varied to observe its effect on the NPSHA for the Therminol®66 pump. The vapor pressure of the aqueous NaCl solution in the recirculation loop will be calculated by utilizing Equation A3 in the Appendix. An equation for calculating the vapor pressure of Therminol®66 is listed in Table 7.

$$\text{Head in Feet} = 2.31\text{P(psi)}/\text{SG} \qquad \textbf{Equation 29}$$

The value of h_{el} will be a variable for both pumps. This will be done by varying the length of the vertical pipe leading down to the pump. This length will also affect the value of h_f. The friction head loss can be divided into two categories, which are minor and major losses. Minor losses are losses incurred through pipe fittings such as valves and elbows. Equation 30 [39] can be utilized to calculate the minor loss through a fitting. In Equation 30, K_L is the loss coefficient of the fitting, V is the average fluid velocity, and g is the gravitational constant. Young et al. [39] provide values for the loss coefficient for a variety of fittings and entrance flow conditions.

$$h_{L,\text{minor}} = K_L V^2/(2g) \qquad \textbf{Equation 30}$$

Major losses are losses incurred through a length of pipe. Equation 31 [39] can be utilized to calculate the major loss through a section of pipe. In Equation 31, f is the friction factor, l is the length of the pipe, and D is the pipe diameter. The friction factor is dependent upon the Reynolds number of the flow, the pipe material, and the pipe size. Equation 32 [39] can be utilized to calculate the friction factor if the flow is laminar, and the Moody chart can be utilized

for this purpose if the flow is turbulent. The Moody chart can be found in most fluid mechanics textbooks. The Moody chart utilizes the Reynolds number of the flow and the relative roughness of the pipe to estimate the friction factor. Equation 33 can be utilized to calculate the relative roughness by dividing the equivalent roughness (ϵ) of the material by the diameter of the pipe.

$$h_{L,major} = f(l/D)[V^2/(2g)] \quad \textbf{Equation 31}$$

$$f = 64/Re \quad \textbf{Equation 32}$$

$$\text{Relative Roughness} = \epsilon/D \quad \textbf{Equation 33}$$

Recirculation Pump

Figure 44 shows a schematic of some assumptions made about the recirculation pump arrangement, as well as some properties of the fluid being pumped. It has been assumed that there will be a sharp edged entrance region, a ball valve, and a 90° elbow in the suction line. Young et al. [39] provide values for the loss coefficient for each of these components. The loss coefficient for a sharp edged entrance region, a fully open ball valve, and a threaded 90° elbow are 0.5, 0.05, and 1.5, respectively. It has also been assumed that the suction line draws fluid from the evaporator/crystallizer 1 ft below the water level. The suction line will extend 1 ft horizontally from the evaporator. The suction line should not be placed at the bottom of the evaporator/crystallizer because salt will accumulate at this location.

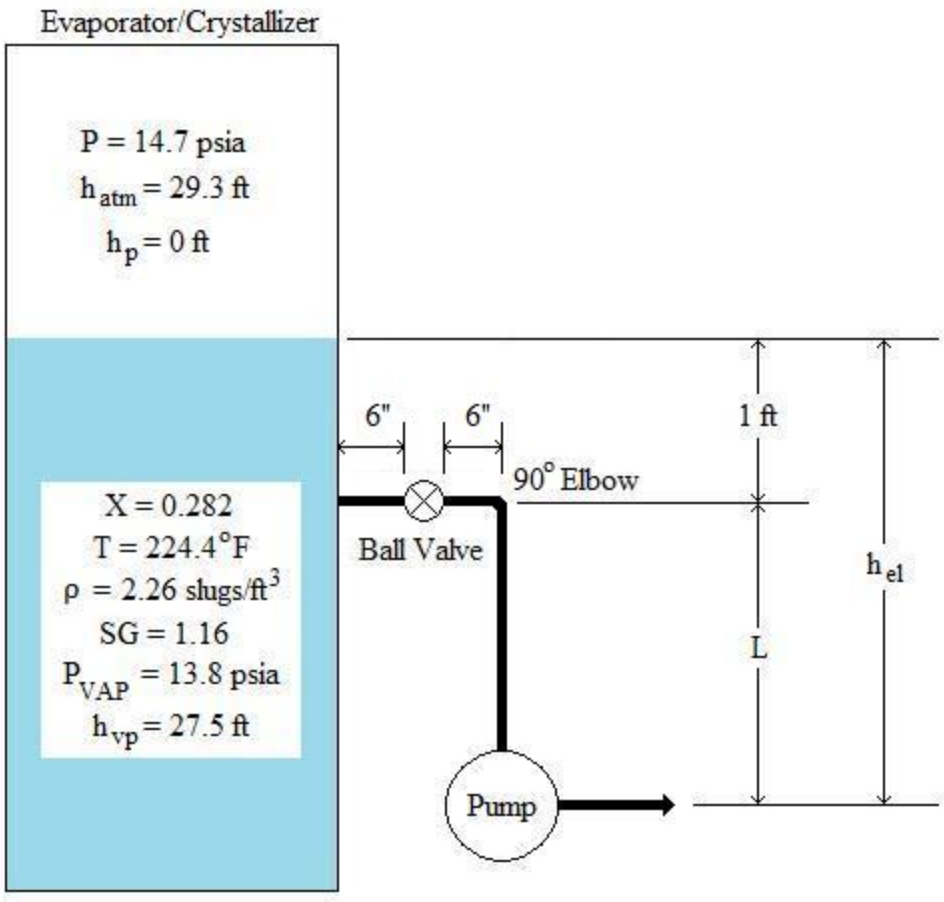

Figure 44: NPSHA Energy Terms for the Recirculation Pump

It has been assumed that the suction line is comprised of 2" NPT stainless steel pipe. Table 19 shows some characteristics of this pipe and flow conditions within the suction line of the recirculation pump. The table shows the flow is turbulent, so the Moody chart was utilized to obtain an approximate friction factor. Figure 45 shows how the NPSHA for the recirculation pump changes by varying L (the distance from the end of the vertical pipe to the centerline of the pump has been neglected). The figure shows that the recirculation pump must have a relatively low NPSHR value in order to function properly without cavitating. From experience with the 1st generation design, an appropriate length of the vertical pipe is approximately 3 ft, so the pump should have an NPSHR value of less than 3 ft.

Table 19: Recirculation Pump Suction Line Conditions

D (ft)	0.172
Equivalent Roughness (ft)	5×10^{-5}
Relative Roughness	3×10^{-4}
Reynolds Number of the Flow	3.11×10^{5}
Velocity of the Flow (ft/s)	9.12
f	0.017

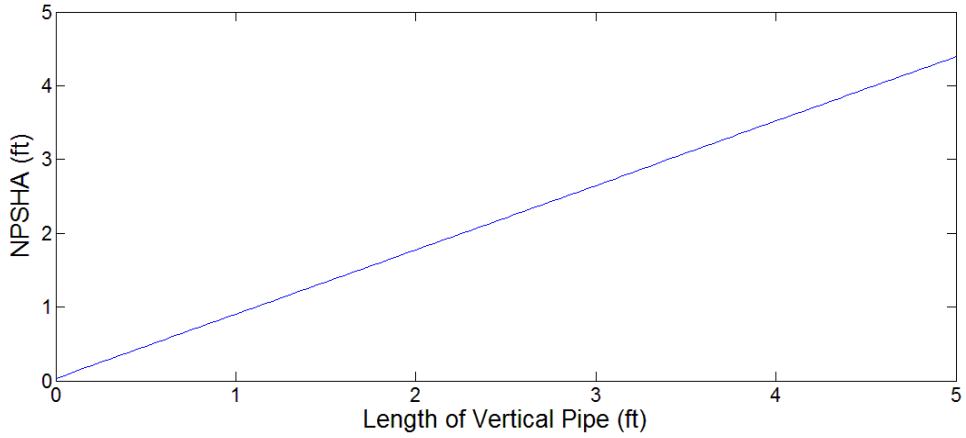

Figure 45: NPSHA vs Length of Vertical Pipe for the Recirculation Pump

Therminol®66 Pump

Figure 46 shows a schematic of some assumptions made about the Therminol®66 pump arrangement. Many of the same assumptions made for the recirculation pump arrangement were also made for the Therminol®66 pump. However, it was assumed that the suction line for this pump was made of 2" NPT steel instead of stainless steel.

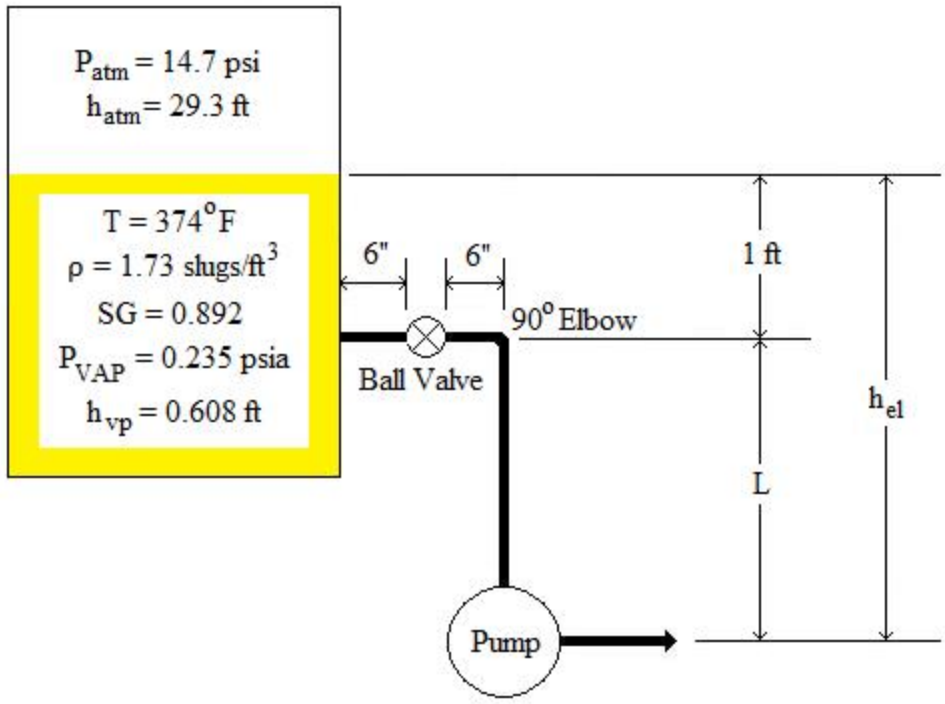

Figure 46: NPSHA Energy Terms for the Therminol®66 Pump

Table 20 shows some characteristics the pipe comprising the suction line of the Therminol®66 pump, as well as flow conditions within the line. The table shows the flow is turbulent, so the Moody chart was utilized to obtain an approximate friction factor. Figure 47 shows how the NPSHA for the Therminol®66 pump changes by varying L (again, the distance from the end of the vertical pipe to the centerline of the pump has been neglected) and the gauge pressure within the holding tank. The figure shows that the Therminol®66 pump has significantly more NPSHA than the recirculation pump, especially if the reservoir is pressurized. This difference in NPSHA is primarily due to the difference in vapor pressures between the fluids.

Table 20: Recirculation Pump Suction Line Conditions

D (ft)	0.172
Equivalent Roughness (ft)	1.5×10^{-4}
Relative Roughness	8.7×10^{-4}
Reynolds Number of the Flow	4404
Velocity of the Flow (ft/s)	0.29
f	0.041

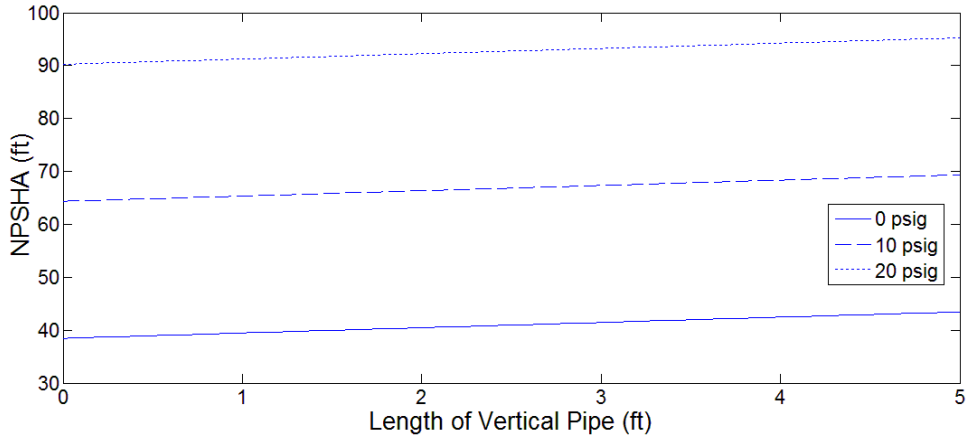

Figure 47: NPSHA vs Length of Vertical Pipe for the Therminol®66 Pump

4.13 Thermodynamic Model of the 2nd Generation Distiller

Figure 48 shows the thermodynamic model for each of the four modes of operation of the 2nd generation distiller. Figure 48A is the beginning of the distillation process in which an aqueous NaCl solution is pumped into the distiller. Heat and work interactions are assumed to be negligible for this process. Figure 48B is the bypass mode where aqueous NaCl is utilized to cool the output water in Heat Exchanger A, but it does not remain in the distiller and is sent back to the input IBC. Figure 48C is the filling mode for when the height of the fluid in the evaporator has dropped below a certain level and more aqueous NaCl is sent into the distiller. The distiller

will alternate between the bypass and filling modes until it is time to remove salt from the system.

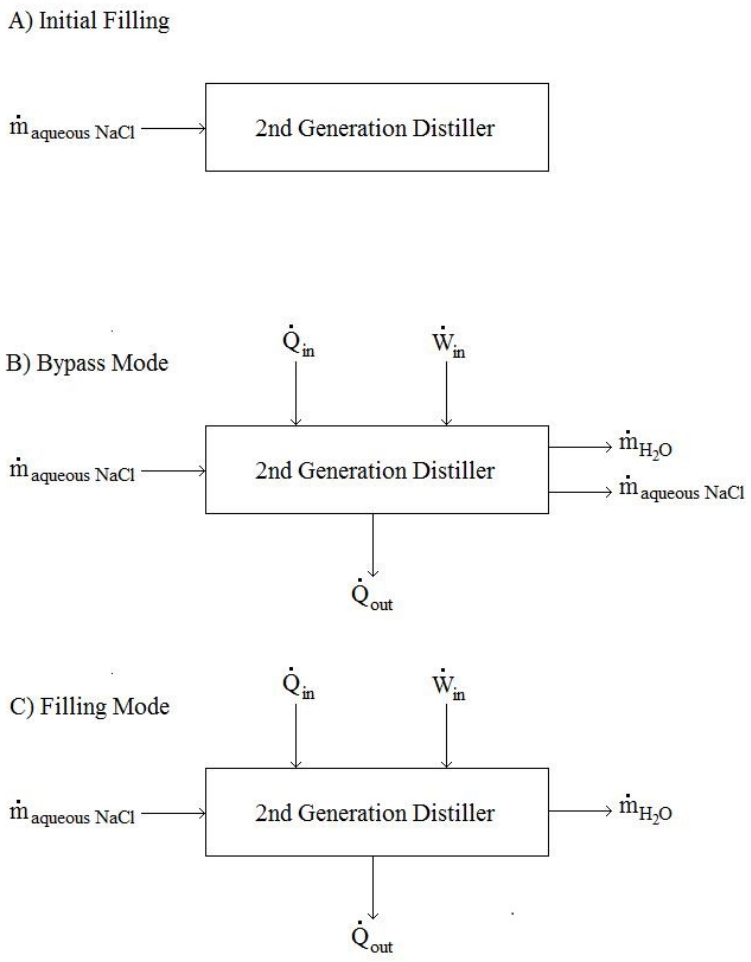

Figure 48: 2nd Generation Thermodynamic Models

Each of the processes shown in Figure 48 is unsteady flow situation. Therefore, there is a change in total energy in the system with respect to time for each mode. The calculations below show the magnitude and direction of the energy flow for each mode.

Initial Filling

$$dE_{system}/dt = (\dot{m}h)_{\text{aqueous NaCl},35°C} = 0.133\,kg/s * 132.1\,kJ/kg = 17.6\,kW$$

Bypass Mode

$$dE_{system}/dt = [\dot{m}(h_{35°C} - h_{43.8°C})]_{\text{aqueous NaCl}} + \dot{Q}_{in} + \dot{W}_{in} - (\dot{m}h)_{H_2O,60°C} - \dot{Q}_{out}$$

$$dE_{system}/dt = [0.133\,kg/s\,(132.1\,kJ/kg - 165.3\,kJ/kg)] + 3.2\,kW + 1.38\,kW - 0.021\,kg/s * 251.2\,kJ/kg - 0.499\,kW = -5.61\,kW$$

Filling Mode

$$dE_{system}/dt = (\dot{m}h)_{\text{aqueous NaCl},35°C} + \dot{Q}_{in} + \dot{W}_{in} - (\dot{m}h)_{H_2O,60°C} - \dot{Q}_{out}$$
$$= 0.133\,kg/s * 132.1\,kJ/kg + 3.2\,kW + 1.38\,kW - 0.021\,kg/s * 251.2\,kJ/kg - 0.499\,kW = 16.4\,kW$$

The calculation for the bypass mode shows energy is leaving the system (the value is negative) at a rate of 5.61 kW. This value is negative because aqueous NaCl is leaving the system at a greater temperature than it entered at while having the same mass flow rate, fresh water is leaving the system, and there is heat loss to the ambient air. The other two modes have positive values because aqueous NaCl is being pumped to the system and the system gains more mass.

4.14 Expected System Performance

Table 21 shows the expected performance of the 2nd generation design. The compressor power was calculated by assuming the steam would be superheated at a temperature and pressure

of 120°C and 143.4 kPa, respectively. It was also assumed that the compressor and its motor had an overall efficiency of 75%. The necessary heat input to the Therminol®66 loop is 3.2 kW if heat loss through 3 cm of mineral fiber insulation (499 W) is added to the 2.7 kW calculated during the assumption of an adiabatic system. The table shows that the design meets the goals for flow rate and performance. Compared to the 1st generation design, the 2nd generation design consumes 64% less power.

Table 21: 2nd Generation Design Performance

	1st Generation Design	2nd Generation Design	% Reduction
Distillate Flow Rate (gal/hr)	20	20	0
Recirculation Pump Power Input (kW)	0.7	0.7	0
Compressor Power Input (kW)	4.3	0.68	84.2
Heat Transfer Fluid Heat Input (kW)	5	3.2	36
Total Power Input (kW)	10	4.58	54.2
Performance (kWh/gal)	0.5	0.229	54.2

4.15 Preliminary Examination of a Grid-Free Power System

This section explores some solar technologies which could allow the distiller to be grid-independent. PDRs could provide the thermal energy requirements of the Therminol®66 loop, while photovoltaic (PV) cells could provide electricity to run the compressor and pumps. As is discussed in Section 4.16, it is theoretically possible for PDRs to collect enough solar energy

during the day to ensure the Therminol®66 loop can provide 3.2 kW of heat to the distiller for 24 hours. However, it may be impractical to store the volume of Therminol®66 needed to properly store all the energy collected from the PDRs for this to occur. Therefore, a generator may be the best option for meeting the distillation power requirements during the night if 24 hour operation is desired.

4.15.1 Parabolic Dish Reflector

A PDR is a sun-tracking device which collects solar energy at a focal point. A PDR schematic is shown in Figure 49. As described by Kalogirou [40], PDRs are considered to be the most efficient type of solar collector system, and their concentration ratios range from 600 to 2000. The concentration ratio is defined as the area of the aperture divided by the area of the receiver [40].

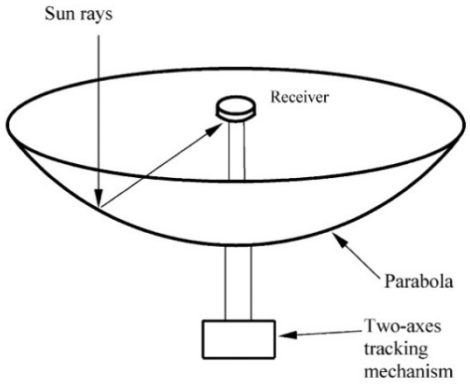

Figure 49: PDR Schematic [40]

PDRs can achieve temperatures greater than 1500°C at their receivers [40]. This technology therefore has great potential for high efficiency when it comes to being coupled to a

heat engine. The efficiency of a Carnot heat engine (the most efficient theoretical heat engine) can be calculated with the following equation [35]:

$$\eta_{\text{Carnot}} = 1 - (T_L/T_H) \qquad \textbf{Equation 34}$$

where T_L and T_H are the thermodynamic temperatures of the low-temperature reservoir and high-temperature reservoir, respectively. Assuming ambient air at 25°C is utilized as the low-temperature reservoir, and the receiver is utilized as a high-temperature reservoir, a PDR and heat engine system could have a Carnot efficiency of approximately 83.2%. However, factors such as heat loss and friction will result in an actual efficiency which is significantly lower than this value.

4.15.2 Photovoltaic Technology

PV cells are used to convert solar energy to electricity. PV technology can be categorized into three generations. The first generation consists of single-junction silicon wafers. The second generation will be thin-film silicon devices which will use less material than the devices of the first generation, but will have the same efficiencies. The third generation (this technology will be available in the near future) will consist of nanostructured solar cells which will improve upon the efficiency of the second generation technology [41].

Figure 50, presented by Razykov et al. [41], is a cost-efficiency analysis of the three generations of PV technologies. Based on Figure 50, a reasonable manufacturing cost and conversion efficiency for first generation technologies is €320/m^2 (approximately \$437/m^2) and 15%, respectively. Also, a reasonable manufacturing cost and conversion efficiency for second generation technologies is €80/m^2 (approximately \$109/m^2) and 10%, respectively. According to

Fröhlich [42], the average solar radiation at Earth over the whole year is 1365 W/m^2. Using this average radiation value and the estimated conversion efficiencies, first generation and second generation technology produce approximately 205 W/m^2 and 137 W/m^2, respectively.

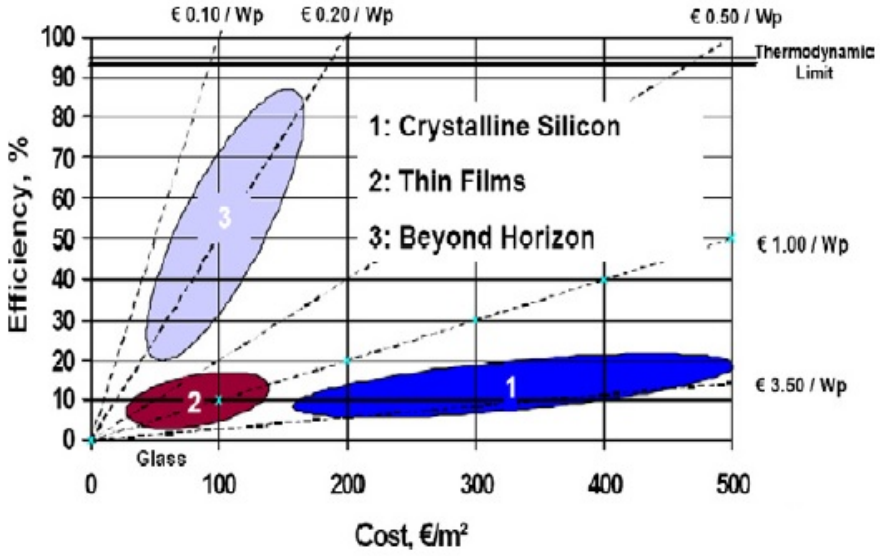

Figure 50: Manufacturing Cost and Conversion Efficiency Analysis of Photovoltaic Technologies [41]

4.16 Preliminary Exploration of the Control of the Therminol®66 Storage Tank Temperature

The National Renewable Energy Laboratory (NREL) has compiled a vast amount of data on solar radiation based on local standard time (LST), date, and location in a National Solar Radiation Database [43]. . Figure 51 shows the average solar radiation for five days in March, June, September, and December, time periods which include the start of Spring, Summer, Fall, and Winter, respectively. Average solar radiation values of less than 10 W/m^2 for an hour were not included in the graph. Figure 51 was developed by utilizing data from Pittsburgh, PA, in 2010. This data was obtained through a Meteorological-Statistical (METSTAT) model in which

it was assumed there was no cloud cover (a clear sky model). This model calculated the amount of solar radiation on a surface normal to the sun. This data provided a theoretical basis for the maximum amount of energy which can be collected by the sun-tracking PDRs

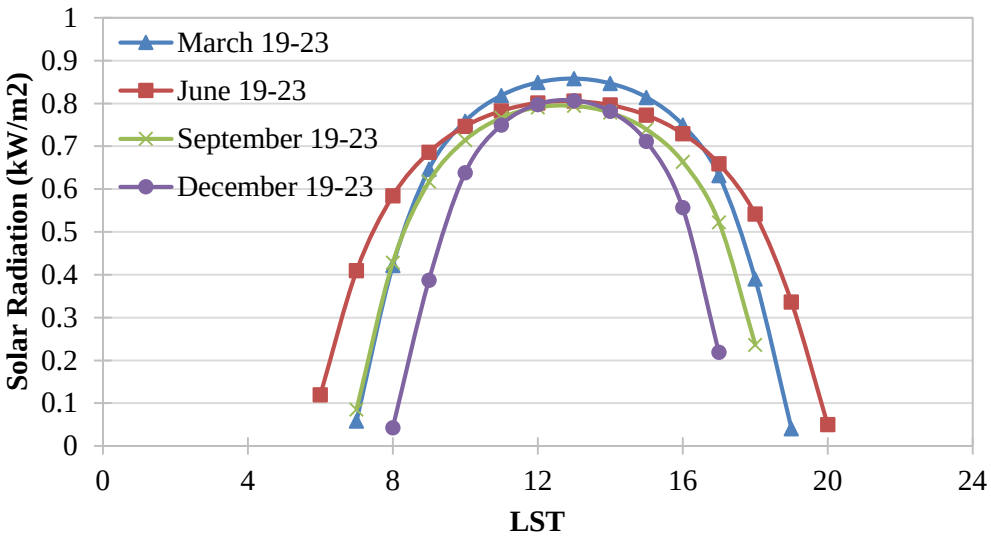

Figure 51: Solar Radiation vs. LST for Pittsburgh, PA, in 2010

Empirical 4th order polynomial equations were developed in Microsoft Excel for the months of December and June. These two months are representative of the most extreme cases where December shows solar radiation over the shortest amount of time, and June over the greatest amount of time. Figure 52 is a graph of the polynomial equations for these two months.

It was assumed that the Therminol®66 would be stored in a standard 55-gallon (0.208 m^3) drum, and the temperature of the fluid would never be greater than 300°C. At 300°C, the density of Therminol®66 is 807.5 kg/m^3, so the total mass contained in the drum should not be more than approximately 168 kg. It was assumed that the average temperature of the Therminol®66 contained in the drum would have an average temperature of 245°C throughout the hours of distiller operation. A heat loss of 0.25 kW from the drum was calculated using the

same process as that used to find the heat loss out of the evaporator/crystallizer if 3” (7.62 cm) of mineral fiber blanket insulation is applied to the drum. Therefore, the total heat transferred from the Therminol®66 loop is 3.45 kW, which includes 3.2 kW of heat transfer to the distiller.

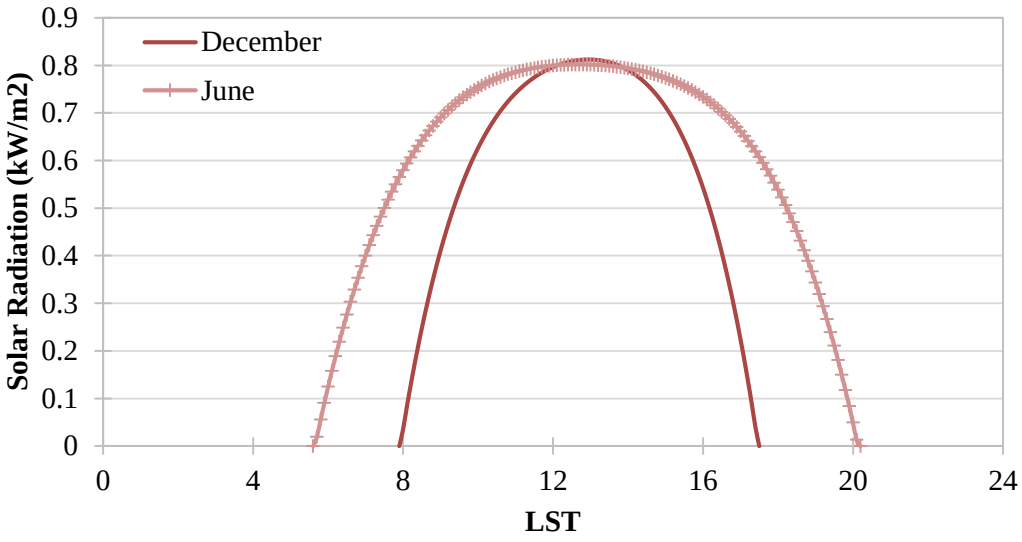

Figure 52: Solar Radiation vs LST for December and June

Integration of the two curves in Figure 52 shows that the total amount of solar radiation during one day for the months of December and June are 5.691 kWh/m^2 and 8.828 kWh/m^2, respectively. If it is assumed that the reflective material of the PDRs is 90% efficient at reflecting light, then 5.122 kWh/m^2 and 7.945 kWh/m^2 of solar energy can be collected during December and June, respectively. If 24-hour operation of the 2nd generation distiller during the month of December is desired, then the total required area of the PDR is 16.17 m^2, so the radius of the dish must be 2.27 m. This is based on a required continuous heat supply of 3.45 kW from the Therminol®66 loop. Fulfilling the heating requirements of the distiller with only one PDR may be impractical based on its size. Another option is to have two PDRs, each with a radius of 1.60 m.

Figure 53 was developed by multiplying the solar radiation curve for December in Figure 52 by 16.17 m^2 and including an efficiency of 90%. 16.17 m^2 is the minimum area required to ensure a continuous heat supply of 3.45 kW (this heat requirement has been included on the graph for reference) can be provided by the PDRs over 24 hours. The PDRs can provide the necessary heating requirements for the distiller from approximately 8:30 am to 5 pm, which is represented by the intersection locations of the two data series in the figure. The area under the PDR heat curve is 81.2 kWh (299,088 kJ), which is the gross heat transfer from the PDRs. Equation 35 is the empirically derived relationship for the PDR heat curve in Figure 53.

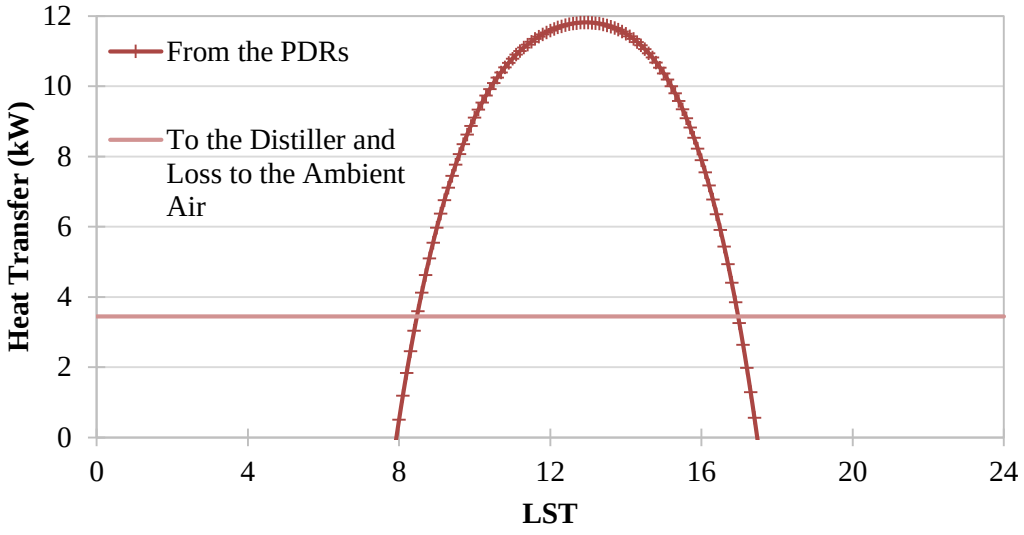

Figure 53: Solar Power vs. Local Standard Time

$$\dot{Q} = -0.01171t^4 + 0.58944t^3 - 11.37593t^2 + 99.81612t - 323.7897 \quad \textbf{Equation 35}$$

The First Law of Thermodynamics can be utilized to calculate the temperature in the Therminol®66 storage tank. If work, kinetic energy, and potential energy contributions are neglected, the First Law of Thermodynamics simplifies to the following expression:

$$\frac{dU}{dt} = \dot{Q}$$

In the above expression, heat transfer to the system and out of the system are positive and negative, respectively. Heat transfer to the Therminol®66 loop is given by Equation 35, and the total heat transfer out of the loop is 3.45 kW. After substituting these values into the equation, the above expression can be integrated with respect to time to find dU:

$$\frac{dU}{dt} = [-0.01171t^4 + 0.58944t^3 - 11.37593t^2 + 99.81612t - 323.7897] - [3.45]$$

$$dU = -0.002342t^5 + 0.14736t^4 - 3.79198t^3 + 49.90806t^2 - 327.2397t \qquad \textbf{Equation 36}$$

For an incompressible substance, it can be assumed that $c_p = c_v = c$. Therefore, the following relationship is valid for the Therminol®66:

$$c = \frac{du}{dT}$$

Utilizing the equation for the heat capacity of Therminol®66 found in Table 7 and integrating with respect to temperature, the following equation was obtained for the specific internal energy (kJ/kg):

$$u = 1.496T + 1.657 * 10^{-3}T^2 + 2.990 * 10^{-7}T^3 \qquad \textbf{Equation 37}$$

Figure 54 was developed by utilizing Equation 36 from approximately 8:30 to 5:00 LST, the time period when dU is positive. The specific internal energy of Therminol®66 at 190°C and 300°C is 346.1 kJ/kg and 606 kJ/kg, respectively. Therefore, the total internal energy of 168

kg of Therminol®66 at 190°C and 300°C is 58,144.8 kJ and 101,808 kJ, respectively. Figure 54 shows that the total internal energy will increase beyond 101,808 kJ during the daylight hours, meaning the PDRs must stop tracking the sun in order for the temperature of the Therminol®66 to stay below 300°C.

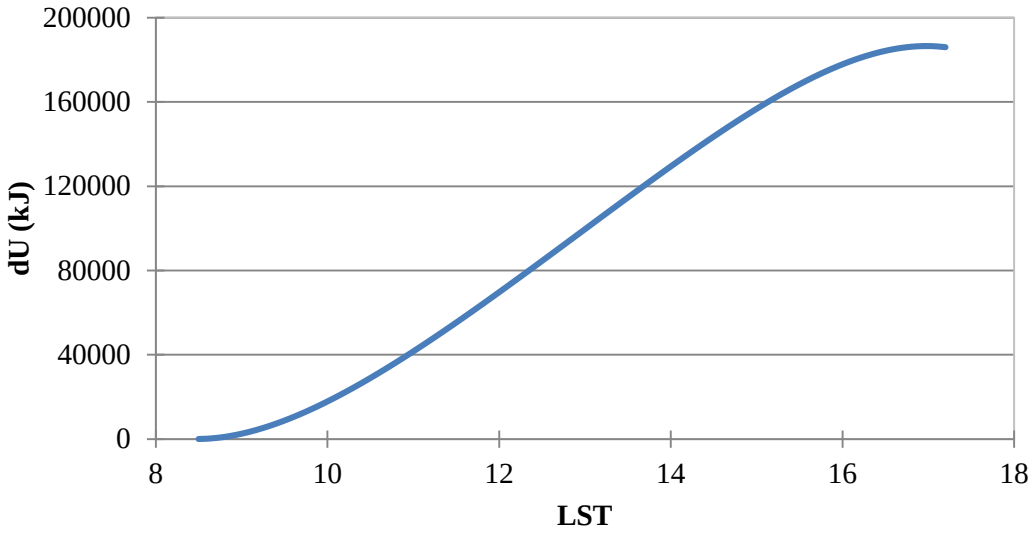

Figure 54: dU vs. LST for the Therminol 66 Storage Tank

The PDRs can provide a maximum of 186,627 kJ of additional energy during the daylight hours, represented by the area bound by the PDR heat curve and the heat transfer requirement line in Figure 53. In order for the storage tank to reach a maximum temperature of 300°C from a starting temperature of 190°C and receive all the energy from the PDRs, there must be 718 kg of Therminol®66 in the storage tank. This is an impractical solution because this would require five 55-gallon drums to store the fluid at 300°C. A practical approach would be to ensure a 55-gallon drum of Therminol®66 has a temperature of 300°C at 17:00 LST, the time at which the total internal energy in the storage tank will begin to decrease. One such approach would be to start tracking the sun with the PDRs at sunrise, stop tracking at approximately 11:00 LST, start

tracking again from approximately 14:30 LST until sunset. The variation of the total internal energy of 168 kg of Therminol®66 during the day for this method is shown in Figure 55. The resulting temperature variation in the storage tank is shown in Figure 56, which was obtained by utilizing Equation 37 along with the total internal energy values shown in Figure 55. Figure 56 shows that the temperature of the fluid will always be between 190°C and 300°C, and the distiller will be able to operate without additional heat input to the Therminol®66 loop until approximately 20:45 LST, which is about 3 hours and 15 minutes after sunset.

Figure 57 shows how the mass flow rate of the Therminol®66 loop must be varied in order for it to provide a constant heat input of 3.2 kW to the distiller. The graphs shows that a controller will be needed to adjust the flow rate as the temperature in the storage tank varies. The minimum and maximum mass flow rate of the loop are approximately 0.011 kg/s and 0.19 kg/s, respectively.

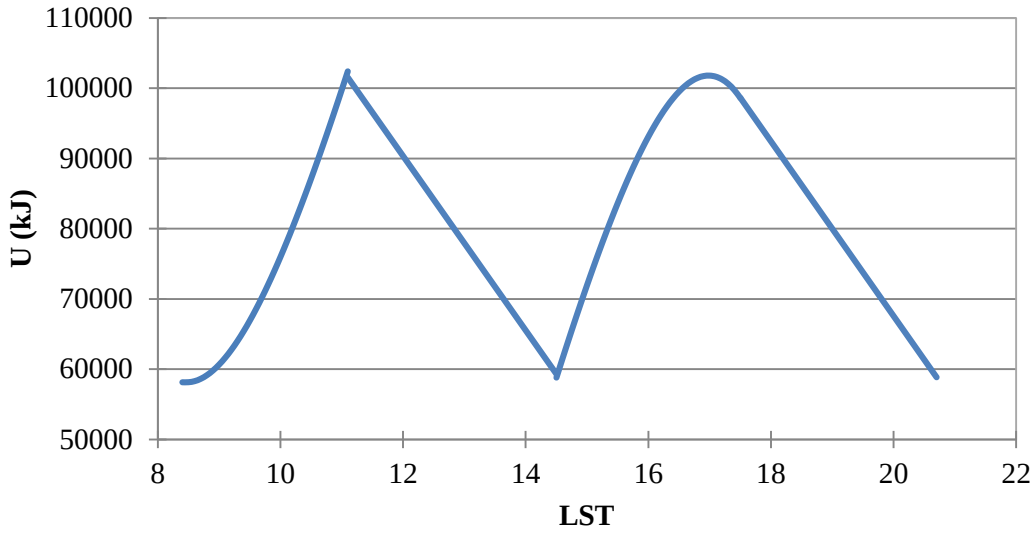

Figure 55: Total Internal Energy of the Therminol®66 vs. Time

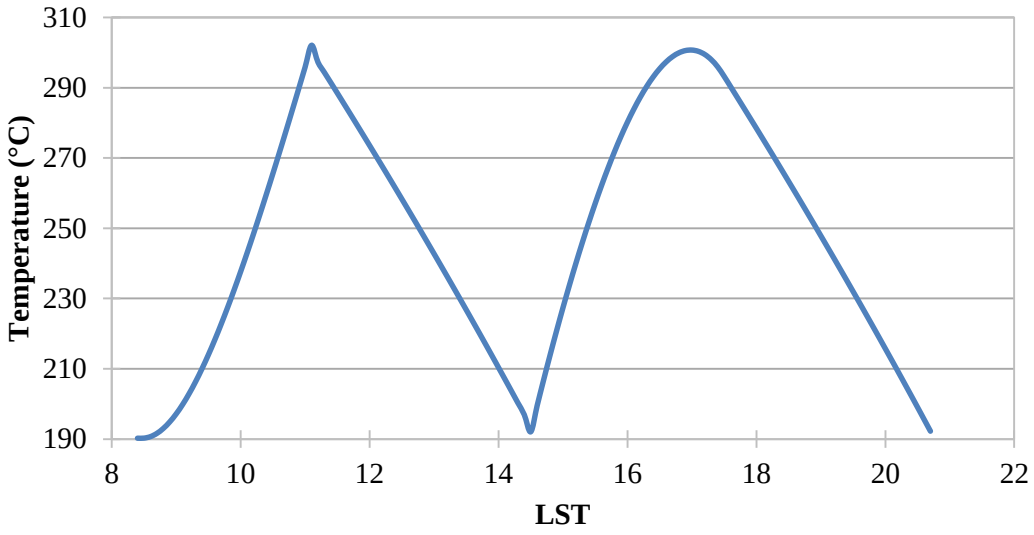

Figure 56: Temperature in the Therminol®66 Storage Tank vs. Time

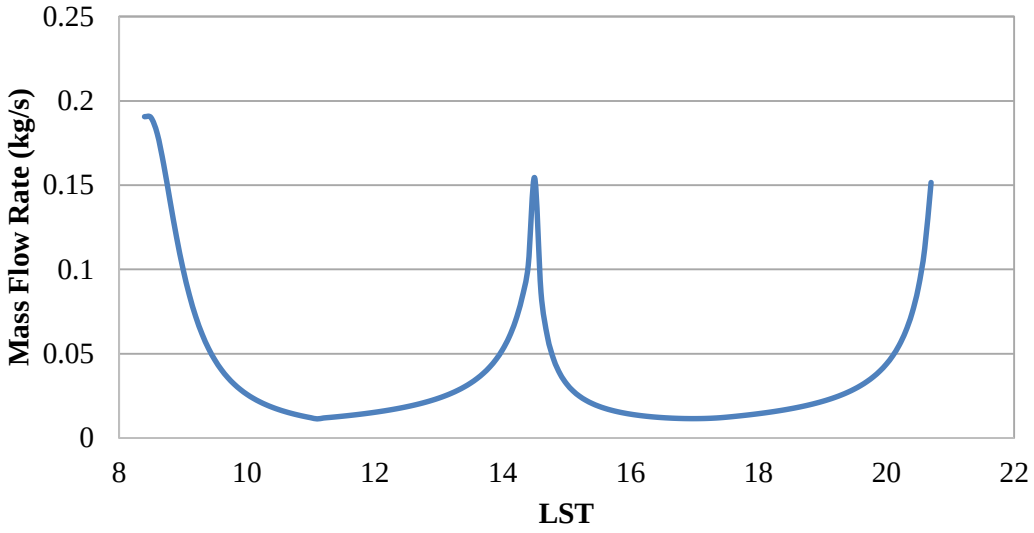

Figure 57: Mass Flow Rate of the Therminol®66 vs. Time

Chapter 5: Conclusions and Recommendations

5.1 Conclusions

The objective of this research was to develop a solar-power assisted mechanical vapor-compression distiller capable of processing produced water from the shale gas industry to environment friendly water with salt recovery. The system was required to process produced water at a rate of 20 gal/hr with an energy consumption of less than 0.5kWh/gallon. The research works completed include the in-house and onsite demonstration of the 1st generation vapor compression system, and the design of the 2nd generation system. The in-house examination and the onsite demonstration of the 1st generation system confirmed the capability of the 1st generation system in distilling the produced water. The potential issues of the 1st generation system were identified. The 2nd generation distiller included a system designed to recover the energy released during the condensation of superheated water vapor and its cooling, the selection of heat exchangers, calculation of power input for the compressor, and the examination of the potential of system insulation in reducing the consumption of solar energy. A thermodynamic model was developed to examine the performance of the designed system and the potential of the compressor, waste heat recovery system, and insulation in reducing energy consumption. Based on the results obtained in this research, the following conclusions can be drawn:

- The in-house and on-site demonstration confirmed that the proposed solar-power assisted mechanical vapor-compression distiller was able to process the produced water at a rate of 20 gallon/hour. The analysis verified that the distilled water met the requirement of water quality for direct disposal to rivers and lakes.

- The 2nd generation design was able to meet the design goal of separating fresh water from produced water at a rate of 20 gal/hr with the consumption of approximately 4.6 kW, which includes 3.2 kW from solar energy for heating purposes and 1.4 kW from electricity to run the compressor and the recirculation pump. The estimated energy consumption was 0.23 kWh/gal, which was 64% lower than design goal.

- The selection of the proper compressor has the potential to reduce energy consumption from 4.3 to 0.68 kW.

- The regeneration system of the MVC distiller was able to recover approximately 91% of the thermal energy released during the condensation and cooling process of the distilled water vapor, which dramatically decreased the consumption of thermal energy and the size of the PDRs.

- The insulation system was able to reduce heat loss to the ambient air by approximately 86% compared to an un-insulated system.

- It is possible to develop a grid-electricity free water distiller system with the thermal energy provided by the PDRs, and the electricity needed for compressor and pump provided by a photovoltaic system. All energy requirements could be met by utilizing a generator if 24 hour operation of the distiller is desired.

8.2 Recommendations

The work presented in this thesis was the preliminary design of the 2nd generation solar-power assisted mechanical vapor-compression distiller. There are many things that need to be done before fabrication and commercialization of the system can take place. The following are recommendations for future works:

- It is necessary to select a compressor which can handle the required flow rate of steam. The new compressor must be able to move the increased flow rate of generated steam and produce an outlet pressure which is greater than the saturation temperature of the brine within the recirculation loop.
- The operation of the pumps and compressor of the system consumes electricity, which is not convenient for its application in rural areas. The author recommends examining the possibility of developing a grid-electricity free system. The electricity can be provided by PV technology or a small spark ignition internal combustion engine operated on shale gas produced onsite. Table 22 shows the area required and cost of PV technology completely or partially providing the required power input to the distiller. If the power input is not completely handled by PV technology (in which case the power required from the PV panels is 1.88 kW), then a PDR can be utilized to provide the remaining 2.7 kW of heat. The table shows 1st or 2nd generation PV technology could be utilized in a practical manner in order to make the entire system operate entirely on sunlight if desired.
- There is a need to develop a control system capable of maintaining the distillation of produced water at a rate of 20 gallon/hour while managing the Therminol®66 loop. Control of the Therminol®66 loop includes managing its temperature and mass flow rate.

- The most uncertainty in this research is the selection of Heat Exchanger B, which serves to condense the output water from a saturated vapor to a saturated liquid. The physical model of the 1st generation design was not always able to completely condense the output water, and if this continues to be a problem then a heat exchanger with more surface area for heat transfer must be selected.

Table 22: Power Supply from Photovoltaic Technology

Power Requirement	PV Technology	Area (m^2)	Cost ($)
4.58 kW	1st Generation	22.3	9,374
4.58 kW	2nd Generation	33.4	3,640
1.88 kW	1st Generation	9.23	4,034
1.88 kW	2nd Generation	13.8	1,504

Bibliography

[1] Epiphany Solar Water Systems, [Online]. Available: http://epiphanysws.com/technology/hybrid/.

[2] D. Grottenthaler, "Recycling Water for Hydraulic Fracturing," *Mechanical Engineering,* vol. 133, no. 12, pp. 21-22,24, 2011.

[3] K. B. Gregory, R. D. Vidic and D. A. Dzombak, "Water Management Challenges Associated with the Production of Shale Gas by Hydraulic Fracturing," *Elements,* vol. 7, no. 3, pp. 181-186, 2011.

[4] G. P. Thiel and J. H. Lienhard V, "Treating Produced Water from Hydralic Fracturing: Composition Effects on Scale Formation and Desalination System Selection," *Desalination,* vol. 346, pp. 54-69, 2014.

[5] T. J. Tofflemire and G. P. Brezner, "Deep-Well Injection of Wastewater," *Water Pollution Control Federation,* vol. 43, no. 7, pp. 1468-1479, 1971.

[6] L. F. Greenlee, D. F. Lawler, B. D. Freeman, B. Marrot and P. Moulin, "Reverse osmosis desalination: Water sources, technology, and today's challenges," *Water Research,* vol. 43, no. 9, pp. 2317-2348, 2009.

[7] S. Sethi and G. Wetterau, "Seawater Desalination Overview," in *Desalination of Seawater*, First ed., American Water Works Association, 2011, p. 121.

[8] S. M. Rao, "Reverse Osmosis," *Resonance,* vol. 16, no. 12, pp. 1333-1336, 2011.

[9] T. Younos and K. E. Tulou, "Overview of Desalination Techniques," *Journal of Contemporary Water Research & Education,* vol. 132, no. 1, pp. 3-10, 2005.

[10] R. Saidur, E. Elcevvadi, A. Safari and H. Mohammed, "An Overview of Different Distillation Methods for Small Scale Applications," *Renewable and Sustainable Energy Reviews,* vol. 15, no. 9, pp. 4756-4764, 2011.

[11] W. V. Collentro, "Distillation," *Journal of Validation Technology,* 2011.

[12] T. Asano, F. Burton and H. Leverenz, Water Reuse: Issues, Technologies, and Applications, McGraw-Hill, 2007.

[13] J. A. Nathanson, "Water Supply System," 2012. [Online]. Available:

http://www.britannica.com/EBchecked/topic/637296/water-supply-system. [Accessed 14 November 2012].

[14] H. Ettouney, H. El-Dessouky and Y. Al-Roumi, "Analysis of Mechanical Vapour Compression Desalination Process," *International Journal of Energy Research,* vol. 23, no. 5, pp. 431-451, 1999.

[15] R. Dev and G. N. Tiwari, "Solar Distillation," in *Drinking Water Treatment*, C. Ray and R. Jain, Eds., Springer Netherlands, 2011, pp. 159-210.

[16] R. Sinnott and G. Towler, Chemical Engineering Design, Fifth ed., Butterworth-Heinemann, 2009.

[17] S. McAleese, Operation Aspects of Oil and Gas Well Testing, Elsevier, 2000.

[18] R. Kouhikamali, H. Hesami and A. Ghavamian, "Convective heat transfer in a mixture of cooling water and superheated steam," *International Journal of Thermal Sciences*, vol. 60, pp. 205-211, 2012.

[19] K. Donohue, "Desuperheater & Optimization," *Chemical Engineering,* vol. 108, no. 8, pp. 80-83, 2001.

[20] R. Semiat, "Energy Issues in Desalination Processes," *Environmental Science and Technology*, vol. 42, no. 22, pp. 8193-8201, 2008.

[21] J. M. Veza, "Mechanical Vapour Compression Desalination Plants -- A Case Study," *Desalination ,* vol. 101, no. 1, pp. 1-10, 1995.

[22] N. H. Aly and A. K. El-Fiqi, "Mechanical vapor compression desalination systems--a case study," *Desalination,* vol. 158, no. 1-3, pp. 143-150, 2003.

[23] R. Bahar, M. Hawlader and L. S. Woei, "Performance evaluation of a mechanical vapor compression desalination system," *Desalination,* vol. 166, pp. 123-127, 2004.

[24] P. E. Minton, Handbook of Evaporation Technology, William Andrew Publishing/Noyes, 1986.

[25] J. C. Cowan and D. J. Weintritt, Water-Formed Scale Deposits, Knovel, 1976.

[26] J. d. B. Doelman, "Controlling Scale Deposition and Industrial Fouling," *Water Engineering & Management,* vol. 148, no. 7, pp. 19-21, July 2001.

[27] J. W. Gooch, Ed., Encyclopedic Dictionary of Polymers, Springer Science+Business Media, LLC., 2007.

[28] J. Speight, Lange's Handbook of Chemistry, Sixteenth ed., McGraw-Hill Education, 2005.

[29] F. J. Millero, R. Feistel, D. G. Wright and T. J. McDougall, "The Composition of Standard Seawater and the Definition of the Reference-Composition Salinity Scale," *Deep-Sea Research Part I: Oceanographic Research Papers,* vol. 55, no. 1, pp. 50-72, 2008.

[30] R. R. Langteau, "Cavitation in Pumps: Its Nature and Control," *Water Pollution Control Federation,* vol. 38, no. 4, pp. 585-600, 1966.

[31] J. Askew, "Centrifugal Pumps: Avoiding Cavitation," *World Pumps,* vol. 2011, no. 7-8, pp. 34,36,38-39, 2011.

[32] G. Hetsroni, Ed., Handbook of Multiphase Systems, Hemisphere Publishing Corporation, 1982.

[33] M. Mikheyev, Fundamentals of Heat Transfer, Moscow: Mir Publishers, 1977.

[34] J. W. Mullin, Crystallization, London: Butterworth & Co, 1972.

[35] Y. A. Çengel and M. A. Boles, Thermodynamics: An Engineering Approach, Sixth ed., New York, NY: McGraw-Hill, 2008.

[36] Solutia, "Therminol 66," [Online]. Available: http://twt.mpei.ac.ru/TTHB/HEDH/HTF-66.PDF.

[37] H. S. Aybar, "Analysis of a mechanical vapor compression desalination system," *Desalination,* vol. 142, no. 2, pp. 181-186, 2002.

[38] T. L. Bergman, A. S. Lavine, F. P. Incropera and D. P. Dewitt, Introduction to Heat Transfer, Sixth ed., John Wiley & Sons, Inc., 2011.

[39] D. F. Young, B. R. Munson, T. H. Okiishi and W. W. Huebsch, A Brief Introduction to Fluid Mechanics, 4th ed., John Wiley & Sons, Inc., 2007.

[40] S. A. Kalogirou, "Solar Thermal Collectors and Applications," *Progress in Energy and Combustion Science,* vol. 30, no. 3, pp. 231-295, 2004.

[41] T. M. Razykov, C. S. Ferekides, D. Morel, E. Stefanakos, H. S. Ullal and H. M. Upadhyaya, "Solar Photovoltaic Electricity: Current Status and Future Prospects," *Solar Energy,* vol. 85,

no. 8, pp. 1580-1608, 2011.

[42] C. Fröhlich, "Solar Radiation," in *McGraw-Hill Concise Encyclopedia of Science and Technology*, 2006.

[43] NREL, "National Solar Radiation Data Base," [Online]. Available: http://rredc.nrel.gov/solar/old_data/nsrdb/.

[44] B. S. Sparrow, "Empirical Equations for the Thermodynamic Properties of Aqueous Sodium Chloride," *Desalination*, vol. 159, no. 2, pp. 161-170, 2003.

[45] A. A. Aleksandrov, E. V. Dzhuraeva and V. F. Utenkov, "Themal Conductivity of Sodium Chloride Aqueous Solutions," *Thermal Engineering*, vol. 60, no. 3, pp. 190-194, 2013.

[46] A. A. Aleksandrov, E. V. Dzhuraeva and V. F. Utenkov, "Viscosity of Aqueous Solutions of Sodium Chloride," *High Temperature*, vol. 50, no. 3, pp. 378-383, 2012.

[47] D. L. Reger, S. R. Goode and D. W. Ball, Chemistry: Principles and Practices, Third ed., Cengage Learning, 2010.

[48] D. J. Kukulka, "An Evaluation of Heat Transfer Surface Materials Used in Fouling Applications," *Heat Transfer Engineering*, vol. 26, no. 5, pp. 42-46, 2005.

[49] C. J. Chartres and S. Varma, Out of Water: From Abundance to Scarcity and How to Solve the World's Water Problems, Upper Saddle River, New Jersey: FT Press, 2011.

[50] T. Lohan, Ed., Water Matters: Why We Need to Act Now to Save Our Most Critical Resource, San Francisco, CA: AlterNet Books, 2010.

[51] I. C. Escobar and A. I. Schafer, Eds., Sustainable Water for the Future, Volume 2 - Water Recycling versus Desalination, Elsevier B.V., 2010.

[52] M. A. Darwish and H. El-Dessouky, "The Heat Recovery Thermal Vapour-Compression Desalting System: A Comparison With Other Thermal Desalination Processes," *Applied Thermal Engineering*, vol. 16, no. 6, pp. 523-537, 1996.

[53] H. El-Dessouky and H. Ettouney, "Single-Effect Thermal Vapor-Compression Desalination Process: Thermal Analysis," *Heat Transfer Engineering*, vol. 20, no. 2, pp. 52-68, 1999.

[54] F. Cardarelli, Materials Handbook: A Concise Desktop Reference, 2nd ed., Springer-Verlag London Limited, 2008.

[55] J. C.-S. Chou, *Thermodynamic Properties of Aqueous Sodium Chloride Solutions from 32 to 350 Degrees F,* ProQuest Dissertations and Theses, 1968.

[56] K. H. Mistry, R. K. McGovern, G. P. Thiel, E. K. Summers, S. M. Zubair and J. H. Lienhard V, "Entropy Generation Analysis of Desalination Technologies," *Entropy,* vol. 13, no. 10, pp. 1829-1864, 2011.

[57] M. Al-Sahali and H. M. Ettouney, "Humidification Dehumidification Desalination Process: Design and Performance Evaluation," *Chemical Engineering Journal,* vol. 143, no. 1-3, pp. 257-264, 2008.

[58] H. El-Dessouky, H. Ettouney, I. Alatiqi and G. Al-Nuwaibit, "Evaluation of Steam Jet Ejectors," *Chemical Engineering and Processing: Process Intensification,* vol. 41, no. 6, pp. 551-561, 2002.

[59] E. Curcio and E. Drioli, "Membrane Distillation and Related Operations--A Review," *Separation & Purification Reviews,* vol. 34, no. 1, pp. 35-86, 2005.

[60] J. Lara, G. Noyes and M. Holtzapple, "An investigation of high operating temperatures in mechanical vapor compression desalination," *Desalination,* vol. 227, no. 1-3, pp. 217-232, 2008.

[61] A. Behan, Convection Heat Transfer, Third ed., John Wiley & Sons, 2004.

[62] V. Gnielinski, "Heat Transfer Coefficients for Turbulent Flow in Concentric Annular Ducts," *Heat Transfer Engineering,* vol. 30, no. 6, pp. 431-436, 2009.

[63] M. H. Sharqawy, J. H. Lienhard V and S. M. Zubair, "The thermophysical properties of seawater: A review of existing correlations and data," *Desalination and Water Treatment,* vol. 16, pp. 354-380, 2010.

[64] K. W. Whitten, R. E. Davis, L. M. Peck and G. G. Stanley, Chemistry, Tenth ed., Brooks/Cole, Cengage Learning, 2014.

[65] J. Bird, "Water Supply," in *Pump Handbook,* Fourth ed., I. J. Karassik, J. P. Messina, P. Cooper and C. C. Heald, Eds., McGraw-Hill, 2008.

[66] A. G. Fane, R. Wang and Y. Jia, "Membrane Technology: Past, Present, and Future," in *Handbook of Environmental Engineering,* vol. 13, J. P. C. Y. H. N. K. S. Lawrence K. Wang, Ed., Humana Press, 2011, pp. 1-45.

[67] G. M. Masters, Renewable and Efficient Electric Power Systems, Hoboken, New Jersey:

John Wiley & Sons, Inc. , 2004.

[68] C. A. Gueymard and D. Thevenard, "Revising ASHRAE Climatic Data for Design and Standards--Part 2: Clear-Sky Solar Radiation Model," *ASHRAE Transactions*, vol. 119, no. 2, pp. 194-209, 2013.

Appendix A

Thermodynamic Properties of Aqueous NaCl Solutions

The thermodynamic properties of aqueous NaCl solutions differ from those of pure water. Many sources in the literature present certain properties of these solutions as a result of experimentation and/or theoretical calculation. Several properties of great importance are discussed below.

Sparrow [44] provides empirical equations for the solubility, vapor pressure, density, enthalpy, and entropy as functions of temperature and mass fraction of NaCl of the solution. All these equations will be utilized in this document except for that of entropy. The mass fraction is related to the molality of the solution by utilizing Equation A1 [44]:

$$X = mM_{NaCl}/(1000 + mM_{NaCl}) \qquad \textbf{Equation A1}$$

In Equation A1, X is the mass fraction of salt, m is the molality (mol NaCl/kg H_2O), and M_{NaCl} is the molar mass of NaCl (58.44 g/mol). The solubility of salt in water can be calculated by utilizing Equation A2 [44]:

$$X_{SAT} = 0.2628 + 62.75 \times 10^{-6}T + 1.084 \times 10^{-6}T^2 \qquad \textbf{Equation A2}$$

The vapor pressure (MPa) of the solution is calculated by utilizing Equation A3 [44]:

$$P_{VAP} = A + BT + CT^2 + DT^3 + ET^4 \qquad \textbf{Equation A3}$$

Where

$$A = (0.9083 - 0.569X + 0.1945X^2 - 3.736X^3 + 2.82X^4) \times 10^{-3}$$

$$B = (-0.0669 + 0.0582X - 0.1668X^2 + 0.6761X^3 - 2.82X^4) \times 10^{-3}$$

$$C = (7.541 - 5.143X + 6.482X^2 - 52.62X^3 + 115.7X^4) \times 10^{-6}$$

$$D = (-0.0922 + 0.0649X - 0.1313X^2 + 0.8024X^3 - 1.986X^4) \times 10^{-6}$$

$$E = (1.237 - 0.753X + 0.1448X^2 - 6.964X^3 + 14.61X^4) \times 10^{-9}$$

Figure 58 is a graph which shows how the temperature and the NaCl mass fraction affect the vapor pressure of the solution. As with pure water, the vapor pressure of a NaCl solution increases with temperature. However, the vapor pressure decreases slightly with NaCl mass fraction for a given temperature.

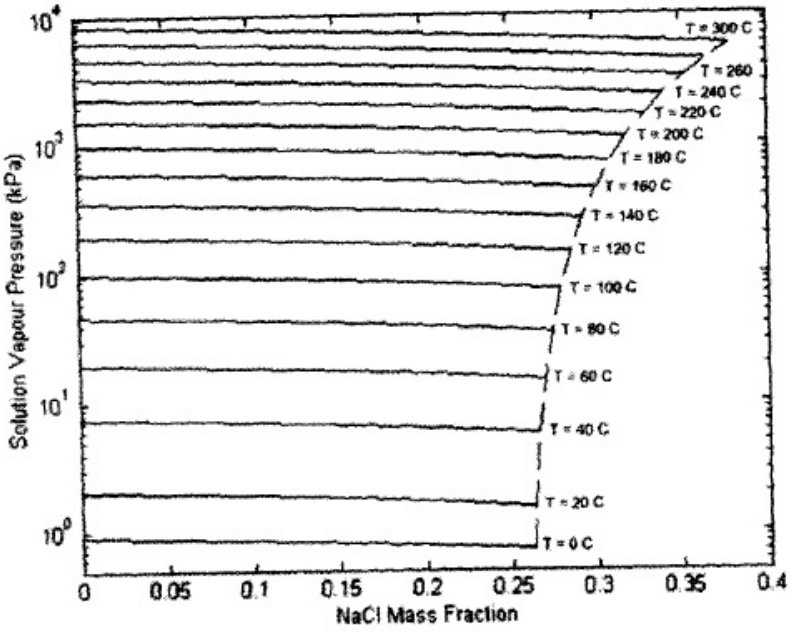

Figure 58: Aqueous NaCl Vapor Pressure vs. Mass Fraction [44]

The density (kg/m^3) of the solution is calculated by utilizing Equation A4 [44]:

$$\rho = A + BT + CT^2 + DT^3 + ET^4 \qquad \textbf{Equation A4}$$

where

$$A = (1.001 + 0.7666X - 0.0149X^2 + 0.2663X^3 + 0.8845X^4) \times 10^3$$

$$B = -0.0214 - 3.496X + 10.02X^2 - 6.56X^3 - 31.37X^4$$

$$C = (-5.263 + 39.87X - 176.2X^2 + 363.5X^3 - 7.784X^4) \times 10^{-3}$$

$$D = (15.42 - 167X + 980.7X^2 - 2573X^3 + 876.6X^4) \times 10^{-6}$$

$$E = (-0.0276 + 0.2978X - 2.017X^2 + 6.345X^3 - 3.914X^4) \times 10^{-6}$$

Figure 59 shows how the density changes with temperature and NaCl mass fraction. Similar to most substances (including pure water), the density of an aqueous NaCl solution decreases with temperature. However, the density increases with NaCl mass fraction for a given temperature.

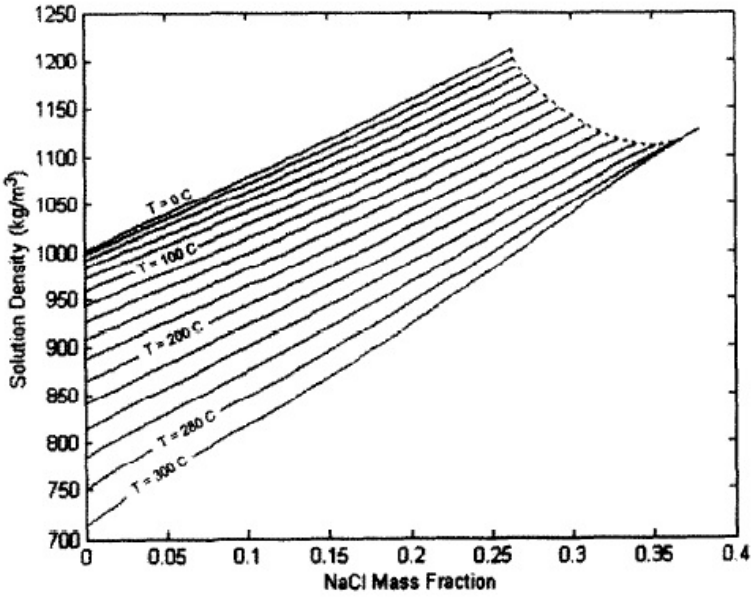

Figure 59: Aqueous NaCl Density vs. Mass Fraction [44]

The specific enthalpy (kJ/kg) of the solution is calculated by utilizing Equation A5 [44]:

$$h = A + BT + CT^2 + DT^3 + ET^4 \qquad \textbf{Equation A5}$$

where

$$A = (0.0005 + 0.0378X - 0.3682X^2 - 0.6529X^3 + 2.89X^4) \times 10^3$$

$$B = 4.145 - 4.973X + 4.482X^2 + 18.31X^3 - 46.41X^4$$

$$C = 0.0007 - 0.0059X + 0.0854X^2 - 0.4951X^3 + 0.8255X^4$$

$$D = (-0.0048 + 0.0639X - 0.714X^2 + 3.273X^3 - 4.85X^4) \times 10^{-3}$$

$$E = (0.0202 - 0.2432X + 2.054X^2 - 8.211X^3 + 11.43X^4) \times 10^{-6}$$

Figure 60 shows how the enthalpy of a solution changes with temperature and NaCl mass fraction based on Equation A5. The enthalpy of the solution increases with temperature. However, the enthalpy decreases with NaCl mass fraction, and the trend is more pronounced at higher temperatures.

The latent heat of vaporization is described by Equation A6:

$$h_{fg} = h_g - h_f \qquad \textbf{Equation A6}$$

where h_{fg} is the latent heat of vaporization, h_g is the enthalpy of the fluid in the vapor phase, and h_f is the enthalpy in the liquid phase. The tabulated data from Çengel and Boles [35] and Equation A5 will be utilized to find h_g and h_f at a certain temperature, respectively. The latent heat of vaporization for the aqueous NaCl solution can be calculated once these values are

known. Equation A7 can then be applied to calculate the amount of heat transfer required to obtain a specific mass flow rate of distilled water from the evaporator/crystallizer:

$$\dot{Q} = \dot{m}h_{fg} \qquad \textbf{Equation A7}$$

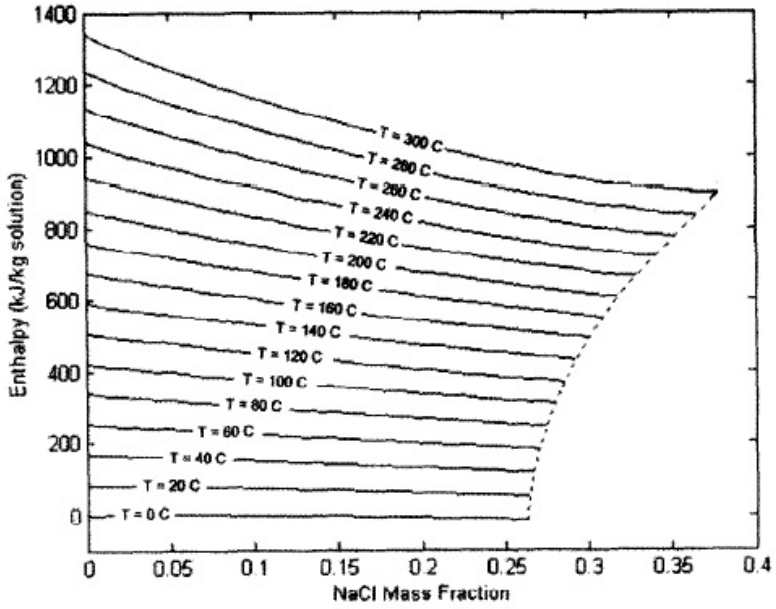

Figure 60: Aqueous NaCl Enthalpy vs. Mass Fraction [44]

The specific heat can be approximated from Equation A5 by utilizing Equation A8:

$$c_p = (\partial h/\partial T)_P \cong (h_2 - h_1)/(T_2 - T_1) \qquad \textbf{Equation A8}$$

The above relation is more accurate when the step between data points is small. Equation A5 will be solved for the temperature in question, and then solved at a temperature 0.5°C greater than that temperature. After the specific enthalpies of these two points are calculated, Equation A8 will then be applied to find the specific heat.

Aleksandrov et al. [45] presented equations for calculating the thermal conductivity of aqueous NaCl solutions derived from experimental results. The temperature range of the

equations is 20 to 325°C, the pressure range is from 0.1 to 100 MPa, and the molality range is from 0 to 5 mol NaCl/kg H_2O. Table 23 shows thermal conductivity of aqueous NaCl solutions at 0.1 and 10 MPa. Linear interpolation or extrapolation techniques will be utilized to calculate the thermal conductivity at a specific temperature and molality. Since the greatest design pressure for the distiller in this document is approximately 0.2 MPa, there will be negligible error in utilizing only the tabulated data for 0.1 MPa when calculating the thermal conductivity.

Table 23: Thermal Conductivity (mW/(m K)) of Aqueous NaCl Solutions [45]

t, °C	Molality, mol/kg H_2O				
	1	2	3	4	5
$p = 0.1$ MPa					
20	590	586	582	575	570
50	636	630	623	617	611
75	661	654	647	642	636
100	675	668	661	657	653
$p = 10$ MPa					
20	595	591	586	579	573
50	641	634	627	621	615
75	666	658	651	646	640
100	680	673	666	662	657
150	685	678	672	668	664
200	661	655	649	645	640
250	614	606	600	594	588
300	540	531	524	516	507
325	489	479	471	461	452

Aleksandrov et al. [46] present equations for dynamic viscosity in the same manner as in [45]. The temperature range of the equations is 0 to 325°C, the pressure range is from 0 to 40 MPa, and the molality range is from 0 to 6 mol NaCl/kg H_2O. Table 24 shows the dynamic viscosity of aqueous NaCl solutions at 0.1 and 10 MPa. Similar to the calculation of thermal conductivity mentioned in the previous paragraph, linear interpolation or extrapolation

techniques will be utilized to calculate the dynamic viscosity at a specific temperature and molality. It will also be assumed using the tabulated data for 0.1 MPa will provide negligible error for the calculations in this document.

Table 24: Dynamic Viscosity (µPa s) of Aqueous Solutions of Sodium Chloride [46]

t, °C	mol/(kg of water)					
	1	2	3	4	5	6
			P = 0.1 MPa			
0	1884	2052	2288	2583	2923	3298
25	974	1074	1199	1349	1528	1737
50	610	679	759	853	964	1097
75	426	478	535	601	678	768
100	321	361	405	455	512	577
			P = 10 MPa			
0	1860	2036	2272	2562	2901	3281
25	973	1078	1203	1354	1533	1744
50	613	684	765	859	971	1104
75	430	482	540	606	683	774
100	324	365	409	459	516	581
150	212	241	271	303	339	378
200	158	181	204	228	253	279
250	127	145	164	184	203	222
300	103	119	135	150	165	179
325	92	105	117	129	142	160

Equation A9 is one method for calculating the BPE [47]:

$$T = T_b + \ iE_b m_b \qquad \textbf{Equation A9}$$

In the above equation, T is the boiling point of solution, T_b is the boiling point of the solvent, *i* is the van't Hoff factor, E_b is the ebullioscopic constant, and m_b is the molality of the solution. The van't Hoff factor for salt solutions is greater than 1, whereas for solutions of typical nonelectrolytes it is less than 1. NaCl has a van't Hoff factor of 2 [47]. The value of the ebullioscopic constant for water is 0.515 K*kg/mol.